(4)

ENGINEERING AND TECHNICAL EFFORTS TO DESIGN AND CONSTRUCT A 10 MW GYROTRON LABORATORY

J206-89-001/6261

JAYCOR

1608 Spring Hill Road
Vienna, Virginia 22180-2270

(4)

JAYCOR

ENGINEERING AND TECHNICAL EFFORTS TO DESIGN AND CONSTRUCT A 10 MW GYROTRON LABORATORY

J206-89-001/6261

Final Report by
George L. Bergeron, III
Robert C. Lee
Marc L.Barsanti
Terry D. Hahn
Mark A. Czarnaski
Richard P. Fischer

January 18, 1989

Prepared For:

Naval Research Laboratory
4555 Overlook Avenue, SW
Washington, DC 20375-5000

Under:
Contract Number N00014-86-C-2322

1608 Spring Hill Road • Vienna, Virginia 22180-2270 • (703) 847-4000

REPORT DOCUMENTATION PAGE

1a. REPORT SECURITY CLASSIFICATION Unclassified	1b. RESTRICTIVE MARKINGS N/A
2a. SECURITY CLASSIFICATION AUTHORITY N/A	3. DISTRIBUTION/AVAILABILITY OF REPORT
2b. DECLASSIFICATION/DOWNGRADING SCHEDULE N/A	
4. PERFORMING ORGANIZATION REPORT NUMBER(S) J206-89-001/6261	5. MONITORING ORGANIZATION REPORT NUMBER(S)
6a. NAME OF PERFORMING ORGANIZATION JAYCOR 6b. OFFICE SYMBOL (*If applicable*)	7a. NAME OF MONITORING ORGANIZATION Naval Research Laboratory
6c. ADDRESS (*City, State, and ZIP Code*) 1608 Spring Hill Road Vienna, VA 22182	7b. ADDRESS (*City, State, and ZIP Code*) 4555 Overlook Avenue, SW Washington, DC 20375
8a. NAME OF FUNDING/SPONSORING ORGANIZATION Naval Research Laboratory 8b. OFFICE SYMBOL (*If applicable*) Code 4740	9. PROCUREMENT INSTRUMENT IDENTIFICATION NUMBER N00014-86-2322
8c. ADDRESS (*City, State, and ZIP Code*) 4555 Overlook Avenue, SW Washington, DC 20375	10. SOURCE OF FUNDING NUMBERS PROGRAM ELEMENT NO.: B003 / PROJECT NO. / TASK NO. / WORK UNIT ACCESSION NO.
11. TITLE (*Include Security Classification*) *Engineering and Technical Efforts to Design and Construct a 10 MW Gyrotron Laboratory*	
12. PERSONAL AUTHOR(S) G.L.Bergeron, III, R.C.Lee, M.L.Barsanti, T.D.Hahn, M.A.Czarnaski & R.P.Fischer	
13a. TYPE OF REPORT Final 13b. TIME COVERED FROM 07/15/86 TO 07/14/88	14. DATE OF REPORT (*Year, Month, Day*) 89 JAN 18 15. PAGE COUNT 110 pages
16. SUPPLEMENTARY NOTATION	
17. COSATI CODES FIELD / GROUP / SUB-GROUP	18. SUBJECT TERMS (*Continue on reverse if necessary and identify by block number*) Gyrotron Quasi-optical gyrotron Phase-locked oscillator

19. ABSTRACT (*Continue on reverse if necessary and identify by block number*)

This report describes the results of efforts performed under Contract Number N00014-86-C-2322. The scope of this effort was diverse with emphasis placed on five major tasks: experiment design and construction of 10 GHz 10 MW long pulse gyrotron; numerical and computational analysis for the gyrotron laboratory; technical efforts for pulsed power microwave experiments; operation of the Gyrotron Test Facility, and; the quasi-optical gyrotron. Also included is a section identified as additional efforts. These efforts include the tunable oscillator and low power phase-locked oscillator experiments and are an extension of work done under the pulsed power experiments.

Keywords:

20. DISTRIBUTION/AVAILABILITY OF ABSTRACT ☐ UNCLASSIFIED/UNLIMITED ☒ SAME AS RPT ☐ DTIC USERS	21. ABSTRACT SECURITY CLASSIFICATION Unclassified
22a. NAME OF RESPONSIBLE INDIVIDUAL Max Rhinewine	22b. TELEPHONE (*Include Area Code*) (202)767-3821 22c. OFFICE SYMBOL Code 4740

DD FORM 1473, 84 MAR — 83 APR edition may be used until exhausted. All other editions are obsolete.

SECURITY CLASSIFICATION OF THIS PAGE
UNCLASSIFIED

TABLE OF CONTENTS

TABLE OF FIGURES

TABLE OF TABLES

ABSTRACT

This report describes the results of efforts performed under Contract Number N00014-86-C-2322. The scope of this effort was diverse with emphasis placed on five major tasks:

- Experiment design and construction of 10 GHz 10 MW long pulse gyrotron;
- Numerical and computational analysis for the Gyrotron laboratory;
- Technical efforts for pulsed power microwave experiments;
- Operation of the Gyrotron Test Facility, and;
- The Quasi-Optical gyrotron.

Also included is a section identified as "Additional Efforts." These efforts include the Tunable Oscillator and Low Power Phase-locked Oscillator experiments and are an extension of work done under the pulsed power experiments.

SECTION I
INTRODUCTION

I. INTRODUCTION

This contract was funded to a large extent through NRL by Walter Reed Army Medical Research Center (WRAMRC) for the development of two 10 GHz, 10 MW gyrotron oscillators. Due to changes in their requirements, many program modifications were made, with the eventual conclusion being drawn (by WRAMRC) that the program was unnecessary and funding was cut just a few months into this contract. The efforts under this program were successful as far as they went, as is shown in this report.

Performance under this contract also included work in numerical and computational analysis which encompassed electron gun design and beam analysis, magnet coil design and cavity design and analysis. JAYCOR has contributed greatly to the numerical modelling and computational tools used by the High Power Electromagnetic Radiation Branch, both in actual code development and through the modification of existing programs.

With the demise of the effort on the WRAMRC systems came increased emphasis in the areas of microwave interactions, pulsed power systems and the Quasi-Optical device. Also, JAYCOR became a major contributor on the 85 GHz tunable oscillator and low power phase-locked oscillator projects, performing essentially all the engineering and development of the tubes. Each task is approached as listed in the statement of work, and the efforts performed are described.

TASK 1: EXPERIMENT DESIGN AND CONSTRUCTION OF A 10 GHz 10 MW LONG PULSE GYROTRON

This experiment was two years into a three year program at the time of award of this contract. The gun, tube and cavity of the $TE_{1,3}$ device had been manufactured and assembled, and were undergoing testing at half power; the power restricted by the existing modulator. Also fully designed, but not built, were the electron guns, tube structure and cavities for the $TE_{1,4}$ device. A new modulator that could reach the design goal of 60 MW nominal beam power had yet to be designed, but the required codes to accomplish this end had been assembled.

After the award of this contract, the modulator design was realized through the efforts of JAYCOR and David Bacon of SAIC. The parts were ordered and preparations were made to begin in-house construction of the pulse line. In conjunction with the preparations for the construction of the modulator, the tube was being tested, with emphasis being placed on mode and frequency purity and the identification of the parameter ranges necessary to produce these desired goals at half beam power.

During the course of the next few months the parts for the new modulator were coming in and the tube had been removed from the experimental area for cavity alterations. The tube had been found to have stray oscillations, giving a broad spectrum of frequencies (8-12 GHz, simultaneously) at several operating points. The rf power of the device was measured calorimetrically to be between 1.5-3 MW at 50 percent final design beam power. Unfortunately, it was at this stage of the experiment that the program was cut. Below is a short description of the final modulator design and a brief summary of the operation of the device before the modified cavity had been installed. A more complete write-up of the 10 GHz systems for WRAMRC can be found in "Design

of a 10 GHz, 10 MW Gyrotron", by M.E. Read and G. Bergeron, NRL Memorandum Report 5629, Nov. 27, 1985.

The Modulator

The conclusion to build a modulator in-house was reached for reasons of economics. A commercially produced system was quoted at around $875,000 by the lowest bidder for a 60 MW, 100 Hz system, and after several iterations, a minimum requirement system was found to be producible internally for around $250,000, including design and construction labor. This did represent a reduction in the average power capability of the system, but WRAMRC had re-examined their needs and found 5 Hz pulse rate satisfactory, as long as a peak power of 5 MW (-3 dB of original specifications) could be guaranteed. The modulator decided upon was a three-section, multiple element line type using a hydrogen thyratron switch and a bi-filar output transformer to achieve the final output pulse. The final modulator design allowed for a repetition rate of approximately 25 Hz with the following parameters:

Modulator Type:	LC Line Discharge
Number of Lines:	3
Pulse Widths:	1,3,10 microseconds
Power:	62.5 MW peak
Voltage:	250 kV peak
Impedance:	1 k-ohm
Current:	250 Amperes peak
Output Transformer turns ratio:	16:1

Tube Operation

The initial operation of the $TE_{1,3}$ device strongly indicated that a final design goal of a 5 MW, at 10 GHz was not only attainable, but could probably be exceeded by at least another 25 percent. This is based on the fact that an input beam power of 31.2 MW yielded output powers to 3 MW, albeit in an impure mode and over a broad spectrum. With a proper redesign of the cavity structure one can assume that

the efficiency and hence, the output power, would improve. Due to the short period of time that was available, no in depth analysis of the the performance of the tube was done. The limited data collected during the period of actual operation is available in Room 212 of Building 51 at NRL.

As a side light, the operation of the device in the original configuration also served to prove that an alternative did exist to buying commercially produced electron guns. The electrostatic design of this gun was done by a JAYCOR employee at NRL, the electrodynamics by Mike Read formerly of NRL, and the mechanical design by JAYCOR and Robert Boesenberg of Litton Industries. The actual assembly was done by JAYCOR and Mr. Boesenberg using Litton facilities. This represented an important milestone in tube development at NRL, (the first fully successful "home brew" hot cathode electron gun) and served in broadening the knowledge base at NRL.

TASK 2: NUMERICAL AND COMPUTATIONAL ANALYSIS FOR THE GYROTRON LABORATORY

JAYCOR's computational efforts have produced codes which are specific to short-pulse gyrotrons and CARMs, and quasi-optical gyrotrons. In addition, codes which are applicable to cyclotron masers in general have been developed. The following is a description of JAYCOR's major contributions in computational analysis for the gyrotron laboratory.

Coupling Coefficient Code

Gyrotrōn coupling coefficients indicate the strength of the interaction between the electron beam and the rf mode. Coupling coefficients are functions of beam position, rf mode and rf mode polarization (right circularly polarized, left circularly polarized or linearly polarized).

Linearly polarized modes are of interest because this polarization is produced when axial slots are used to suppress modes other than $TE_{1,n}$ modes.[1] Since coupling coefficients are inversely proportional to starting current, they are useful for determining optimum beam position and for predicting which modes will be excited.[2]

The gyrotron coupling coefficients are proptional to the square of the effective electric field at the beam. The effective electric field, E_s, is given in Reference 3,[3] for both circularly polarized and linearly polarized transverse electric modes:

$$E_s^{(c)} = \frac{C_{mn}^{(c)} J_{m-s}(k_{mn}R_0)}{r_w} |f_{max}| e^{-im\Xi_0}$$

where $C_{mn}^{(c)} = \{[\pi(x_{mn}^2 - m^2)]^{1/2} J_m(x_{mn})\}^{-1}$ and

$$E_s^{(l)} = C_{mn}^{(l)} \left[\frac{J_{m-s}(k_{mn}R_0)}{r_w} e^{-im\Xi_0} + (-1)^s \frac{J_{m+s}(k_{mn}R_0)}{r_w} e^{im\Xi_0} \right] |f_{max}|$$

where $C_{mn}^{(l)} = \sqrt{2}\{[\pi(x_{mn}^2 - m^2)]^{1/2} J_m(x_{mn})\}^{-1}$.

---

1. Gold, S. H., et al., "High Peak Power K_a-Band Gyrotron Oscillator Experiments with Slotted and Unslotted Cavities," IEEE Transactions on Plasma Science, Vol. 16, pp. 142-148, 1988.

2. Gold, S. H., et al., "High Peak Power K_a-Band Gyrotron Oscillator Experiment," Phys. Fluids, Vol. 30, pp. 2226-2238, 1987.

3. Fliflet, A. W., "Scaling Calculations for a Relativistic Gyrotron", NRL Memorandum Report 5598, 1985.

This gives the coupling coefficients, $H_s \sim (E_s \cdot E_s^*)^{1/2}$ (where * indicates the complex conjugate) for both circularly and linearly polarized modes:

$$H^{+\,2} = \frac{x_{mn}^2 \, J_{m-s}^2(x_{mn} r)}{J_m^2(x_{mn}) \, [\pi(x_{mn}^2 - m^2)]}$$

$$H^{-\,2} = \frac{x_{mn}^2 \, J_{m+s}^2(x_{mn} r)}{J_m^2(x_{mn}) \, [\pi(x_{mn}^2 - m^2)]}$$

$$H^{1\,2} = \frac{(1/2) \, x_{mn}^2 \left[J_{m-s}^2(x_{mn} r) + J_{m+s}^2(x_{mn} r) \right]}{J_m^2(x_{mn}) \, [\pi(x_{mn}^2 - m^2)]}$$

A computer code was written to calculate and plot the coupling coefficient as a function of radius. Figures 1 and 2 are sample output from the code. A listing of the code is given in Appendix A.

Starting Current Codes

The original starting current code was written by K.R. Chu and was based on his linear theory of the electron cyclotron maser.[4] This code assumed a closed right circular cylindrical cavity and scanned over magnetic fields at fixed beam voltage for a specified range of transverse electric modes at fundamental and harmonic frequencies.

A second version of Chu's code scanned over voltages at fixed magnetic field. The functional dependence of beam current and beam alpha on beam voltage must be supplied

---

4. Chu, K. R., "Theory of Electron Cyclotron Maser Interaction in a Cavity at the Harmonic Frequencies", Phys. Fluids, Vol. 21, pp. 2354-2364, 1978.

Figure 1.

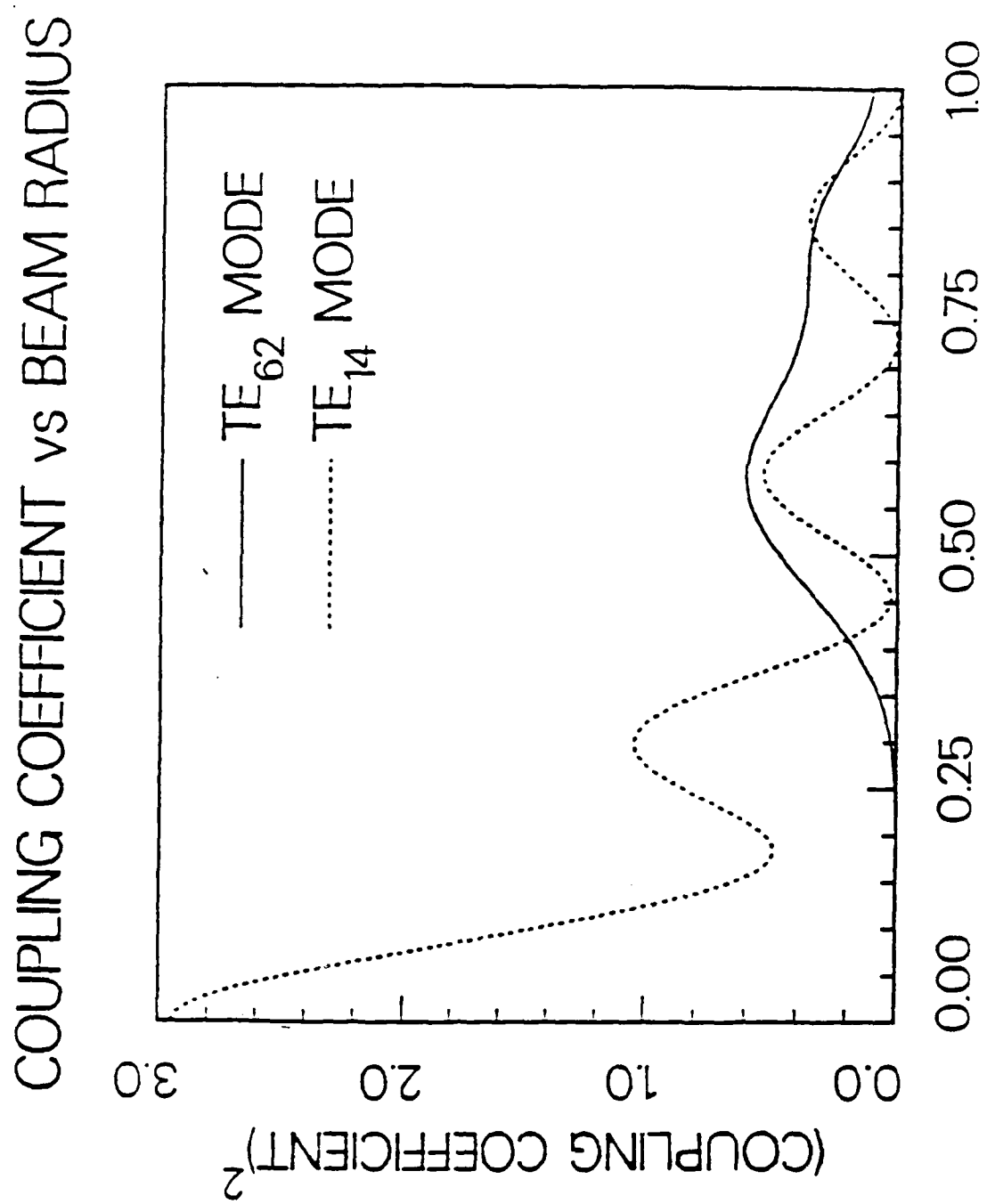
COUPLING COEFFICIENT vs BEAM RADIUS
TE62 MODE
TE14 MODE
(COUPLING COEFFICIENT)2
0.0
1.0
2.0
3.0
0.00
0.25
0.50
0.75
1.00
r/rw

Figure 2.

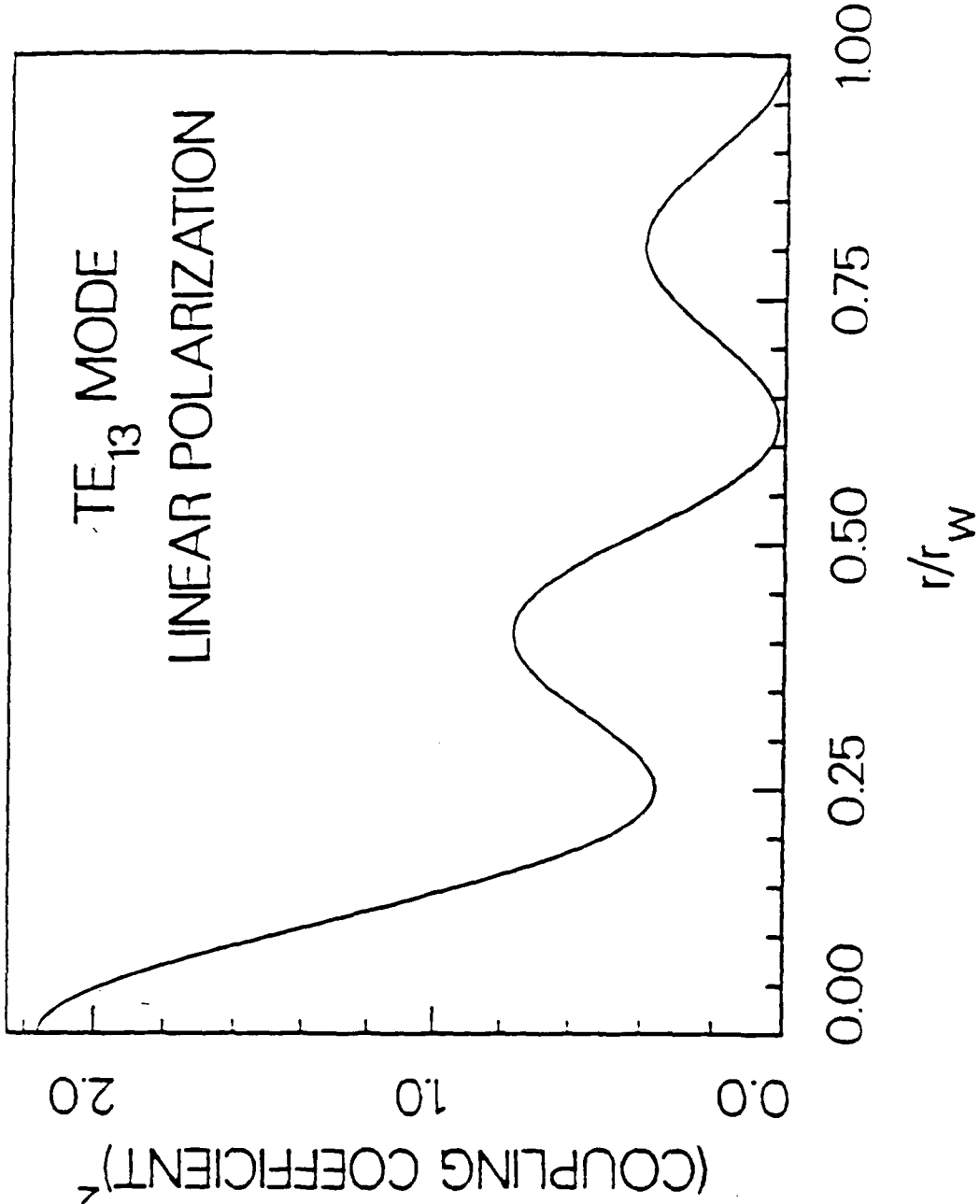
TE13 MODE
LINEAR POLARIZATION
(COUPLING COEFFICIENT)2
0.0
1.0
2.0
0.00
0.25
0.50
0.75
1.00
r/rw

to the code. This version of the code is used for investigating mode excitation as the voltage is increased from zero to peak voltage.

These two original versions of the code generated line printer plots of the starting current map. These codes have been modified to produce vector plots with each starting current curve indexed to its mode number and cyclotron harmonic. This has significantly improved the identification of competing modes.

For gyrotron cavities, a simple analytic formula for diffraction limited quality factor is $Q=(4\pi/l)\cdot(L/\lambda)^2$, where l is the longitudinal mode index, L is the length of the cavity, and λ is the free space wavelength. The Q-factor for each mode scales as $(\omega/l)^2$. Using the formula for diffractive Q, the starting current code was modified to plot current instead of Q times current. Code output relevant to the NRL relativistic gyrotron experiment is given in Figures 3 and 4.

The NRL Cyclotron Auto-Resonance Maser (CARM) experiment features a Bragg reflector cavity. This cavity is characterized by rippled wall sections at both ends. This type of cavity is highly selective with respect to transverse and longitudinal mode indices. Dr. R. McCowan of SAIC has written a code to calculate the eigenfrequencies and Q-factors for Bragg reflector cavities. By interfacing the starting current code with McCowan's Bragg reflector cavity code, the starting current code has been extended to CARMs as well as gyrotrons. A starting current mode map for the NRL CARM is shown in Figure 5. A listing of the CARM starting current code is given in Appendix B.

Cold Cavity Gyrotron Efficiency Code

The cold cavity gyrotron efficiency code is actually composed of two codes. The first part of the code calculates the rf field profile, the Q-factor and resonant fre

Figure 3.

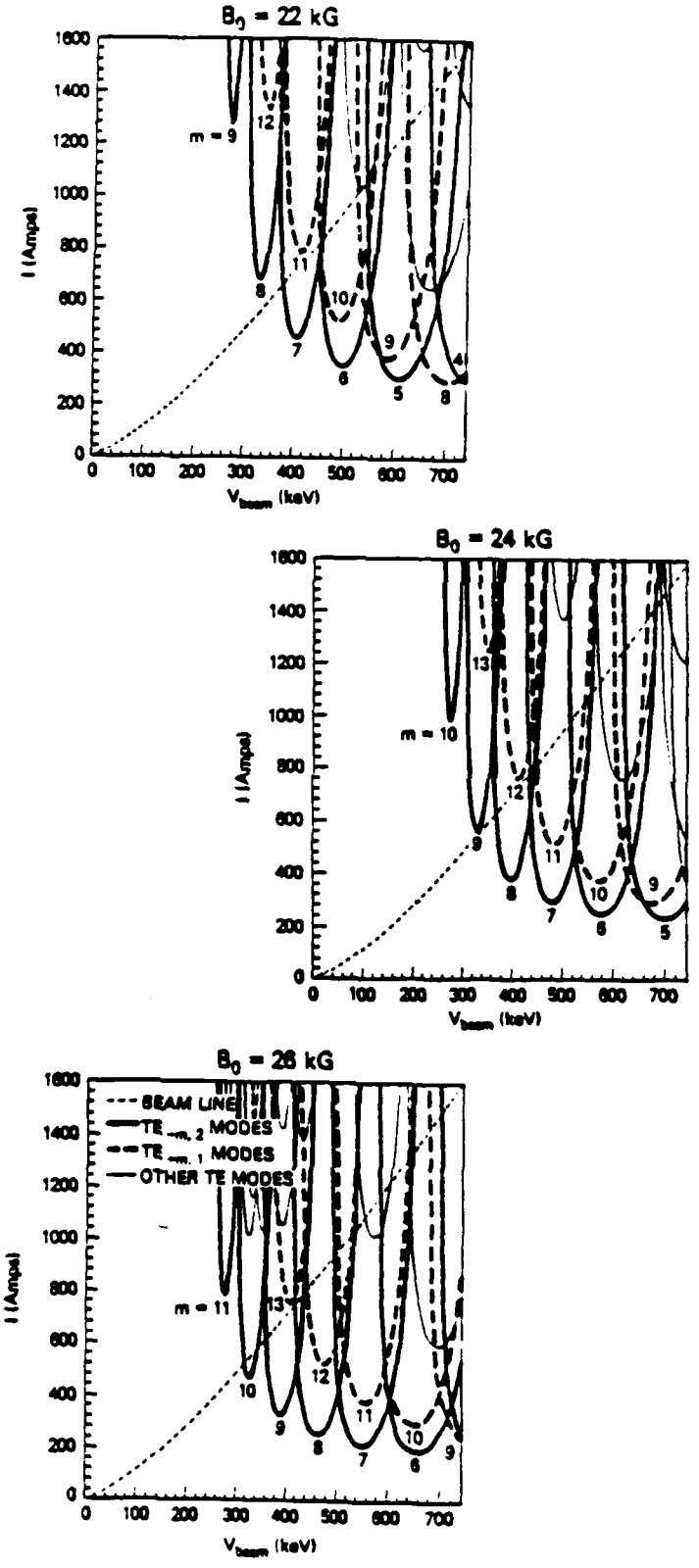
B_0 = 22 kG
m = 9
I (Amps)
V_{beam} (keV)
B_0 = 24 kG
m = 10
I (Amps)
V_{beam} (keV)
B_0 = 26 kG
BEAM LINE
$TE_{-m,2}$ MODES
$TE_{-m,1}$ MODES
OTHER TE MODES
m = 11
I (Amps)
V_{beam} (keV)

Figure 4.

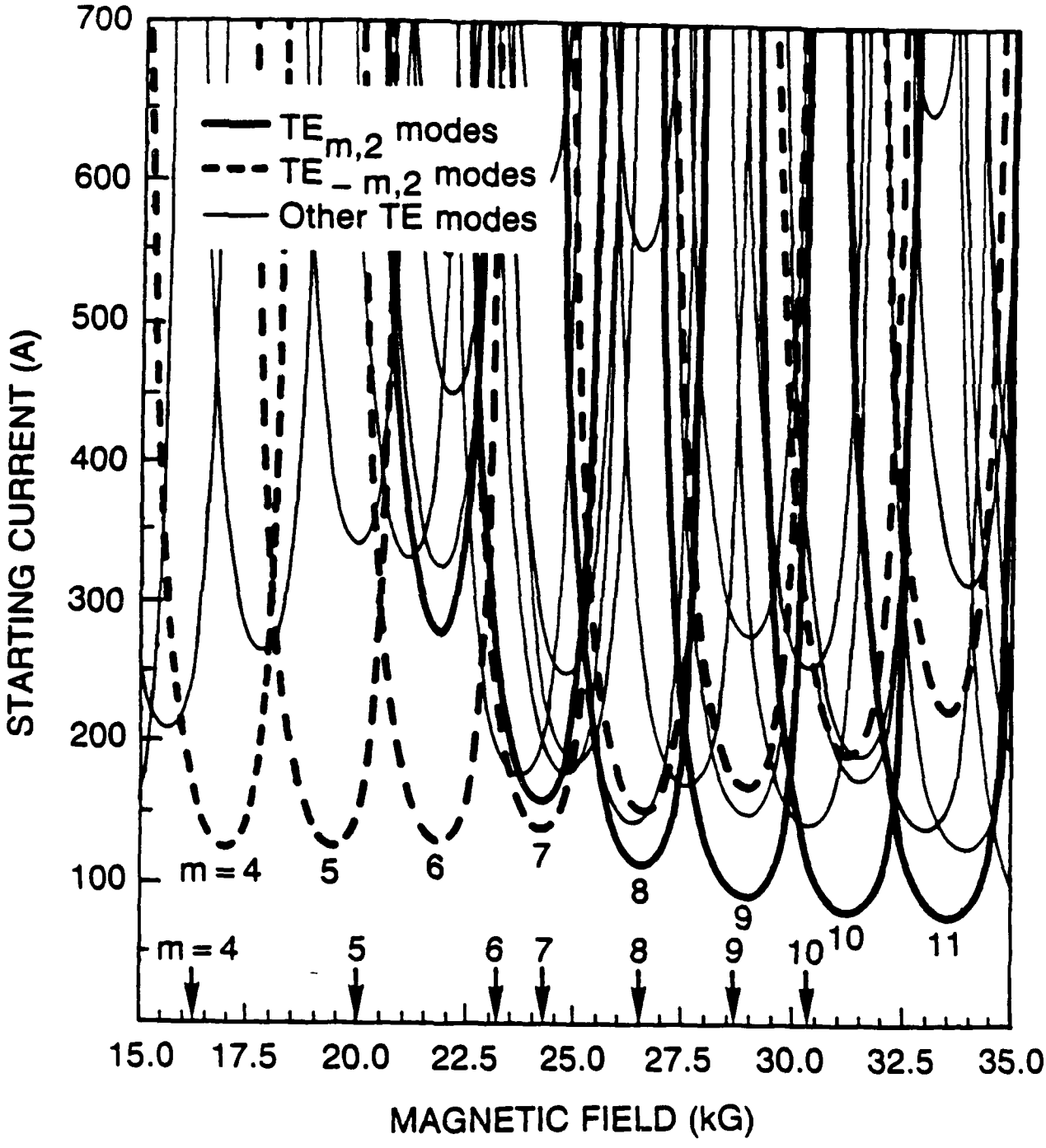
700
600
500
400
300
200
100
STARTING CURRENT (A)
TE m,2 modes
TE - m,2 modes
Other TE modes
m = 4
5
6
7
8
9
10
11
15.0
17.5
20.0
22.5
25.0
27.5
30.0
32.5
35.0
MAGNETIC FIELD (kG)

Figure 5.

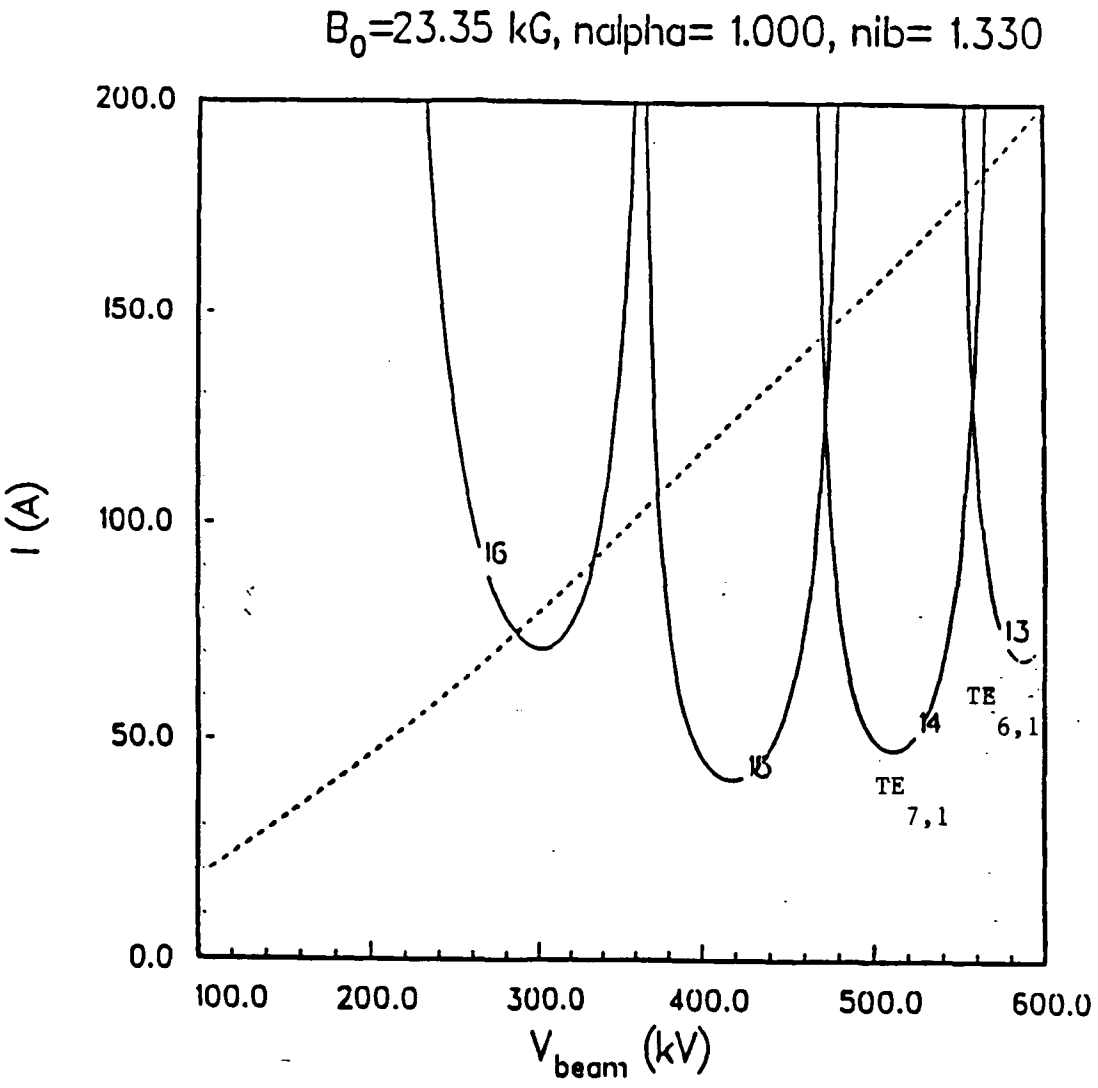
B_0=23.35 kG, nalpha= 1.000, nib= 1.330
200.0
150.0
100.0
50.0
0.0
I (A)
16
15
14
13
TE
7,1
TE
6,1
100.0
200.0
300.0
400.0
500.0
600.0
V_{beam} (kV)

quency in the absence of an electron beam based on weakly irregular waveguide theory.[5] The second part of the code pushes electrons through the cold cavity fields and calculates the energy lost by the electrons. This code has been modified to scan over voltages at fixed magnetic fields (instead of scanning over magnetic fields at fixed voltages). Plots of efficiency versus voltage and current versus voltage at different power levels are generated. The starting current and isopower curves calculated for the NRL $TE_{6,2}$ relativistic gyrotron are shown in Figure 6.

Quasi-Optical Multimode Code

In a quasi-optical gyrotron, the electron beam interacts with the TEM_{mnp} electromagnetic modes of a quasi-optical resonator. Because the diffraction losses for higher order transverse modes are much greater than that of the fundamental transverse mode, transverse mode density is much less than in microwave cavity gyrotrons. However, the number of longitudinal modes which can be excited remains quite high due to the small separation between them. Bondeson has written a code which investigates the time evolution of TEM_{00p} multimoding in a quasi-optical gyrotron.[6]

The basic gyrotron interaction is characterized by five parameters: beam energy, alpha, interaction length, applied magnetic field and the amplitude of the rf electric field at the electron beam. The inputs to the multimode

---

5. Fliflet, A.W. and Read, M.E., "Use of Weakly Irregular Waveguide Theory to Calculate Eigenfrequencies, Q Values, and RF Field Functions for Gyrotron Oscillators", Int. J Electronics, Vol. 51, pp. 475-484, 1981.

6. Bondeson, A., Manheimer, W.M., and Ott, E., "Multimode Analysis of Quasi-Optical Gyrotrons and Gyroklystrons", Int. J. Infrared Millimeter Waves, Vol. 9, pp. 309-339, 1983.

Figure 6.

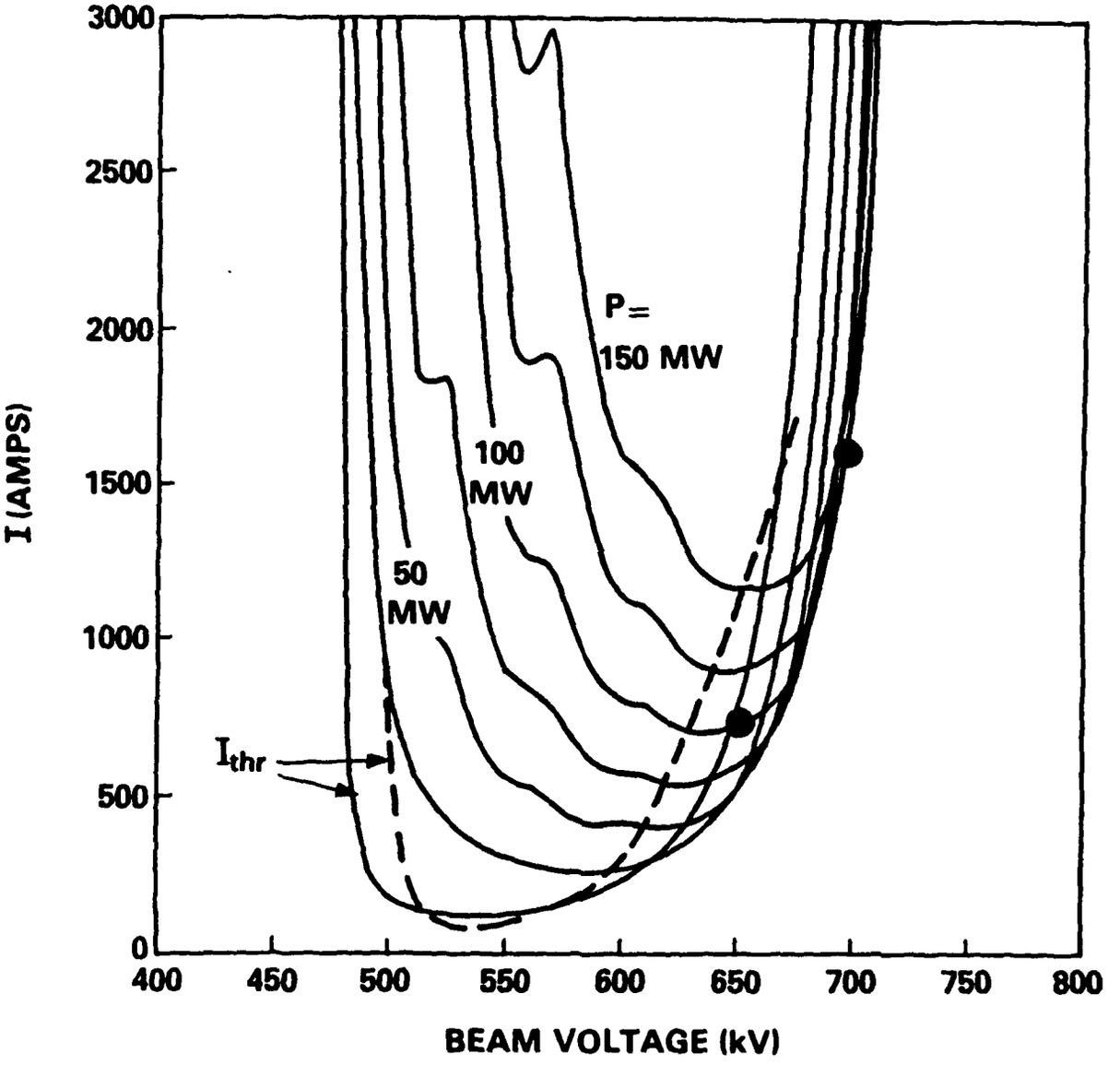
3000
2500
2000
1500
1000
500
0
I (AMPS)
400
450
500
550
600
650
700
750
800
BEAM VOLTAGE (kV)
P=
150 MW
100
MW
50
MW
I_{thr}

code consist entirely of normalized parameters. Electron beam energy is specified by the relativistic factor γ. Interaction length is given by the normalized parameter $on \equiv \omega r_0/c = 2\pi(r_0/\lambda)$, analogous to the conventional gyrotron parameter, L/λ. Beam alpha is specified by the pitch angle, $a \equiv \tan^{-1}(\alpha)$. The rf electric field amplitude is calculated self-consistently by the multimode code. However, the code must be provided with some knowledge of the losses in the cavity and the current which is driving the interaction. This is specified in the combined normalized parameter, $eff \equiv \eta/E^2$, where E is the normalized electric field amplitude and η is the electronic efficiency. The normalized parameter, eff, can be related to the Q-factor, the current and mirror separation through the usual power balance relation, $\eta IV = \omega W/Q$, and the expression for stored energy in a quasi-optical cavity whose mirrors are separated by a distance, d, $W = (1/8)\pi\varepsilon_0 E_0^2 r_0^2 d$:

$$EFF = \frac{\eta}{\hat{E}_0^2} = \frac{1}{8} \frac{\varepsilon_0 mc^2}{e} \frac{\omega}{\gamma_0 - 1} \frac{1}{(QI/d)} ,$$

$$\hat{E}_0 = \frac{\sqrt{\pi}\, eE_0 r_0}{mc^2} .$$

A new graphics post-processing routine which plots the square of the amplitude of modes versus time was developed. This routine is particularly useful for displaying the time at which a steady state has been attained. The routine for plotting bar graphs of mode amplitude versus mode number has been modified to plot the square of the mode amplitude versus detuning. The listings for these two codes are given in Appendices C and D. The normalization for time is:

$$t_0 = \hat{t}_0 \frac{1}{2\mu_0(e/m)} \frac{d}{I}$$

$$= \hat{t}_0 \frac{Q(\gamma_0-1)(eff)}{f} \cdot (6.365 \times 10^5)\ \mu sec$$

Results for a multimode computer run corresponding to the NRL Quasi-Optical experiment with the Seftor gun are shown in Figures 7a-d. This run assumed a flat magnetic field of 5 Tesla, a beam voltage of 75 kV and a mirror separation of 20 cm.

Time-Dependent Code for Free-Running and Phase-Locked Oscillators

A time-dependent code based on the time-dependent slow-time-scale theory of A. W. Fliflet was developed.[7] This code will be particularly useful for the investigation of gyrotrons and phase-locked gyrotrons which are driven by short-pulse relativistic electron beams. The code is capable of modelling the effect of a voltage ripple and the effect of a phase-locking signal in the form of a prebunched beam.

Results for the free-running oscillator corresponding to the NRL relativistic gyrotron are shown in Figure 8. The parameters of the experiment are taken to be:

Mode	$TE_{-6,2}$
Peak voltage	650 kV
Peak current	1.5 kA, $\sim V^{1.33}$
Beam guiding center radius	1.16 cm

7. Fliflet, A.W., Lee, R.C., Manheimer, W.M., and Ott, E., "Time-Dependent Slow-Time-Scale Theory of Free-Running and Phase-Locked Gyrotron Oscillators", NRL Memorandum Report 6064, 1988.

Figure 7a.

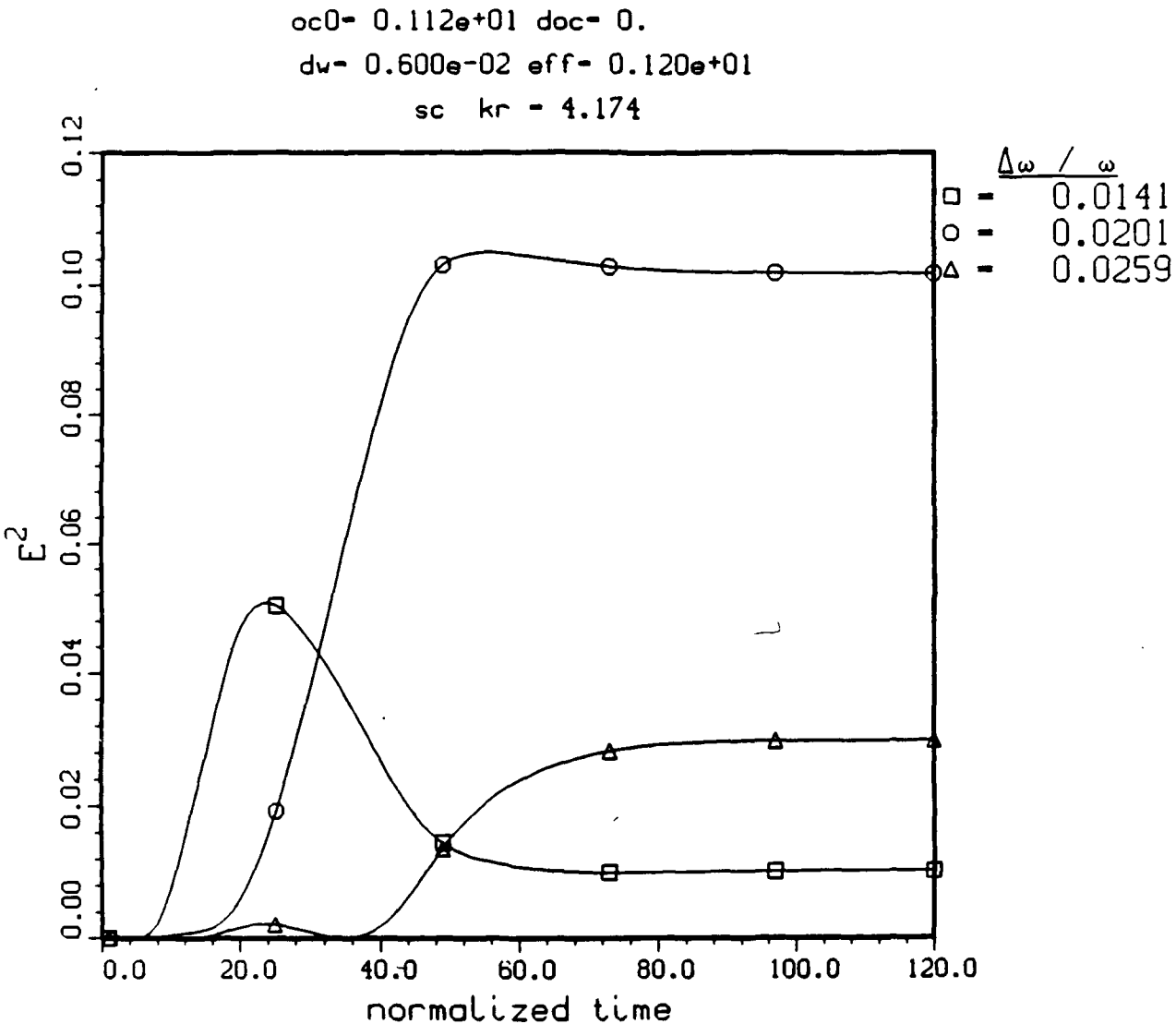
oc0= 0.112e+01 doc= 0.
dw= 0.600e-02 eff= 0.120e+01
sc kr = 4.174
Δω / ω
□ = 0.0141
○ = 0.0201
△ = 0.0259
E²
0.00
0.02
0.04
0.06
0.08
0.10
0.12
0.0
20.0
40.0
60.0
80.0
100.0
120.0
normalized time

Figure 7b.

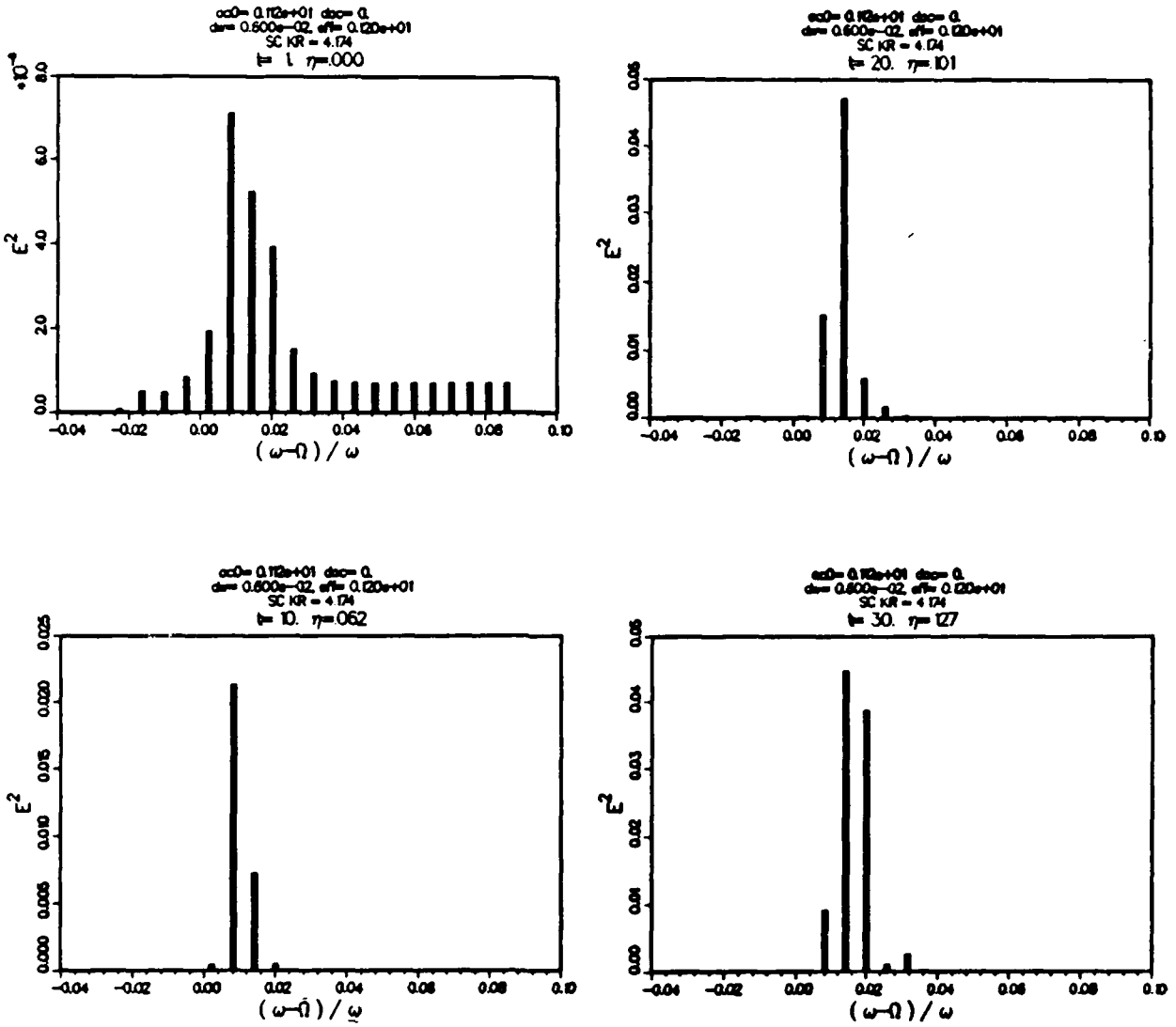

Figure 7c.

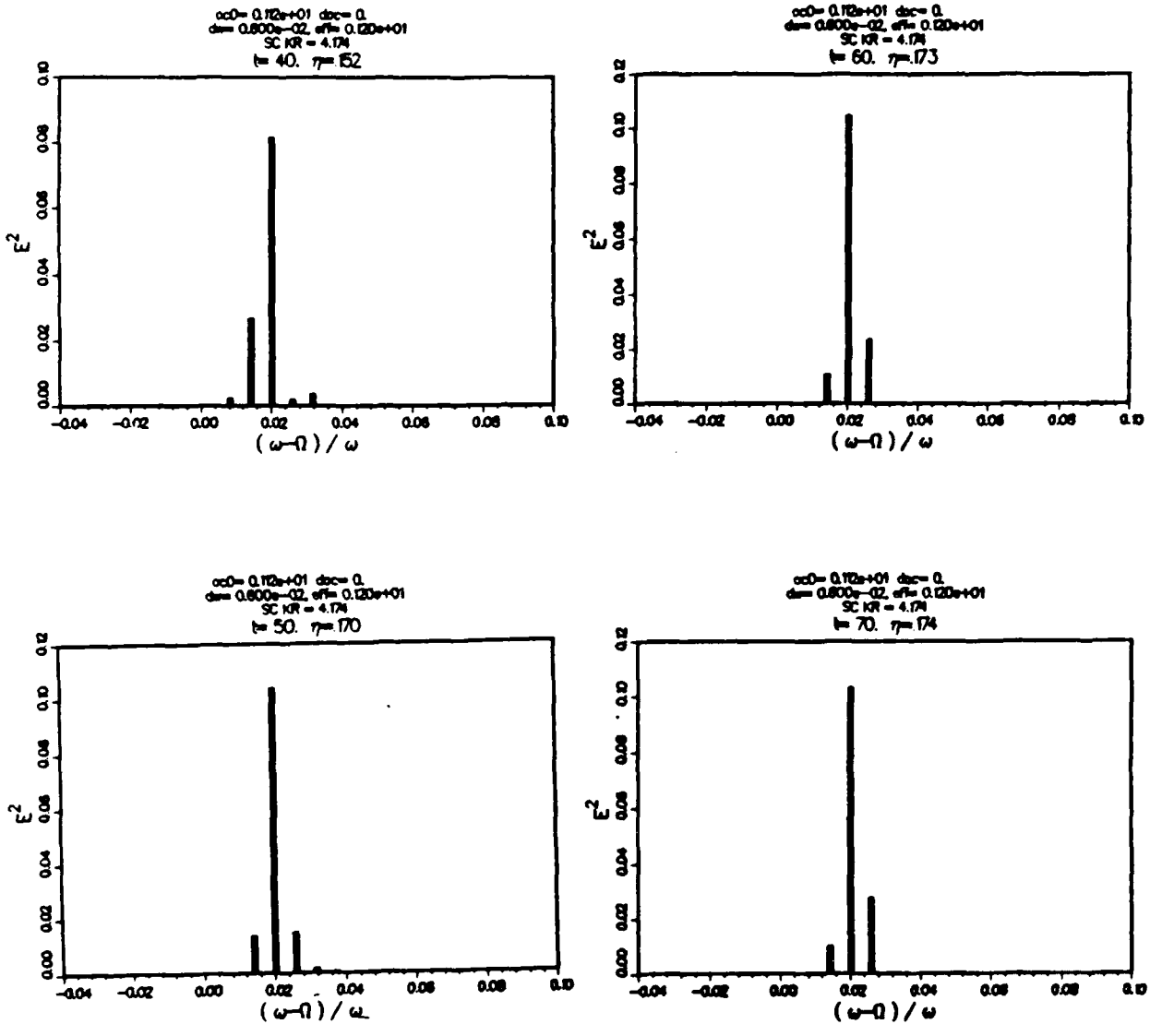
ωc0= 0.172e+01 dωc= 0.
dω= 0.600e-02, eff= 0.120e+01
SC KR = 4.174
t= 40. η= 152
t= 60. η=.173
t= 50. η=170
t= 70. η=174
ε²
(ω-Ω) / ω

Figure 7d.

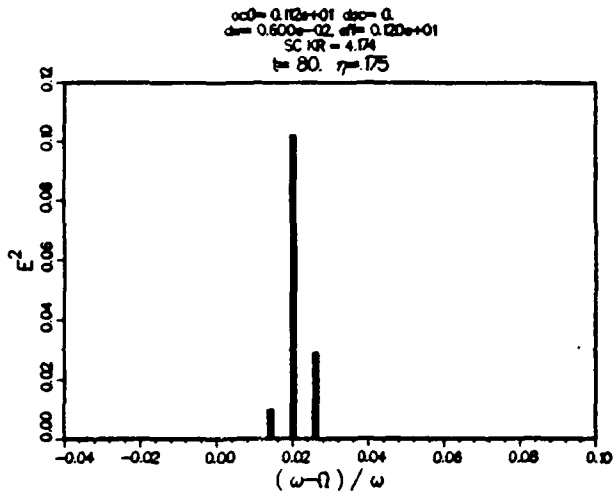
oc0= 0.112e+01 dsc= 0.
dx= 0.600e-02, eff= 0.120e+01
SC KR = 4.174
t= 80. η=.175
E²
0.00
0.02
0.04
0.06
0.08
0.10
0.12
-0.04
-0.02
0.00
0.02
0.04
0.06
0.08
0.10
(ω-Ω) / ω

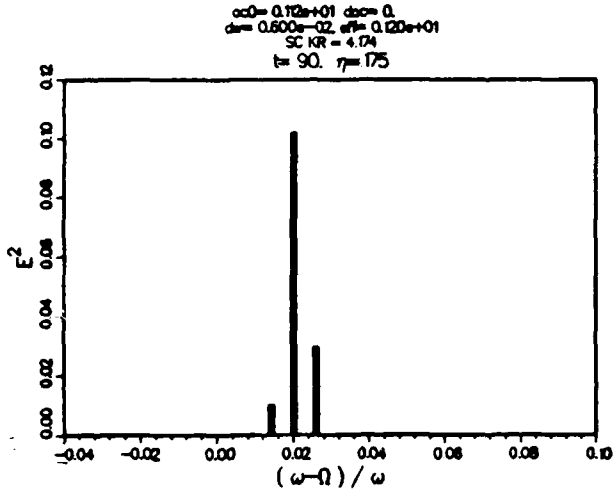
oc0= 0.112e+01 dsc= 0.
dx= 0.600e-02, eff= 0.120e+01
SC KR = 4.174
t= 90. η=.175
E²
0.00
0.02
0.04
0.06
0.08
0.10
0.12
-0.04
-0.02
0.00
0.02
0.04
0.06
0.08
0.10
(ω-Ω) / ω

Figure 8.

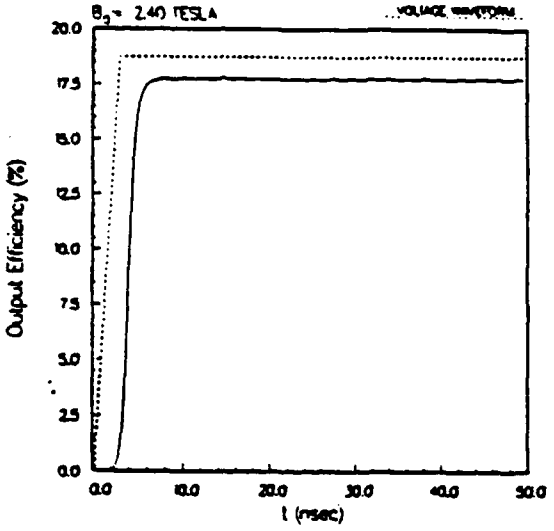
B_0 = 2.40 TESLA
VOLTAGE WAVEFORM
Output Efficiency (%)
20.0
17.5
15.0
12.5
10.0
7.5
5.0
2.5
0.0
0.0
10.0
20.0
30.0
40.0
50.0
t (nsec)

(a)

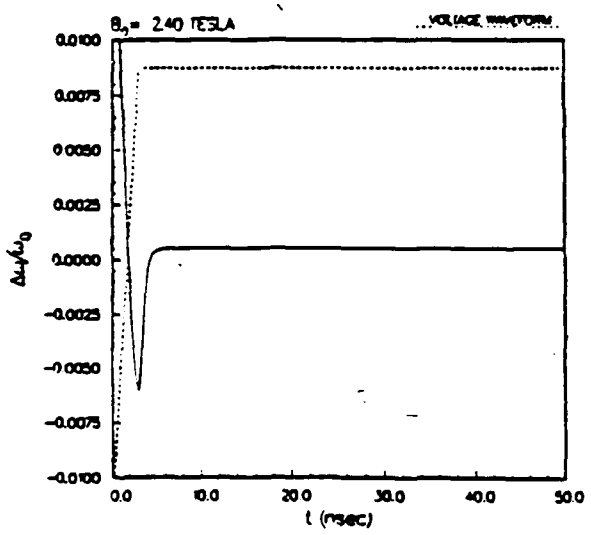
B_0 = 2.40 TESLA
VOLTAGE WAVEFORM
$\Delta\omega/\omega_0$
0.0100
0.0075
0.0050
0.0025
0.0000
-0.0025
-0.0050
-0.0075
-0.0100
0.0
10.0
20.0
30.0
40.0
50.0
t (nsec)

(b)

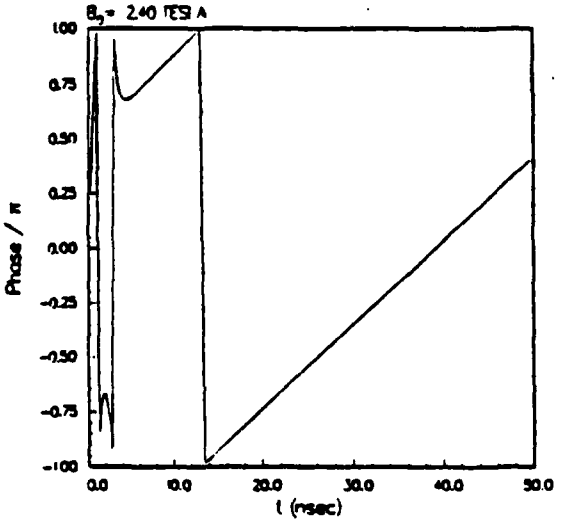
B_0 = 2.40 TESLA
Phase / π
1.00
0.75
0.50
0.25
0.00
-0.25
-0.50
-0.75
-1.00
0.0
10.0
20.0
30.0
40.0
50.0
t (nsec)

(c)

RF field profile	sinusoidal
$\alpha \equiv v_t/v_z$	1.0, $\sim v^{1.33}$
Q	250
Applied magnetic field	2.4 Tesla
Voltage pulse	50 nsec, 3 nsec rise from 75 percent peak to peak

Figure 8 shows the electronic efficiency, operating frequency, and rf phase of the oscillator plotted as a function of time. They indicate that steady-state operation is achieved after ~ 8 nsec.

Results for an oscillator driven by a prebunched beam are shown in Figure 9. The phase-locked condition is indicated by the vanishing frequency shift and the constant rf phase. The plots show that phase-locked operation is obtained after 30 nsec into the voltage pulse.

TASK 3: Technical Efforts for the Pulsed Power Microwave Experiment

Gyrotron oscillators employing thermionic cathode technology have proved to be highly efficient, exceptionally high average power millimeter-wave sources.[8] Operating at moderate currents and voltages (typically, $\leq$ 50 A at $\leq$ 100 keV), they have demonstrated 100s of kW of average power at efficiencies approaching 50 percent.[9] However, some future applications of millimeter-wave radiation may require substantially higher peak power levels than have been demonstrated using conventional thermionic microwave tube technologies. This will require the application of much higher

---

8. V.L. Granatstein, Int. J. Electron., 57, 787 (1984).

9. K. Felch, R. Bier, L. Fox, H. Huey, L. Ives, H. Jory, N. Lopez, J. Manca, J. Shively, and S. Spang; Int. J. Electron.; 57; 815 (1984).

Figure 9.

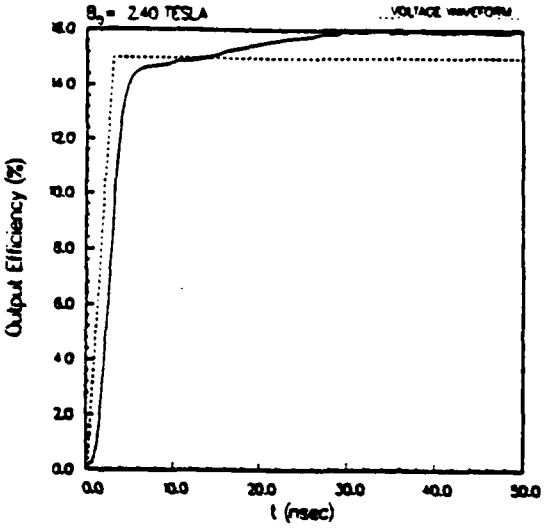
B_0 = 2.40 TESLA
...VOLTAGE WAVEFORM
Output Efficiency (%)
t (nsec)

(a)

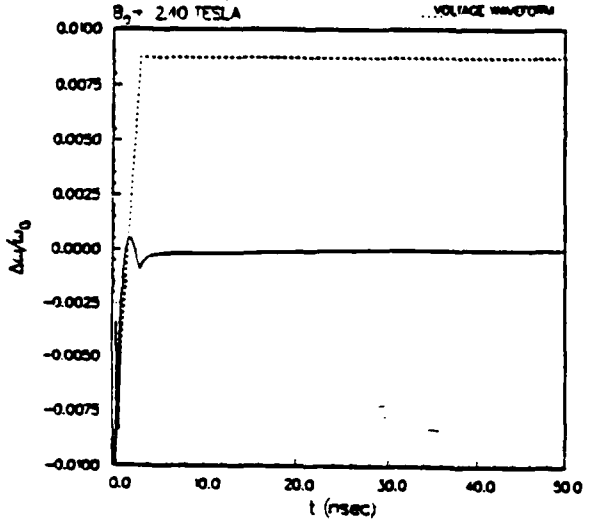
B_0 = 2.40 TESLA
...VOLTAGE WAVEFORM
$\Delta\omega/\omega_0$
t (nsec)

(b)

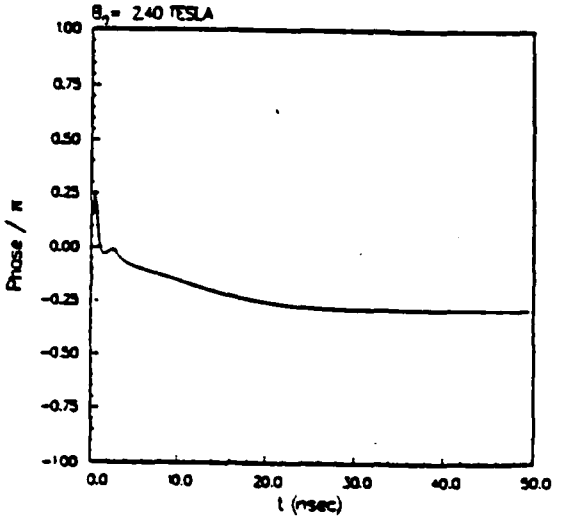
B_0 = 2.40 TESLA
Phase / π
t (nsec)

(c)

beam powers, requiring the use of both higher voltages and currents. In light of these considerations, a research program was initiated to investigate the potential of gyrotron oscillators driven by substantially higher currents and voltages from high voltage pulseline accelerators driving plasma-induced field emission cathodes.

Studies of the gyrotron interaction using pulseline accelerators at NRL have been in progress for years. Some of the recent studies have centered on "whispering-gallery" mode gyrotrons (i.e., TE^{o}_{mn} modes with m>>n) which have good features for very high peak power generation of millimeter waves. The whispering-gallery gyrotrons interact preferentially with annular electron beams of large radius and have superior mode stability.

A previous paper[10] reported the production of 20 nsec pulses with 20 MW peak power at 35 GHz and 8 percent efficiency in a $TE_{6,2}$ mode from a gyrotron oscillator operating at 350 kV and employing currents in the range of 0.5 to 1 kA. This result was produced by a 600 kV Febetron capable of providing 6 kA of current into a matched 100 Ω load.

The most recent paper[11] reported results with an even higher output power. The pulsed power for this study was provided by a "single-shot" 775 kV Febetron with a 55 nsec pulse duration, where the electron beam was drawn from a cold cathode by plasma-induced field emission. The electrons are subsequently given a substantial increase in their transverse momentum by passing through a nonadiabatic dip in

---

10. S.H. Gold, A.W. Fliflet, W.M. Manheimer, W.M. Black, V.L. Granatstein, A.K. Kinkead, D.L. Hardesty, and M. Sucy; IEEE Trans. Plasma Sci.; PS-13; 374 (1985).

11. S.H. Gold, A.W. Fliflet, W.M. Manheimer, R.B. McCowan, W.M. Black, R.C. Lee, V.L. Granatstein, A.K. Kinkead, D.L. Hardesty, and M. Sucy; NRL Memorandum Report 5923 (1987).

magnetic field produced by a pump magnetic coil. Transverse momentum is then further increased between the pump magnet and the gyrotron cavity by adiabatic compression. The experimental configuration is sketched in Figure 10. At 35 GHz, approximately 100 MW of output power was produced in the $TE_{6,2}$ mode with magnetic field in the cavity set at 24.4 kG. This power level corresponds to an efficiency of 8 percent based on a current of 1.6 kA flowing through the gyrotron cavity. By tuning the cavity magnetic field, it proved possible to achieve a stepwise frequency tuning ability with the gyrotron operating at high power in a family of $TE_{m,2}$ modes. Stepwise tuning ability was achieved over a frequency range of 28 to 49 GHz.

The short term goals, Phase I, are to set up the experiment as in the previous studies with two important differences: the Febetron will be fitted with long pulse (~ 250 nsec) modules to produce long pulse microwaves at approximately 100 MW at 8 percent efficiency and to design, fabricate and install a new diode that will function properly under this longer electron beam pulse length. The long term goals, Phase II, are to repetitively pulse the Febetron at 10 Hz for two seconds. This will require direct current magnets (possible superconducting or battery powered) instead of the pulsed magnets. Another new diode may have to be designed for the repetitively-pulsed study. This diode will have to function properly under a long pulse length and at a repetition rate. The experiment is also being configured for mobility as the final goal is to have a mobile repetitively-pulsed system.

This report will describe the progress made in Phase I: the diode design, the microwave circuit and gyrotron tube assembly, the long pulse Febetron, the magnets and capacitor banks for the experiment, and general laboratory equipment.

Figure 10.

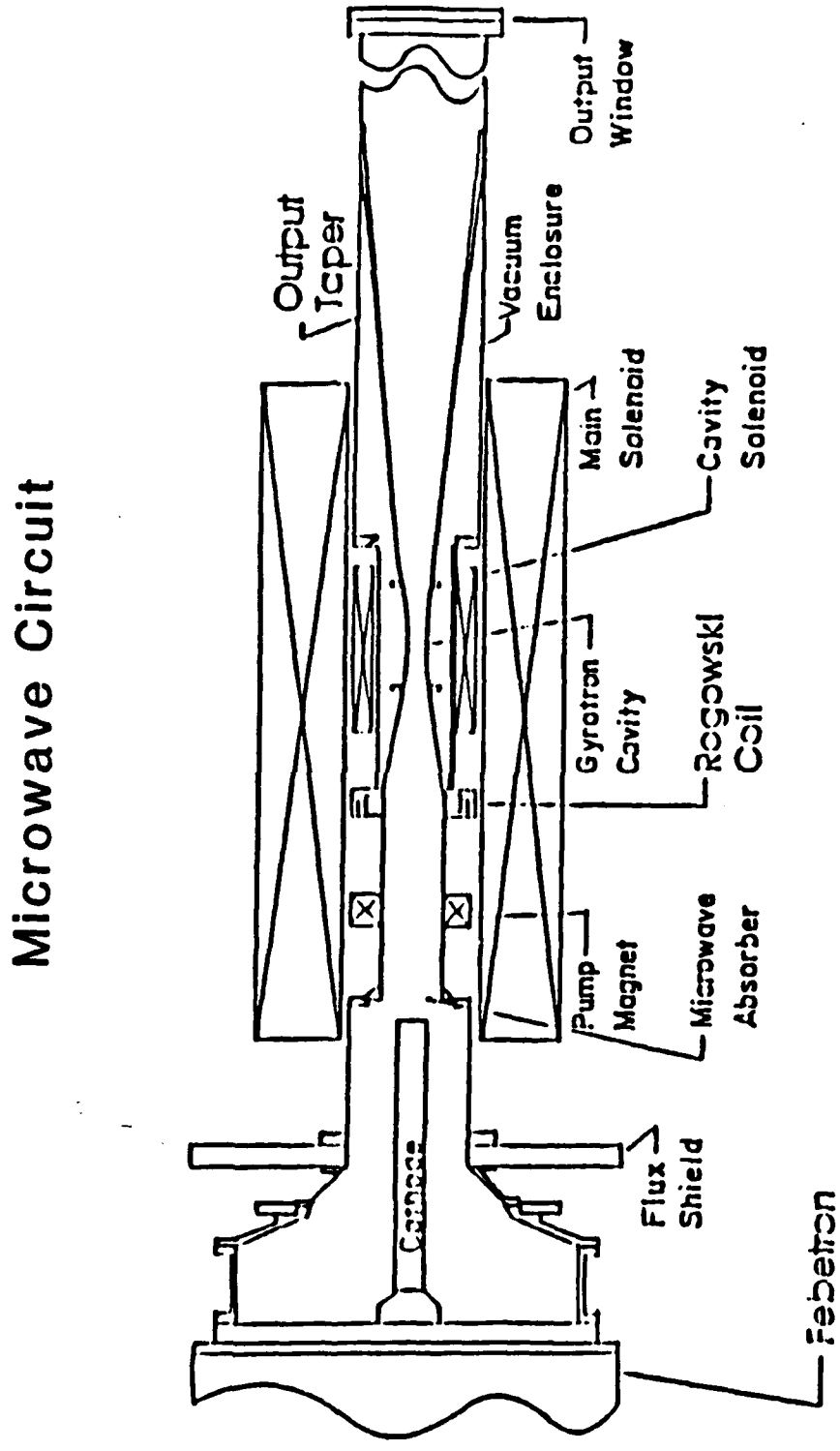
Microwave Circuit
Output Taper
Vacuum Enclosure
Output Window
Main Solenoid
Cavity Solenoid
Gyrotron Cavity
Rogowski Coil
Pump Magnet
Microwave Absorber
Flux Shield
Cathode
Febetron

Design

A new diode has been designed for the Febetron (Figure 11). This diode design was completed by using the NRL Potential Computing and Plotting Program for Axially Symmetric and Two Dimensional Configurations including Different Dielectrics and Floating Electrodes Code, developed by John Shipman at NRL. This code was especially useful since the diode is designed using materials with different dielectrics and floating electrodes. A few of the input parameters include the number of floating electrodes and their position, the dielectric constants of the dielectrics and their position and a voltage of 1 MeV between the highest voltage electrode and the lowest voltage electrode.

Figure 12 shows the results of the code for our diode design by plotting equipotential electrostatic field lines across the diode. Each line represents a five percent step in voltage. As can be seen, the field lines are spaced quite evenly across the floating electrode region of the diode.

The capacitor banks were designed; each bank having a specified capacitance and voltage. These parameters were determined by a computer code, developed by Murray Black of NRL, that calculated the necessary capacitances and voltages for the banks to generate the required fields for the main, trim and kicker magnets while maintaining a minimum thermal gradient across the magnets (Tables 1-5).

Figures 13 and 14 show the results of a computer code, also developed by Murray Black at NRL, that plots the radial magnetic field (B_R) and the axial magnetic field (B_Z) versus distance from the cathode for a given magnet design. The trim magnet is shown in Figure 13. Note that the trim field is very flat around the region of the cavity and gradually falls off away from the cavity region. The main magnet is shown in Figure 14. This field needs to be flat to

Figure 11.

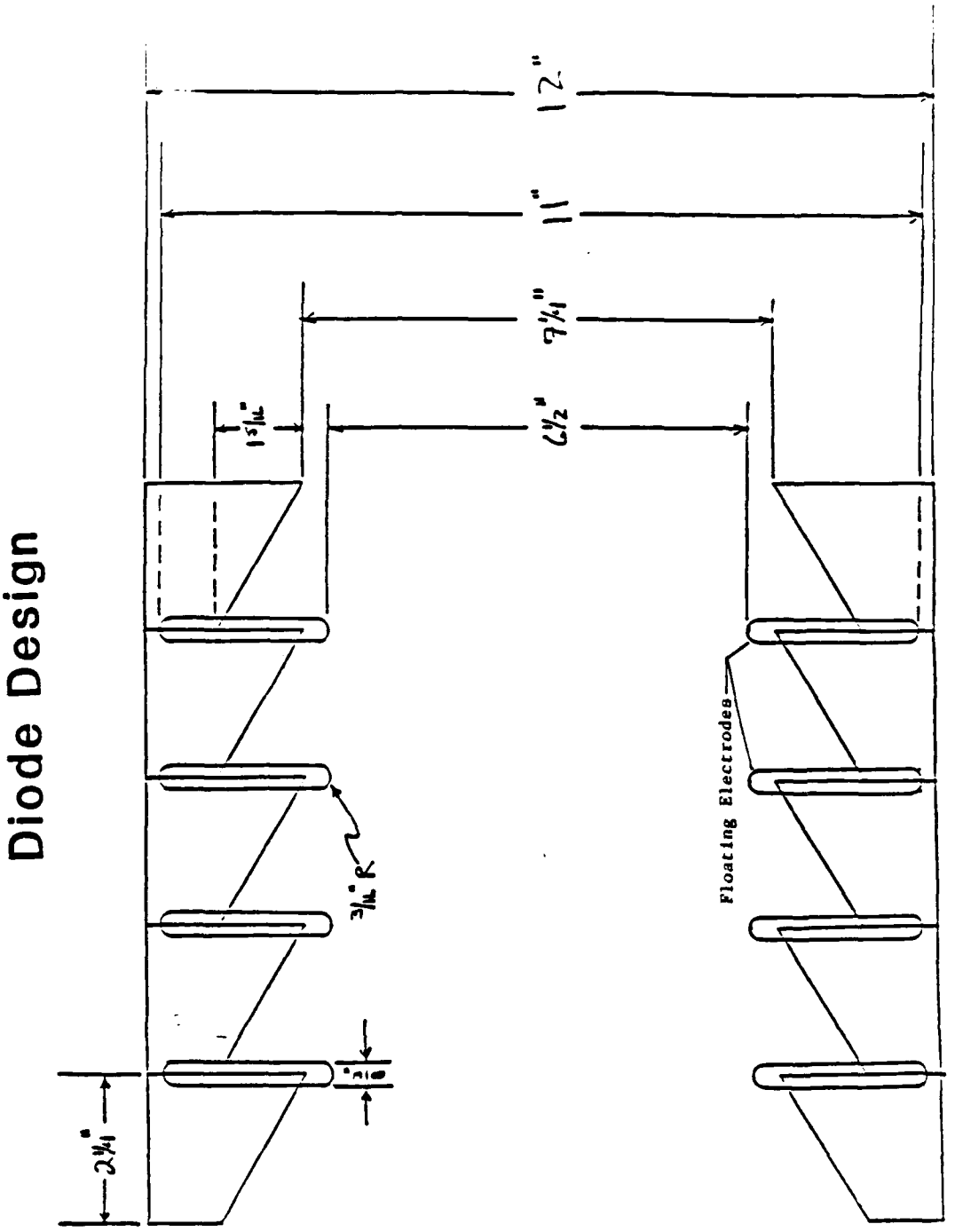

Figure 12.

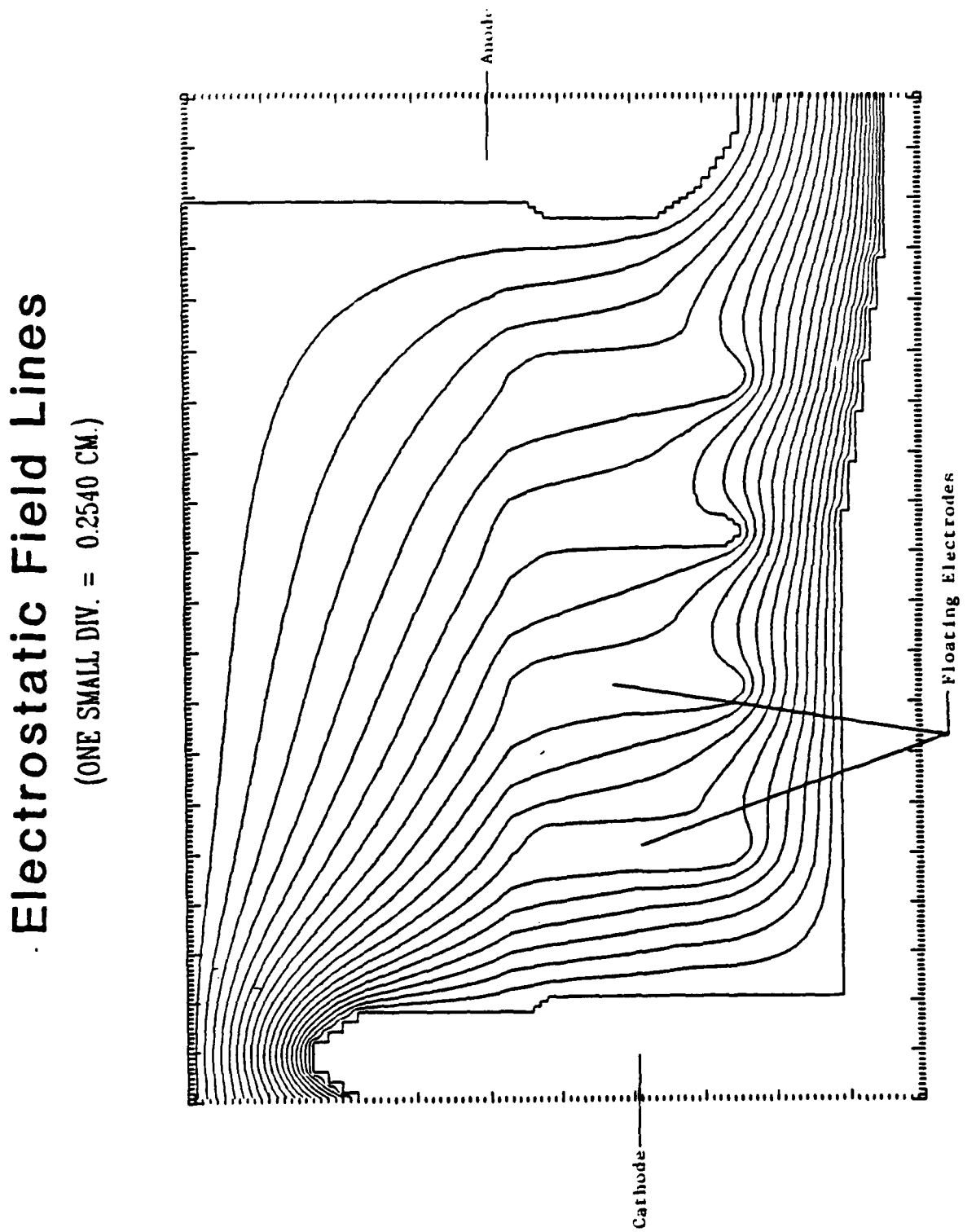
Electrostatic Field Lines
(ONE SMALL DIV. = 0.2540 CM.)
Anode
Floating Electrodes
Cathode

Table 1.

THE MAIN MAGNET

Pancake coils
Coil inside radius = 3.1 inches
Max. field strength = 10.0 kG
Total capacitance = 1060.0 microfarads
Spacer width between coils = 1.10 inches
At each end, 2 pancakes are adjacent (no spacer)

coils	turns	time max	i max (kA)	r	l	kV(0)	alpha	beta	theta
8	400	0.561E-02	0.955	0.13E+00	0.12E-01	3.35	1.89	2.66	0.97E-08
9	450	0.610E-02	0.944	0.14E+00	0.15E-01	3.61	1.89	3.04	0.91E-08
10	500	0.654E-02	0.936	0.16E+00	0.17E-01	3.84	1.89	3.42	0.85E-08
11	550	0.691E-02	0.931	0.18E+00	0.19E-01	4.05	1.89	3.80	0.78E-08
12	600	0.723E-02	0.928	0.19E+00	0.21E-01	4.23	1.89	4.17	0.72E-08
→13	650	0.748E-02	0.926	0.21E+00	0.22E-01	4.37	1.89	4.55	0.66E-08
14	700	0.765E-02	0.925	0.23E+00	0.23E-01	4.48	1.89	4.93	0.60E-08
15	750	0.823E-02	0.924	0.24E+00	0.27E-01	4.81	1.89	5.30	0.60E-08
16	800	0.878E-02	0.924	0.26E+00	0.30E-01	5.13	1.89	5.68	0.60E-08
17	850	0.933E-02	0.924	0.27E+00	0.34E-01	5.45	1.89	6.06	0.60E-08
18	900	0.988E-02	0.924	0.29E+00	0.38E-01	5.77	1.89	6.44	0.60E-08
19	950	0.104E-01	0.924	0.31E+00	0.43E-01	6.10	1.89	6.81	0.60E-08
20	1000	0.110E-01	0.924	0.32E+00	0.47E-01	6.42	1.89	7.19	0.60E-08

Table 2.

THE MAIN MAGNET

Pancake coils
Coil inside radius = 3.1 inches
Max. field strength = 18.0 kG
Total capacitance = 1060.0 microfarads
Spacer width between coils = 1.25 inches
At each end, 2 pancakes are adjacent (no spacer)

coils	turns	time max	i max (kA)	r	l	kV(0)	alpha	beta	theta
8	400	0.564E-02	1.692	0.13E+00	0.12E-01	5.97	1.89	2.61	0.98E-08
9	450	0.612E-02	1.684	0.14E+00	0.15E-01	6.46	1.89	3.01	0.92E-08
10	500	0.654E-02	1.682	0.16E+00	0.17E-01	6.90	1.89	3.41	0.85E-08
11	550	0.690E-02	1.682	0.18E+00	0.19E-01	7.30	1.89	3.81	0.78E-08
12	600	0.719E-02	1.685	0.19E+00	0.20E-01	7.64	1.89	4.21	0.71E-08
→13	650	0.741E-02	1.688	0.21E+00	0.22E-01	7.91	1.89	4.61	0.65E-08
14	700	0.768E-02	1.692	0.23E+00	0.23E-01	8.23	1.89	5.02	0.60E-08
15	750	0.823E-02	1.696	0.27E+00	0.27E-01	8.83	1.89	5.42	0.60E-08
16	800	0.878E-02	1.700	0.26E+00	0.30E-01	9.45	1.89	5.82	0.60E-08
17	850	0.933E-02	1.704	0.27E+00	0.34E-01	10.06	1.89	6.22	0.60E-08
18	900	0.988E-02	1.708	0.29E+00	0.38E-01	10.68	1.89	6.62	0.60E-08
19	950	0.104E-01	1.712	0.31E+00	0.43E-01	11.29	1.89	7.02	0.60E-08
20	1000	0.110E-01	1.715	0.32E+00	0.47E-01	11.91	1.891	7.42	0.60E-08

Table 3.

THE TRIM MAGNET

Coil wire restivity = 0.18E-05 ohm-cm
Coil wire type = AWG 10 Magnet Wire
Coil length = 25.237 cm
Coil inside radius = 4.60 cm
Max. field strength = 10.0 kG
Total capacitance = 500.0 microfarads
Wall thickness = 0.1250 inches
Penetration time = 0.12E-03 sec.
Number of beams = 1
Connection of multiple beams = not applicable
Turns lie in grooves of lower layer

layers	turns	outrad (cm)	time max I (msec)	max I (kA)	ind. (mH)	r r (temp)	kV(0) kV(0) (temp)	temp chng (deg C) alpha	stress (kg/cm2) beta	length (ft) theta
1	92	4.87	0.55 0.55	2.33	0.26	0.09 0.09	1.86 1.86	1.75 1.06	207.3 2.74	90.0 0.67E-08
2	184	5.11	1.11 1.11	1.17	1.08	0.19 0.19	1.90 1.90	0.89 1.11	104.0 2.74	184.4 0.69E-08
→ 3	276	5.35	1.69 1.69	0.78	2.51	0.29 0.30	1.93 1.93	0.60 1.16	69.6 2.74	283.4 0.72E-08
4	368	5.59	2.28 2.28	0.59	4.58	0.40 0.40	1.97 1.97	0.45 1.21	52.3 2.74	386.9 0.74E-08
5	460	5.82	2.89 2.28	0.47	7.36	0.51 0.52	2.01 2.01	0.37 1.27	42.0 2.74	494.9 0.78E-08
6	552	6.06	3.52 3.52	0.40	10.89	0.63 0.63	2.04 2.04	0.31 1.32	35.1 2.74	607.5 0.78E-08
7	644	6.30	4.15 4.15	0.34	15.22	0.75 0.75	2.08 2.08	0.27 1.37	30.2 2.74	724.5 0.80E-08
8	736	6.54	4.81 4.81	0.30	20.39	0.88 0.88	2.11 2.11	0.24 1.42	26.5 2.74	846.0 0.82E-08
9	828	6.77	5.47 5.47	0.27	26.46	1.01 1.01	2.15 2.15	0.22 1.47	23.7 2.74	972.1 0.84E-08
10	920	7.01	6.15 6.15	0.24	33.47	1.15 1.15	2.19 2.19	0.20 1.52	21.4 2.74	1102.7 0.86E-08

Table 4.

THE TRIM MAGNET

Coil wire resistivity = 0.18E-05 ohm-cm
Coil wire type - AWG 10 Magnet Wire
Coil length = 25.237 cm
Coil inside radius = 4.70 cm
Max. field strength = 18.0 kG
Total capacitance = 500.0 microfarads
Wall thickness = 0.1250 inches
Penetration time = 0.12 msec
Number of beams = 1
Connection of multiple beams = not applicable
Turns lie in grooves of lower layer

layers	turns	outrad (cm)	time max I (msec)	max I (kA)	ind. (mH)	r r (temp)	kV(0) kV(0) (temp)	temp chng (deg C) alpha	stress (kg/cm2) beta	length (ft) theta
1	92	4.97	0.55 0.55	4.21	0.27	0.10 0.10	3.40 3.41	5.70 1.06	688.2 2.68	91.9 0.67E-08
2	184	5.21	1.12 1.12	2.11	1.10	0.20 0.20	3.46 3.47	2.89 1.11	345.2 2.68	188.2 0.69E-08
→ 3	276	5.45	1.70 1.70	1.41	2.56	0.30 0.30	3.53 3.53	1.95 1.16	230.9 2.68	289.1 0.71E-08
4	368	5.69	2.30 2.30	1.06	4.67	0.41 0.41	3.59 3.60	1.48 1.21	173.7 2.68	394.5 0.73E-08
5	460	5.92	2.92 2.92	0.35	7.50	0.52 0.53	3.66 3.66	1.20 1.26	139.5 2.68	504.4 0.75E-08
6	552	6.16	3.55 3.55	0.71	11.09	0.64 0.65	3.72 3.72	1.02 1.31	116.6 2.68	618.9 0.77E-08
7	644	6.40	4.19 4.19	0.61	15.49	0.77 0.77	3.79 3.79	0.38 1.36	100.3 2.68	737.8 0.79E-08
8	736	6.64	4.85 4.85	0.54	20.75	0.90 0.90	3.85 3.85	0.78 1.41	88.1 2.68	861.2 0.81E-08
9	828	6.37	5.52 5.52	0.48	26.91	1.03 1.03	3.92 3.92	0.70 1.46	78.6 2.68	989.2 0.84E-08
10	920	7.11	6.20 6.20	0.43	34.03	1.17 1.17	3.98 3.98	0.64 1.51	71.0 2.68	1121.7 0.86E-08

Table 5.

THE KICKER MAGNET

Coil wire resistivity = 0.18E-05 ohm-cm
Coil wire type = RG 58 Coax Center Cable
Coil length = 3.797 cm
Coil inside radius = 3.81 cm
Max. field strength = 5.00 kG
Total capacitance = 250.0 microfarads
Wall thickness = 0.1250 inches
Penetration time = 0.10 msec
Number of beams = 1
Connection of multiple beams = not applicable
Turns lie in grooves of lower layer

layers	turns	outrad (cm)	time max I (msec)	max I (kA)	L (mH) damping factor	R(w/extra) R (temp)	kV(0) kV(0) (temp)	temp chng (deg C) alpha	stress (kg/cm2) beta	length (ft) theta
1	13	4.10	0.08	2.69	0.01	0.08	0.80	10.38	751.5	10.6
			0.08		0.04	0.09	0.81	1.08	0.50	0.21E-07
2	26	4.36	0.16	1.38	0.05	0.17	0.83	5.43	385.3	21.6
			0.16		0.04	0.18	0.84	1.14	0.50	0.21E-07
3	39	4.61	0.25	0.94	0.12	0.27	0.86	3.79	263.2	33.9
			0.25		0.04	0.27	0.87	1.21	0.50	0.21E-07
4	52	4.86	0.33	0.72	0.22	0.37	0.89	2.97	202.1	46.5
			0.33		0.04	0.37	0.90	1.28	0.50	0.22E-07
5	65	5.11	0.42	0.59	0.35	0.47	0.93	2.48	165.4	59.9
			0.41		0.04	0.48	0.93	1.34	0.50	0.22E-07
6	78	5.37	0.50	0.50	0.52	0.58	0.96	2.15	140.9	73.9
			0.50		0.04	0.59	0.96	1.41	0.50	0.22E-07
7	91	5.62	0.59	0.44	0.71	0.70	0.99	1.92	123.3	88.6
			0.59		0.04	0.71	0.99	1.48	0.50	0.23E-07
→ 8	104	5.87	0.67	0.39	0.94	0.82	1.03	1.75	110.2	103.9
			0.67		0.05	0.83	1.03	1.54	0.50	0.23E-07
9	117	6.15	0.76	0.36	1.21	0 95	1.06	1.61	99.9	120.0
			0.76		0.05	0.95	1.06	1.61	0.50	0.23E-07
10	130	6.38	0.85	0.33	1.52	1.08	1.09	1.51	91.7	136.7
			0.85		0.05	1.09	1.10	1.67	0.50	0.24E-07

Figure 13.

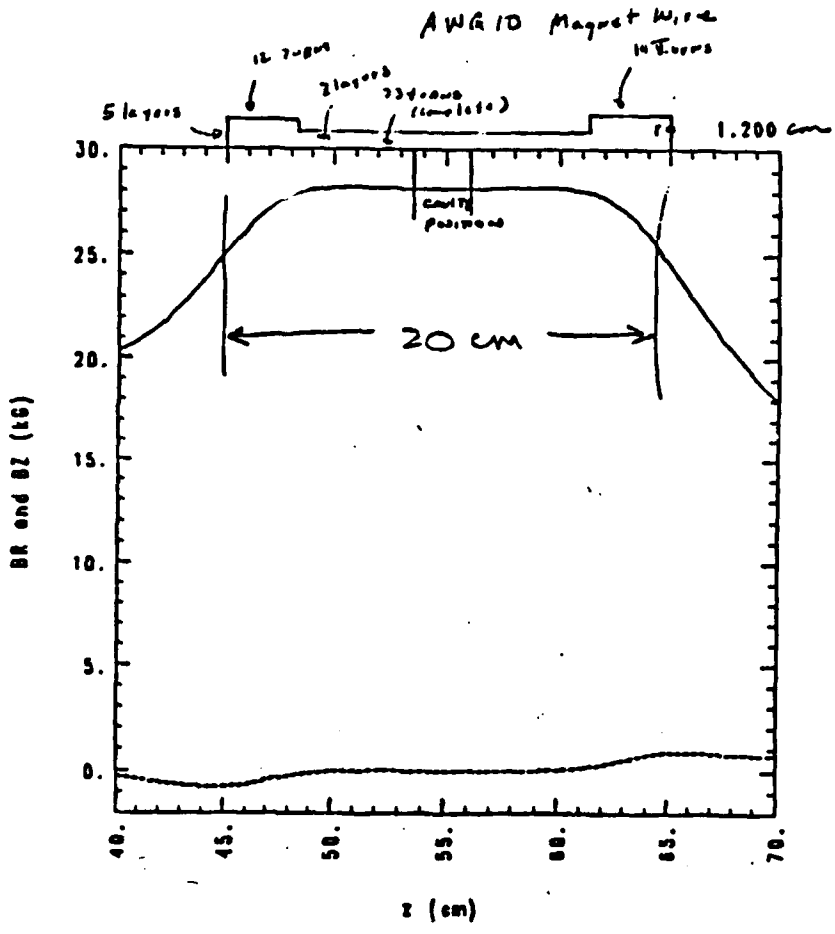
Trim Magnet
AWG 10 Magnet Wire
5 layers
1.200 cm
30.
25.
20.
15.
10.
5.
0.
20 cm
BR and BZ (kG)
40.
45.
50.
55.
60.
65.
70.
z (cm)

Figure 14.

Main Magnet

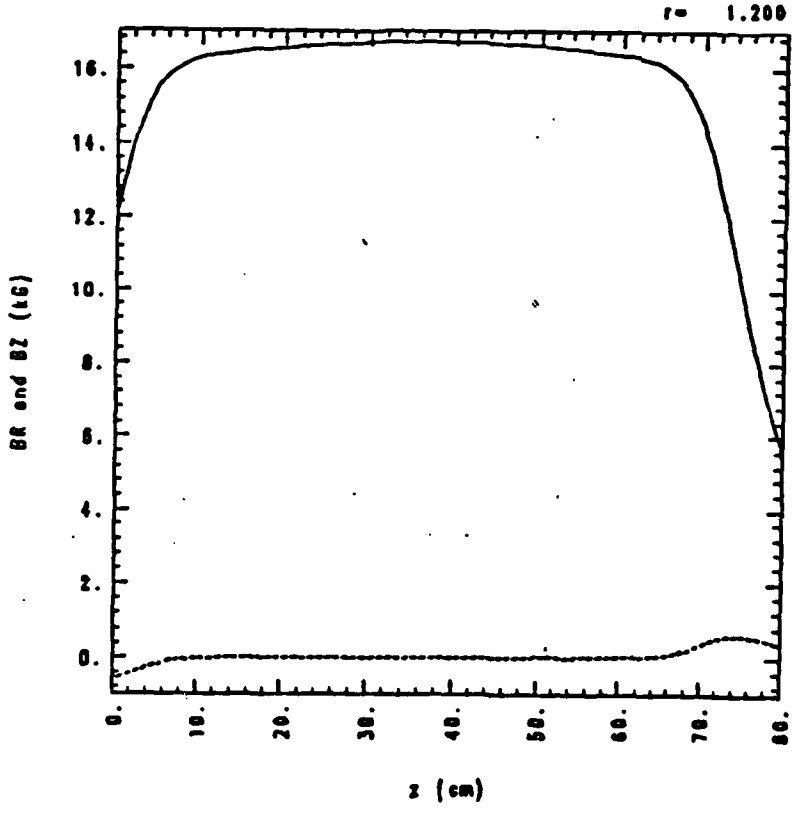

within a few percent between 10 cm and 60 cm from the cathode. A gradual fall-off on both ends was achieved by having two coils at each end with no spacers. All of the other coils have a spacer of 1.25 inches between them.

Experimental Set-up

A Hewlett Packard electron beam accelerator, known as a Febetron, is used as the source of the electron beam for this experiment. To fire the Febetron, a power supply rated at 50 kV, 500 mA was acquired, and repaired. The Febetron has been fired many times, although it is not yet functioning properly above 22 kV. The parameters that are being varied are the capacitor module spark gap distance (from 0.95" to 0.120") to change the voltage holdoff capability of the capacitor module, the pressure of nitrogen in the module chamber (from 20 psi to 80 psi) varying the voltage holdoff of the capacitor module, the pressure of freon in Febetron case (from 10 psi to 30 psi) to change the amount of voltage standoff between the pulseline and the Febetron case and the sulfur hexafluoride (SF_6) in the pulse tube (10 psi to 40 psi) to vary the amount of voltage standoff between the resistive load and the Febetron case. The resistive load for the beam pulse has been varied from 100 Ω to 1 kΩ and finally settled on at 300 Ω to match the impedance of the Febetron.

Figure 15 shows a voltage pulse of the Febetron. It was charged to 22 kV, the nitrogen pressure in the module chamber was 40 psi, the freon pressure was 25 psi and the SF_6 pressure was 40 psi. Note that the peak is flat to within eight percent and ~ 200 nsec long. The rise time, the small pre-pulse and the overshoot still need to be brought to within operational requirements.

The capacitor banks consist of three power supplies and three trigger units (one for each capacitor bank), three

Voltage Pulse

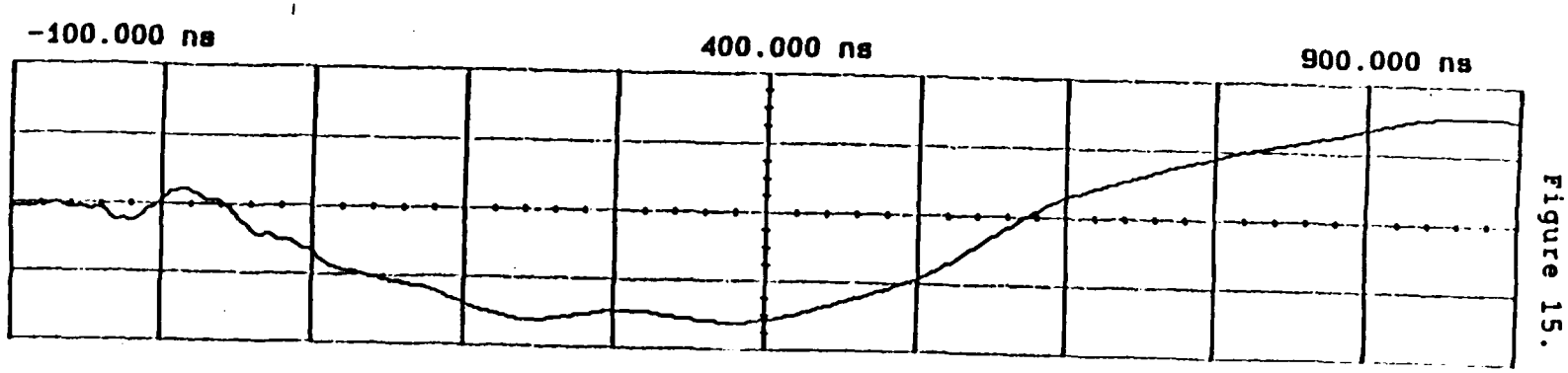

Figure 15.

Ch. 1 = 40.00 mVolts/div
Timebase = 100 ns/div

Offset = 0.000 Volts
Delay = -100.000 ns

banks of capacitors and all of the necessary circuitry needed to charge, measure the voltage, fire and dump the banks. The power supplies for the capacitor banks had to be acquired and repaired as necessary until all three were made functional. The trigger units were designed, fabricated, tested and interfaced with the capacitor banks.

All of the circuitry to charge, measure the voltage, fire and dump the banks had to be designed, fabricated and tested. The components of this circuitry include high voltage resistors, various high voltage switches, high voltage diodes and wiring. Figure 16 shows the circuitry to charge, fire and dump a capacitor bank. When the high voltage "on" switch on the high voltage power supply is pushed, the 110 VAC line and the switch (S_1) are energized. This disconnects the power supply and the capacitor bank from ground through the dump resistors and allows the capacitor bank to be charged. The bank is fired when the trigger amplifier is pulsed into the ignitron. The capacitor bank then discharges through the ignitron and into the magnet.

The main magnet consists of 13 unidirectionally wire wound coils separated by nylon spacers. These coils had to be acquired and the spacers had to be manufactured. The main magnet will be capable of producing 10.0 kG for ~ 50 cm. Once the magnet was assembled it was tested under a direct current load to determine if the magnet had been properly constructed. The main magnet still needs to be tested under a pulsed power load. The trim magnet consists of three layers of windings of AWG 10 magnet wire in the center with two more layers of windings on each end for 12 turns on the cathode end and 14 turns on the other end. The magnet will be capable of producing 18.0 kG for ~ 15 cm. The trim magnet has been designed and fabricated although it still needs to be tested under a pulsed power load. The kicker magnet consists of eight windings of the inner conductor from RG-58 coax cable evenly distributed across the

Figure 16.

Capacitor Bank Circuitry

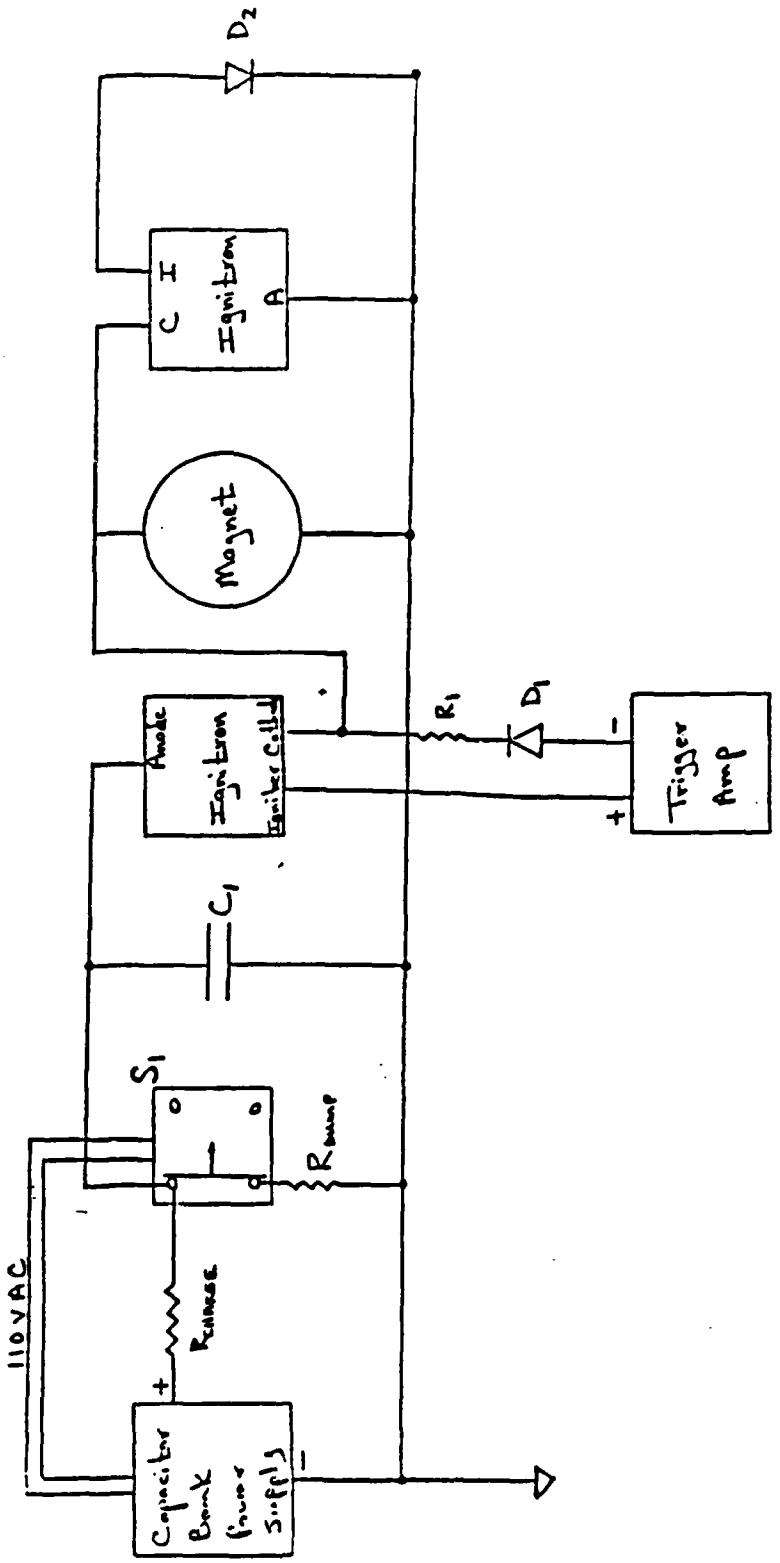

magnet form. This magnet will be able to produce 5.0 kG to give the beam an increase in transverse momentum by passing through a nonadiabatic dip in the magnetic field produced by the magnet. The kicker magnet has been designed, fabricated and tested under a pulsed power load.

The pumping station for the experiment, consisting of a roughing pump, a diffusion pump and all necessary meters, valves and controls, has been repaired. A portable leak detector has been refurbished and used to test the vacuum system for leaks.

Remote digital voltage meters have been installed in the control console to accurately measure the charge voltage of the Febetron and to measure the voltage of the three capacitor banks. Each meter has a three-digit accuracy. A shielded room has been assembled in the laboratory. The room was tested at various RF frequencies to ensure its integrity.

Since the experiment will produce x-rays, the collector and diode regions which generate the x-rays had to be encased in a lead enclosure. The lead shield frames were designed and constructed to hold a total of one inch of lead. The thickness of the lead needed was calculated from such parameters as the electron beam current and voltage, the number of shots per day and the target material of the electron beam. At the present time, one-half inch of lead has been applied to the lead shield frames. An interlock system has been built for the laboratory's four power supplies. If the interlock circuit is open, no high voltage may exist in the laboratory.

In summary, a new diode design has been achieved for the Febetron. All three of the capacitor banks have been completed while the three magnets are in the process of being completed. The Febetron is firing properly at lower voltages and all of the necessary general laboratory experiment is in place.

JAYCOR's work will continue under the new contract. The remaining part of Phase I and Phase II will be completed.

Additional Efforts: Phase locked Oscillator

For the past two years JAYCOR has been supporting, at NRL's request, the high and low power programs in phase-locked oscillator development. The high power experiments have been centered on the operation of slotted cavity configurations at 35 GHz and the fabrication of a three cavity phase-locked gyrotron. At the low power end, efforts have been focused on building an 85 GHz tunable oscillator configured to be modified for operation in a phase-locked state.

Tunable Oscillator

The tunable gyrotron oscillator designed to operate in the $TE_{1,3}$ circular mode has been fabricated. The oscillator (Figure 17) consists of a Varian VUW 8010 (Seftor) electron gun, drift region, tunable cavity holder, non-magnetic hard seal current break, copper collector, pump-out region and a beryllium output window. The design operating parameters for the tube are:

Cathode voltage	50-70 kV
Intermediate anode	50 percent cathode
Beam current	$\leq$ 6 A
Pulse width	1 - 2 μsec
Frequency	85 GHz ($\pm$2 GHz)
Mode	$TE_{1,3}$
Rep rate	20 Hz
Peak power	50 kW
Pressure	10^{-8} Torr

Figure 17.

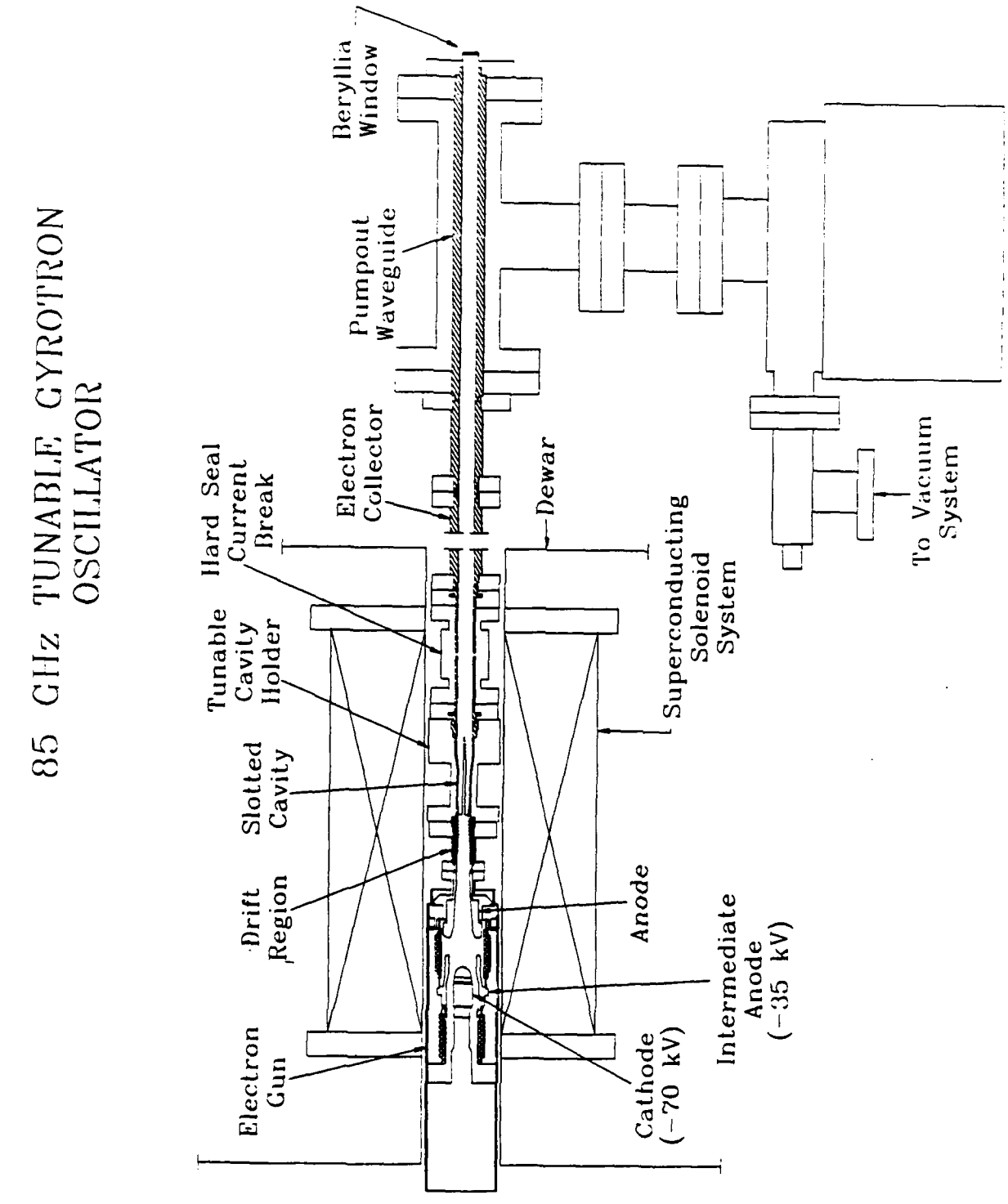
85 GHz TUNABLE GYROTRON
OSCILLATOR
Beryllia Window
Pumpout Waveguide
Electron Collector
Hard Seal Current Break
Dewar
Tunable Cavity Holder
Slotted Cavity
Drift Region
Electron Gun
Superconducting Solenoid System
Anode
Intermediate Anode (-35 kV)
Cathode (-70 kV)
To Vacuum System

Mechanical Design

In deformation bench testing of several test cavities, a free ended, slotted copper cavity with a spring constant of 3000 lbs/in was chosen as the tunable design. This decision was based on the fact that the measurable inside dimension deflection after the application of a few pounds of force was reasonable. Figure 18 shows the gyrotron cavity bilateral slots and the keyed orientation in the holder.

The mechanical tuning of the holder was achieved by a vacuum compatible design which symmetrically transmits action via two miniature stainless steel bellows to the cavity (Figure 19). By dialing in fractions of a turn on each 21 inch feed through, the cavity is compressed a few tens of thousandths of an inch, changing its shape and, in theory, its frequency. In calibrating the tunable cavity holder with all the tube components in place, it was determined that one complete turn from the zero on each tuning rod changed the cut-off region of the oscillator three thousandths of an inch in diameter. This corresponds to an approximate one and half thousandths of an inch change in diameter at the cavity center and should tune the frequency of the oscillator by 1.5 GHz per turn.

The full mechanical range of the cavity holder is 20 turns on each rod and is limited by the transmission design. An eight degree wedge configuration translates the action to a pin that extends the bellows sub-assemblies resting on the cavity. Each vacuum tight bellows assembly is mounted on a custom one inch, ultra high vacuum flange machined to stop the motion at a maximum travel of 40 mils, the extension limit of the stainless steel bellows (Figure 20). The TIG welded, all non-magnetic stainless steel construction of the bellows assemblies allows the units to be cycled ten thousand times.

Figure 18.

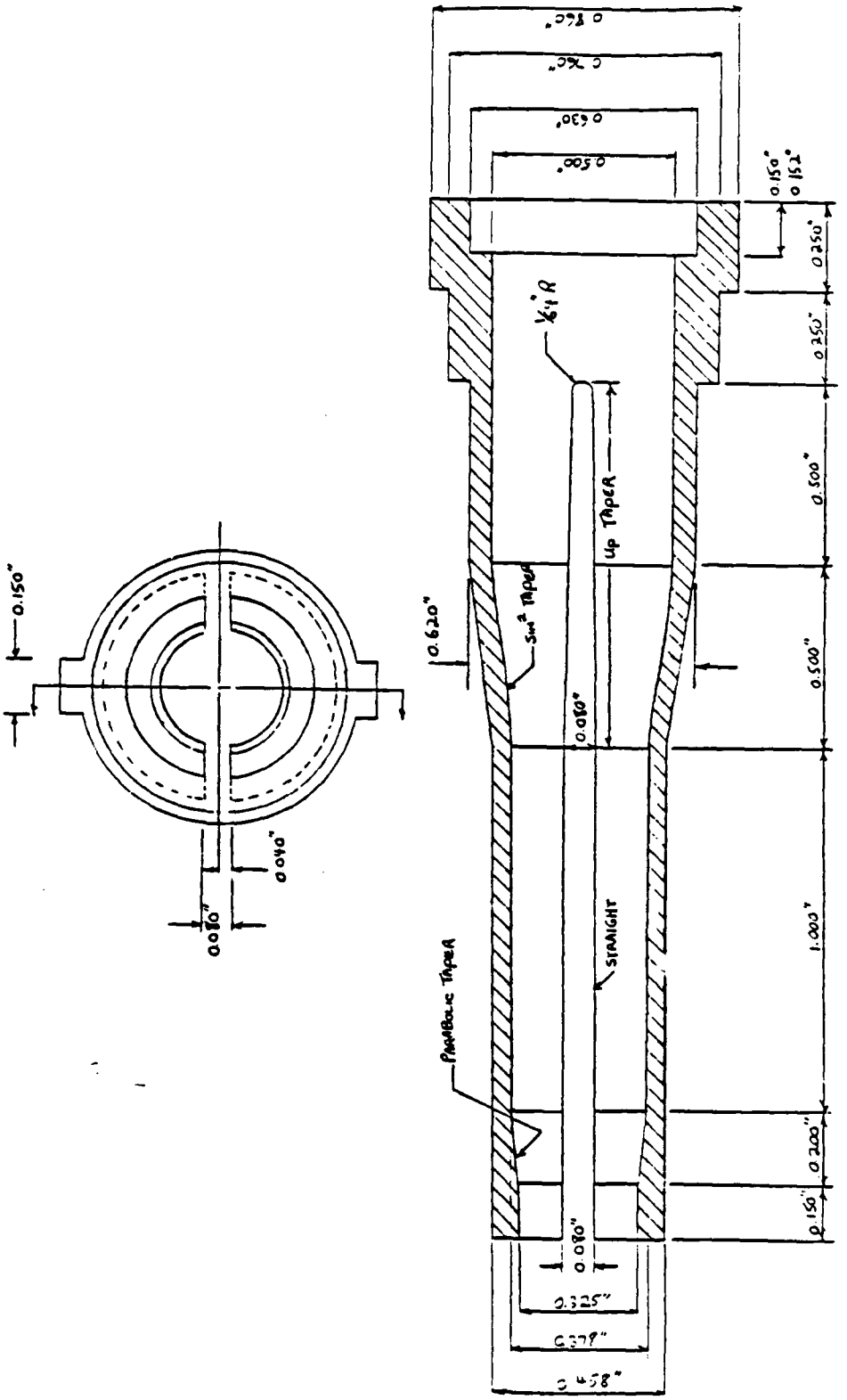
0.150"
0.040"
0.080"
0.620"
1/4" R
Sm² Taper
Up Taper
0.080"
Straight
Parabolic Taper
0.080"
0.325"
0.379"
0.458"
0.150"
0.151"
0.250"
0.250"
0.500"
0.500"
1.003"
0.200"
0.150"

Figure 19.

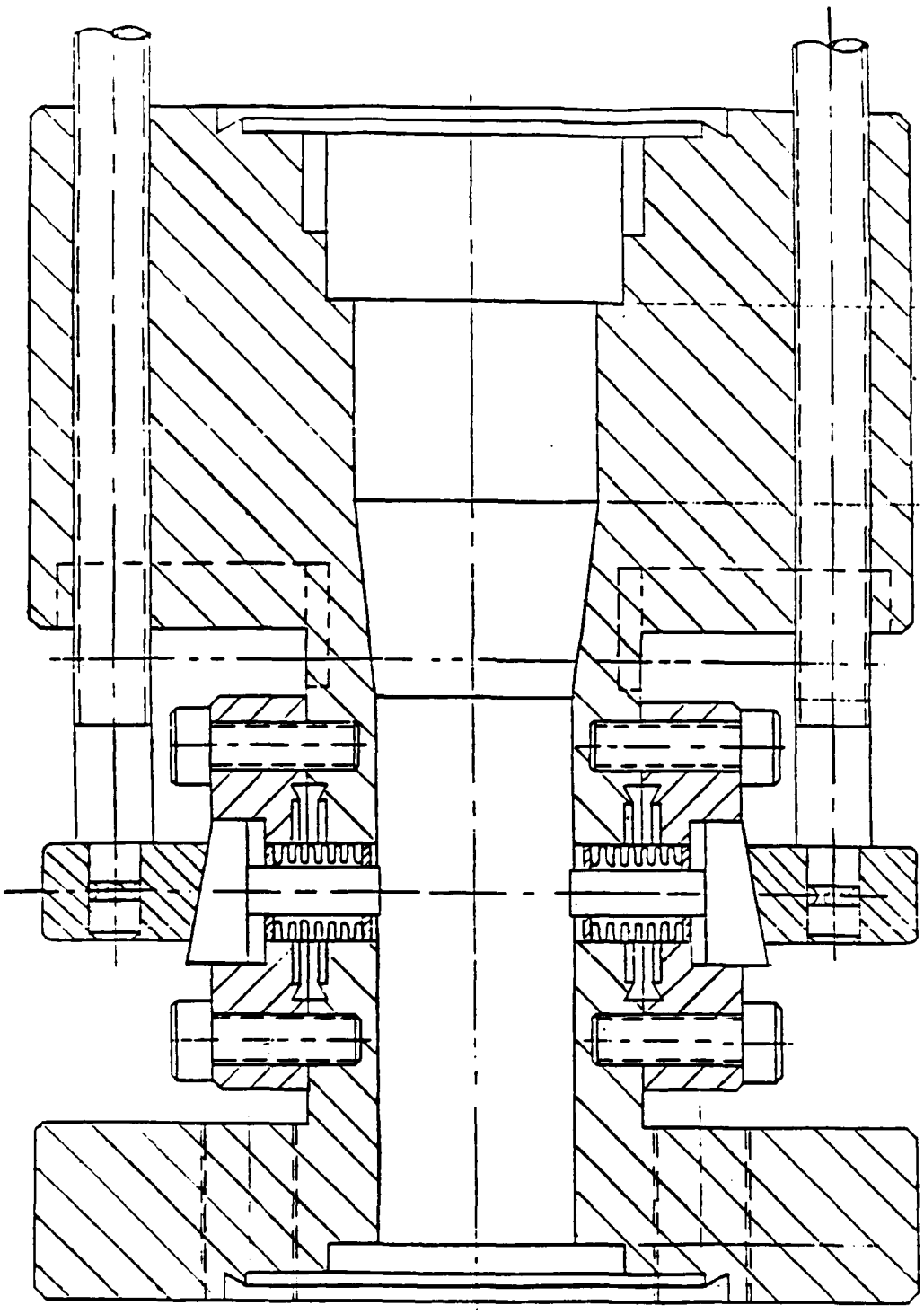

Figure 20.

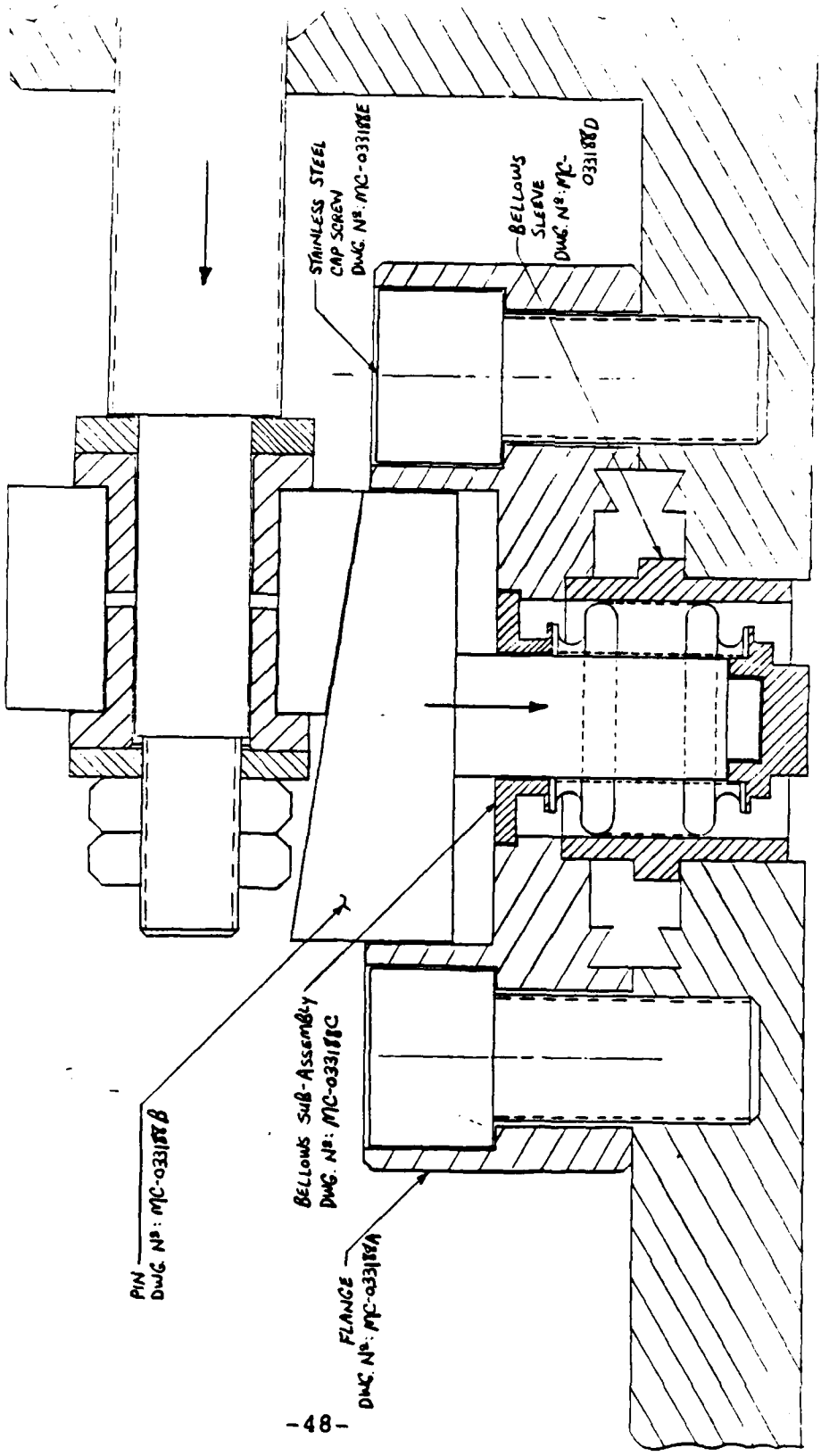
STAINLESS STEEL CAP SCREEN DWG. Nº: MC-033188E
BELLOWS SLEEVE DWG. Nº: MC-033188D
PIN DWG. Nº: MC-033188B
BELLOWS SUB-ASSEMBLY DWG. Nº: MC-033188C
FLANGE DWG. Nº: MC-033188A

A non-magnetic hard seal current break was developed to alleviate shorts in the body current beam diagnostic and baking constraints that previous o-ring designs have experienced. The prototype assembly consists of a ceramic-to-metal adapter, two double sided support flanges and two waveguide inserts (Figure 21). The hard seal is fabricated in 70/30 copper nickel and aluminum with stainless steel weld adapters on each end. The waveguide break is machined to a separation of approximately ten mils and allows the assembly to be baked to 450 degrees centigrade.

Vacuum Systems

The tunable oscillator was evacuated by a cryogenic pump station designed and built around a CTI Cryo-Torr 100 high vacuum pump, monitored by a Varian 580 nude ionization gauge with the RS 880 digital controller. The cryo station incorporates a double valve configuration and a 1.5 liter liquid nitrogen trap which allows the operator to obtain an ultra high vacuum which is virtually free of mechanical pump oil, a major contaminant in these systems. With the 350 liter/sec pumping speed (air) of the station, the gyrotron tube reached a pressure in the 10^{-6} Torr scale within minutes, and a final base pressure after a low temperature bake in the 10^{-8} Torr scale in approximately five days. The cyro pump station speeded the processing of this tube making it a wise choice for ultra high vacuum applications in the future.

Diagnostics/Code Development

A calorimeter was fabricated to measure power at 85 GHz. Several types of absorptive coatings were used during the testing. The finished calorimeter was tested under low and high power. It absorbed 94 percent of the incident power at a frequency of 85 GHz. The calorimeter exhibited unexpectedly good performance from 75 to 120 GHz. This

Figure 21.

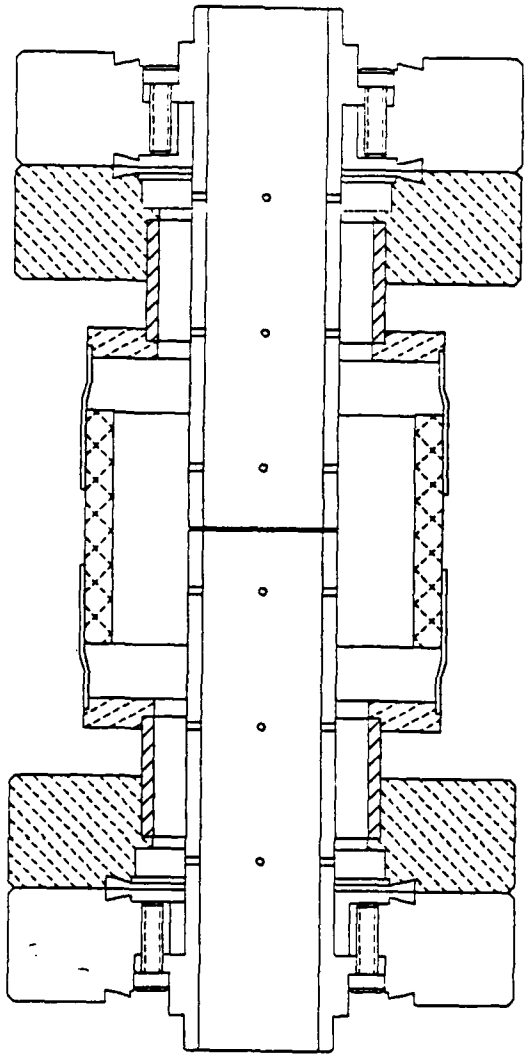

represents a significant improvement over the previous calorimetric systems. Several computer codes are available to NRL to model such devices. One of these, CALPERP.TH, is listed in Appendix C.

Various pieces of overmoded waveguide were designed, built and tested for use with the 85 GHz phase-locked oscillator. Foremost among these is a directional coupler which preferentially couples a $TE_{1,3}$ circular mode. The coupler was tested with a $TE_{1,1}$ circular mode at frequencies around 85 GHz. The coupler has eight coupling holes and is ten inches long. It coupled approximately -30 dB. The directional coupler will be used to sample the microwave output of the oscillator.

A newly acquired scalar network analyzer was used to measure the microwave properties of several components. The analyzer allows for fast, efficient measurements in a swept-mode fashion. It should facilitate many measurements which were previously very lengthy or impossible.

The output window for the tube was tested with a $TE_{1,1}$ circular mode. Microwave transmission was maximum at 82 GHz, which implies that the window will work very well for the $TE_{1,3}$ circular mode at 85 GHz. A balanced mixer/phase detector was acquired and tested. The device is capable of comparing the frequency and phase of two signals. It will ultimately be used to compare the input and output signals to the phase-locked oscillator.

A good deal of effort has gone into analyzing the multimode output of gyrotrons. A set of several computer codes were developed to design a K_z spectrometer. This is a device which characterizes a mode by the angle it makes with the z-axis. Another set of programs analyzes the far field patterns of up to five modes at a time. These codes were used to deconvolve the data from a previous tube.[12] The

---

12. R. Fischer and J. Burke, to be published.

information obtained through this analysis has provided useful data for future measurements.

Tunable Oscillator Data

The goal of the first series of experiments is to characterize the tunability of the 85 GHz gyrotron oscillator. The test area of the Long Pulse Millimeter Device Section has been set up to measure the frequency, power, mode and efficiency of every point to which the oscillator cavity is tuned. To obtain this complete data set on the oscillator, the tube is tuned to a stable operating point. The microwave frequency is observed with a dip meter. The output power is measured by a calorimeter and a calibrated crystal. The efficiency is calculated from information supplied by the beam and cathode voltage diagnostics. The radiating mode is identified by a horn swept in the far field.

The experiment has run for several days and the tube continues to hold an exceptional vacuum. With a design beam current of 6.0 amps at one microsecond pulse width, a peak microwave power of 50 kW has been recorded repetitively pulsed at 20 Hz. Since the tube was designed for low power operation and no cooling is supplied to the electron collector, this seems to be the safe operating point, avoiding the excessive heating that would occur at higher power levels.

The addition of the cavity tuning knob to the existing parameters of the gyrotron has already proven to be a very useful experimental tool. Preliminary experiments have shown that the cavity tunes, though the coupled output radiation is not clearly defined. Understanding the operation of the tunable cavity could prove to be very time consuming, but has become increasingly important to a successful phase-locking experiment.

Phase-Locked Oscillator

Figure 22 shows how the tunable oscillator experimental layout can be modified to run in the phase-locked gyrotron configuration. By venting the system and replacing the drift region of the tunable oscillator with the input holder, the tube is transformed into a two cavity gyroklystron with a heavily slotted input and a tunable output (Figure 23). Adding the designed injection waveguide to the vac-ion roughing port, the input and output microwave diagnostics (Figure 24), and the locking source, a gridded, extended interaction oscillator (EIO), the experiment setup is complete. The design operating parameters for the phase-locked gyroklystron oscillator follow:

Frequency	85 GHz
Mode	$TE_{1,3}$
Beam Voltage	70 kV
Beam Current	< 6 A
Isolation	45 dB
Input Power	< 500 W
Output Power	50 kW

The main issues the experiment will investigate are the maximization of the phase-locking bandwidth, stray oscillations in the drift region and the phase sensitivity to beam parameters.

TASK 4: OPERATION OF THE GYROTRON TEST FACILITY

As the WRAMRC program was decaying, increased emphasis was placed on the development of a permanent test facility for microwave interactions testing. During the last two years, space was allocated to the program and a laboratory has been developed based on the "original" 35 GHz, $TE_{0,1}$ tube. Several tests were successfully performed

85 GHz. PHASE-LOCKED GYROKLYSTRON OSCILLATOR EXPERIMENT LAYOUT

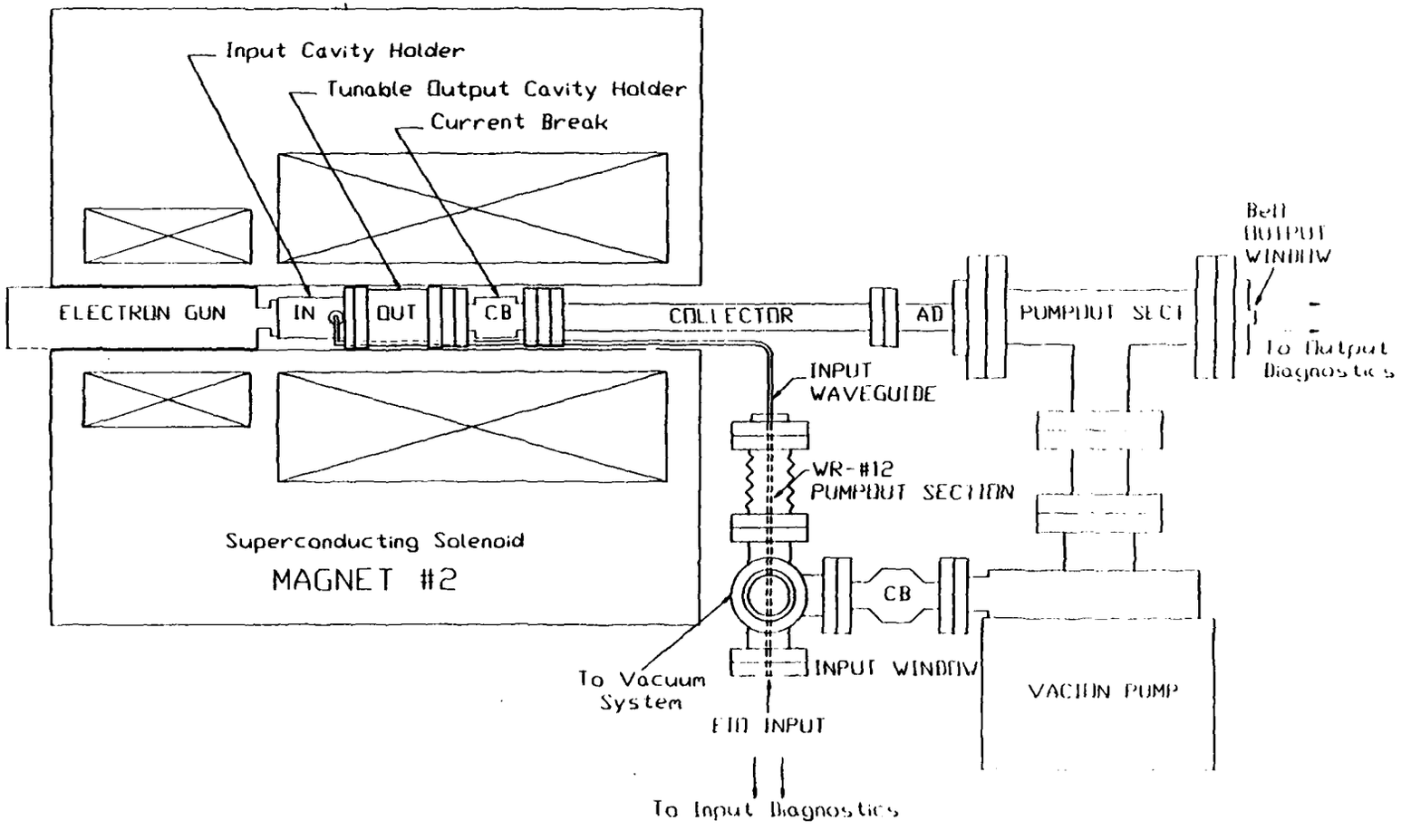

Figure 22.

PHASE-LOCKED GYROKLYSTRON OSCILLATOR

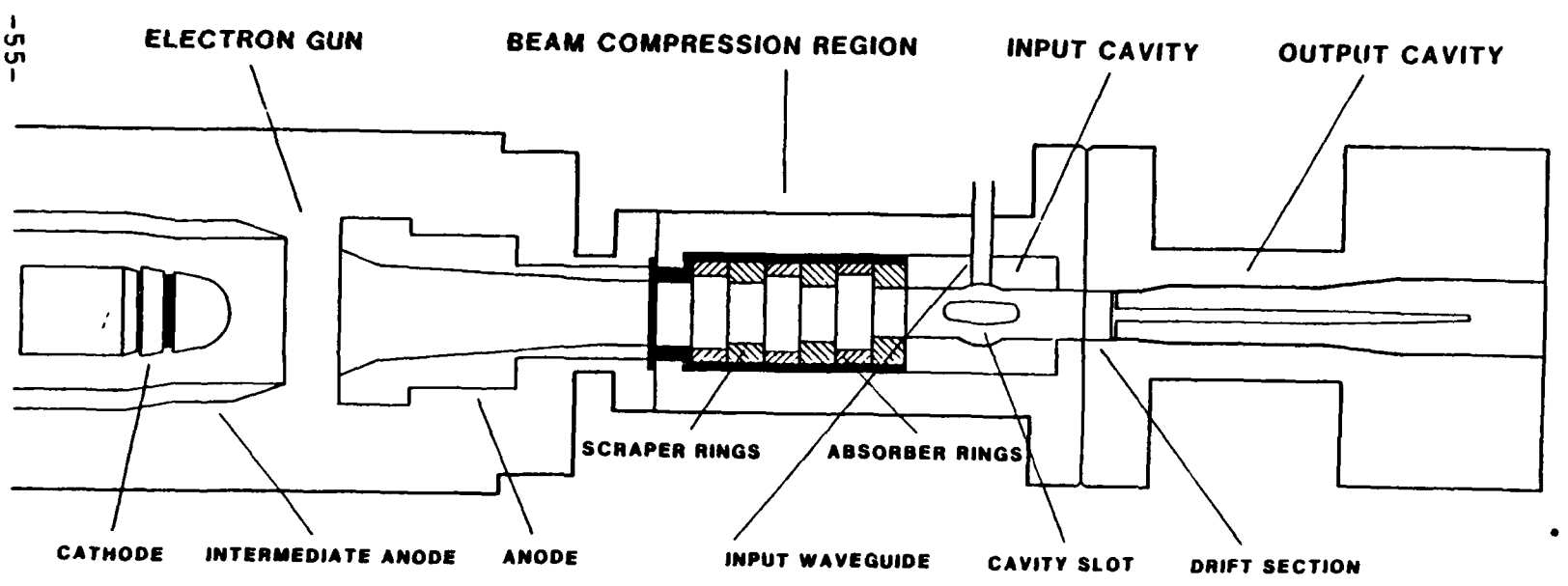

Figure 23.

Figure 24.

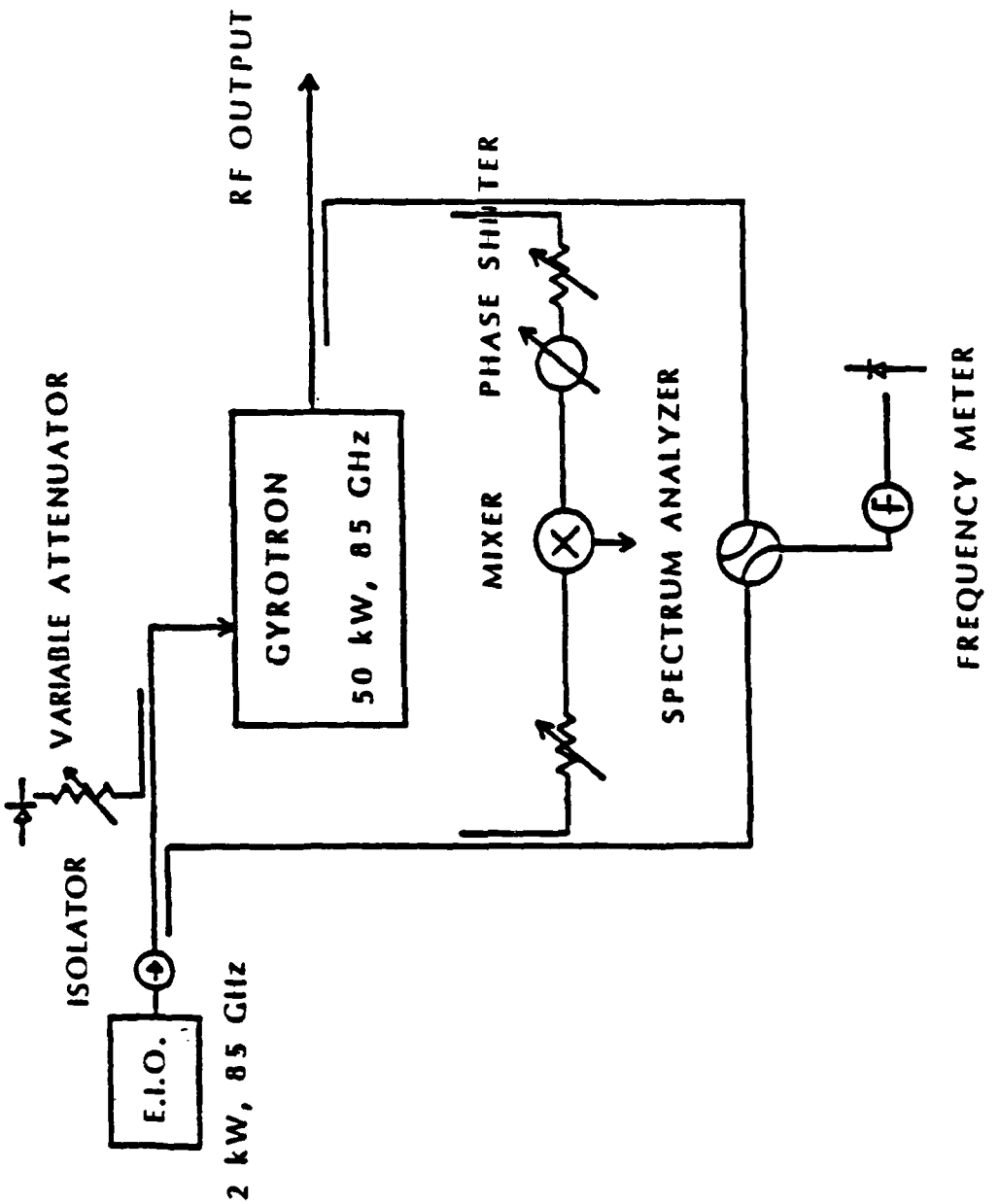
RF OUTPUT
PHASE SHIFTER
VARIABLE ATTENUATOR
GYROTRON
50 kW, 85 GHz
MIXER
SPECTRUM ANALYZER
FREQUENCY METER
ISOLATOR
E.I.O.
2 kW, 85 GHz

in both the old and new locations using this tube on two different modulators. The new facility has been set up to run as a "turn key" operation, using a SLAC type 1, microsecond modulator, and the development of three new tubes and a new modulator was begun. The tubes, though not fully developed at the time of this report, are specified to consist of:

- A remake of the 35 GHz tube using hard seal technology and incorporating a newly designed water cooled collector.
- A 94 GHz $TE_{1,3}$ tube also using the same construction techniques that will be used in the 35 GHz tube.
- The third tube under development is a possible replacement for both of the other tubes, incorporating a novel cavity structure developed by JAYCOR. The realization of this tube would eliminate the need for down time in a test series for tube change-over, a process that would currently take about a day. Only magnetic field and voltage adjustments would be required to make the frequency changes and this could be accomplished in a matter of minutes.

An outgrowth of this design is the development of broad bandwidth and dual frequency windows. The theoretical development of these windows has begun and numerical modelling of several designs is well under way. The manufacturing techniques required to produce broadband windows is also being examined with several possibilities now under consideration.

In addition to the tubes, a new facility modulator has been fully specified and is on order through the government. The modulator will be a hard tube pulsed supply with an average power rating of 1 kW (nominal), giving the operator a very wide latitude in operating parameters.

Much progress has been made in the development of this facility, and although not yet completed, it is well on

its way to becoming an important branch resource. The required support equipment is in place and is being repaired or updated as required. It is now operational on an as needed basis at 35 GHz and the development of a broader range of available test frequencies is also well along, with the added bonus of introducing several useful new technologies to the branch's corporate knowledge.

TASK 5: QUASI-OPTICAL GYROTRON

Large Cavity Experiment

JAYCOR's involvement with the quasi-optical gyrotron (QO), during this contract period, was initially with the creation of an experiment around the original QO magnet from Intermagnetics General Corp.(IGC). The magnet was a 50 kG cross-bore design that had been out for repairs for over two years. When it was apparent that the magnet would be returned before the arrival of a new 50 kG cross-bore magnet purchased from American Magnetics Inc.(AMI), an intense effort was undertaken to set up an experiment. The experiment was designed to use a majority of the existing equipment so that it could be performed without impeding the setup of the new series of experiments based on the AMI magnet and a new mirror holding system.

This immediate system involved a large cavity, approximately 81 cm in length. The cavity consisted of two mirrors of different diameters, to allow for a single output by diffraction around the smaller mirror. A schematic of the gyrotron is shown in Figure 25. The experiment was originally intended to include a larger electron gun from Hughes that was designed for higher frequencies and higher currents. The gun, however, developed a vacuum leak in one of its ceramic to metal seals as it was being prepared for the experiment and was sent back to Hughes for repair. The repair was never satisfactorily completed and the gun failed

Figure 25.

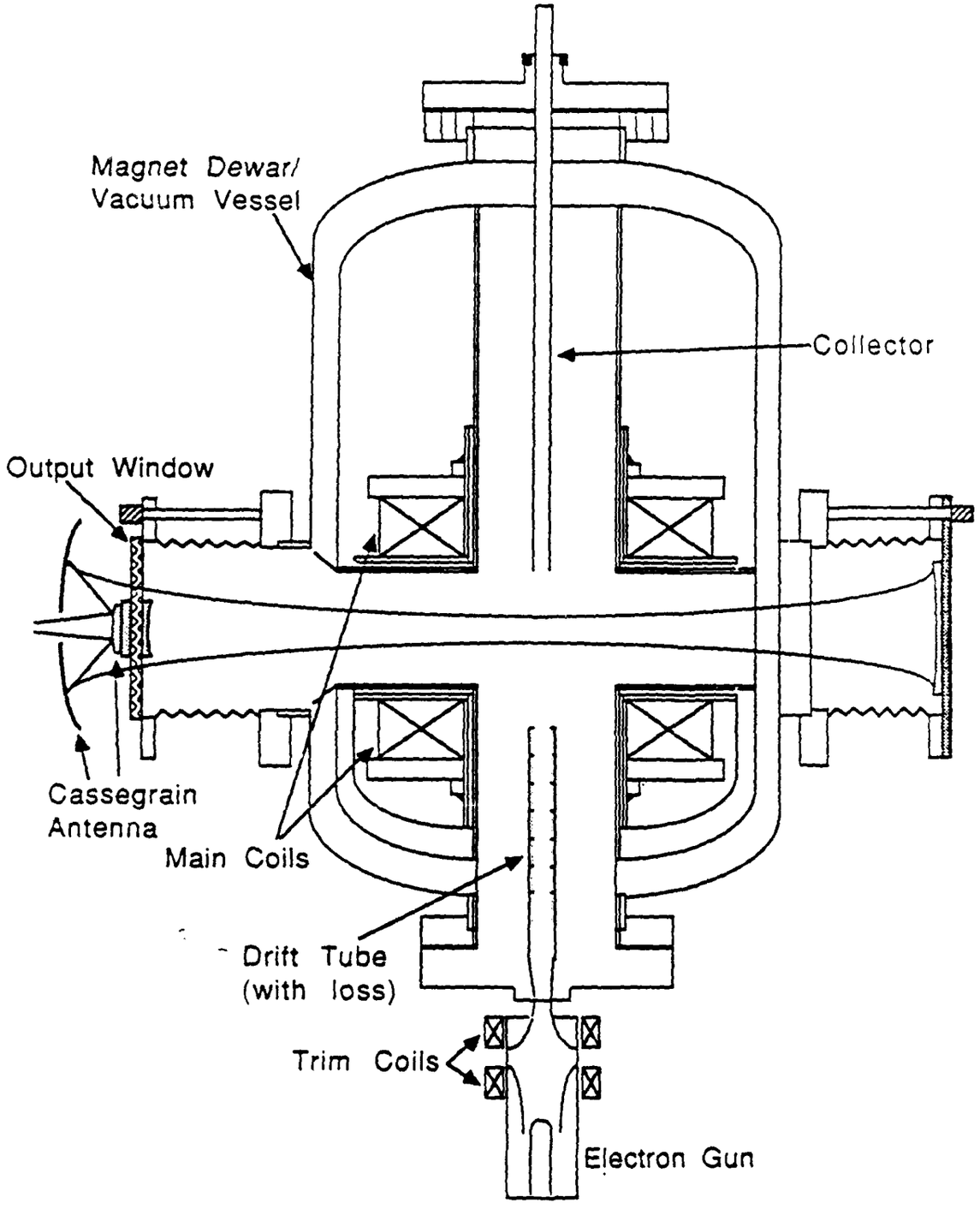
Magnet Dewar/
Vacuum Vessel
Collector
Output Window
Cassegrain
Antenna
Main Coils
Drift Tube
(with loss)
Trim Coils
Electron Gun

almost immediately after its return. The gun has since been sealed and is being stored at NRL. The electro-dynamic design of this gun is considered superior to many electron guns in its power range. Experience, however, indicates the structural design to be weak. Therefore, future use of this gun appears to be quite unlikely.

In place of the failed Hughes gun a Varian VUW-8010 electron gun was installed on the QO. The gyrotron was operated with currents from 0 A to 16 A, and the magnetic field varied from 4.39 Tesla to 4.74 Tesla. At a field of 4.47 Tesla, a magnetic taper of +5 or -5 percent could be produced without exceeding the limits of the magnet. A maximum peak power of 50 kW was reported with the use of a negative tapered magnetic field.[13] The power and efficiency versus beam current results for this negative taper are summarized in Figures 26 and 27.

Certain other aspects of this experiment are noteworthy. This experiment was the first at NRL to use externally adjustable mirrors. This allowed the mirrors to be realigned, translated and/or separated at any time during the experiment without having to break vacuum in the tube, which, in this case, was also the magnet. Because of the amount of time needed to warm and then to recool the magnet, breaking vacuum in the tube involved, at an extreme minimum, a week of down time. The actual time involved was usually longer. Even though this flexibility was not greatly exercised during the experiment,(although they were adjustable, the mirror holders had minimal travel) it did show that external tunability should be a design parameter for all future mirror holders.

---

13. M.E. Read, M.Q. Tran, J. McAdoo, M.L. Barsanti, "Experimental Study of a 115 GHz Quasi-Optical Gyrotron with a Large Cavity", Int. J. Electron., Special issue on Gyrotrons 5, to be published.

Figure 26.

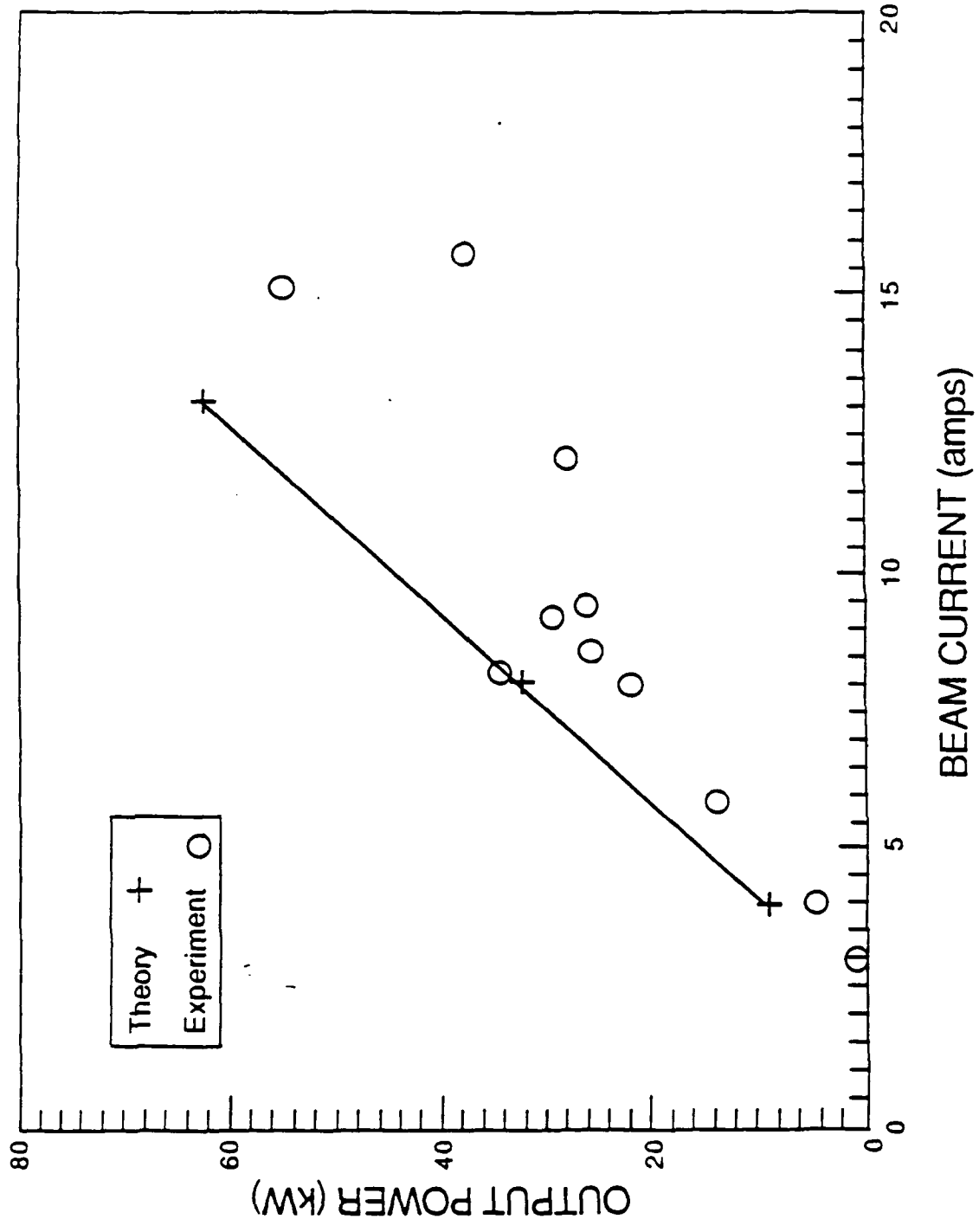
OUTPUT POWER (kW)
0
20
40
60
80
BEAM CURRENT (amps)
0
5
10
15
20
Theory +
Experiment O

Figure 27.

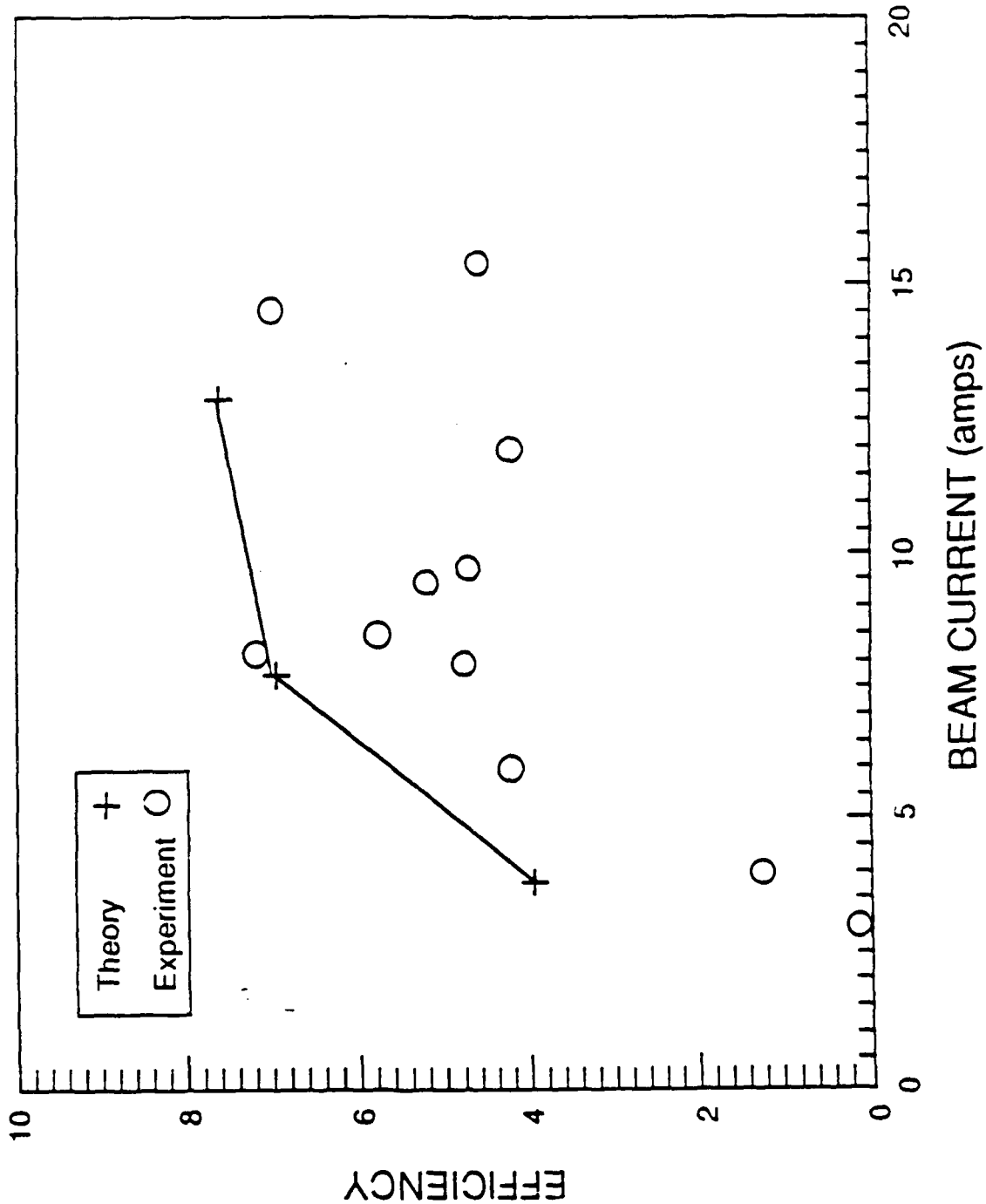
EFFICIENCY
BEAM CURRENT (amps)
Theory
Experiment
0
2
4
6
8
10
0
5
10
15
20

It was also the first NRL QO experiment with a cw relevant cavity design. The cavity is cw relevant in that peak mirror heating due to ohmic dissipation can be cooled with current techniques. Placing the mirrors outside of the vacuum further simplifies the cooling problem. It was the first experiment that was multimoded, which allowed the possibility of comparison with the various multimode theories and codes which have developed over the years. This experiment also marks the first use of the heterodyne frequency measuring system. The heterodyne is an important frequency diagnostic being developed at NRL for use in multimoded systems. It will be explained in greater detail later in this report.

The New Small Cavity Experiment

The large cavity experiment was closed down in late November 1986 in order to allow the set up of the new AMI 50 kG cross-bore magnet. The AMI magnet had a flatter field than the magnet manufactured by IGC, but still retained the same size cross-bore. The calculated field profiles are given in Figures 28, for the IGC, and 29, for the AMI magnets.[14] This flatter field allows a higher possible alpha in the cavity. The AMI magnet also had a much lower operating and at rest boil off rate of its cryogenics. This allowed for lower maintenance and less thermal cycling of the magnet and gyrotron.

The magnet was unpacked and set up to operate. It was then tested to determine that all of the support equipment for the magnet was operating correctly and verify that the magnet could operate at its maximum rated current without going normal. The magnetic field was measured by means of a hall-effect probe placed along the axis of the magnet.

---

14. R.C. Lee, "NCOIL", a numerical solution of axial and transverse magnetic fields in a solenoid.

Figure 28.

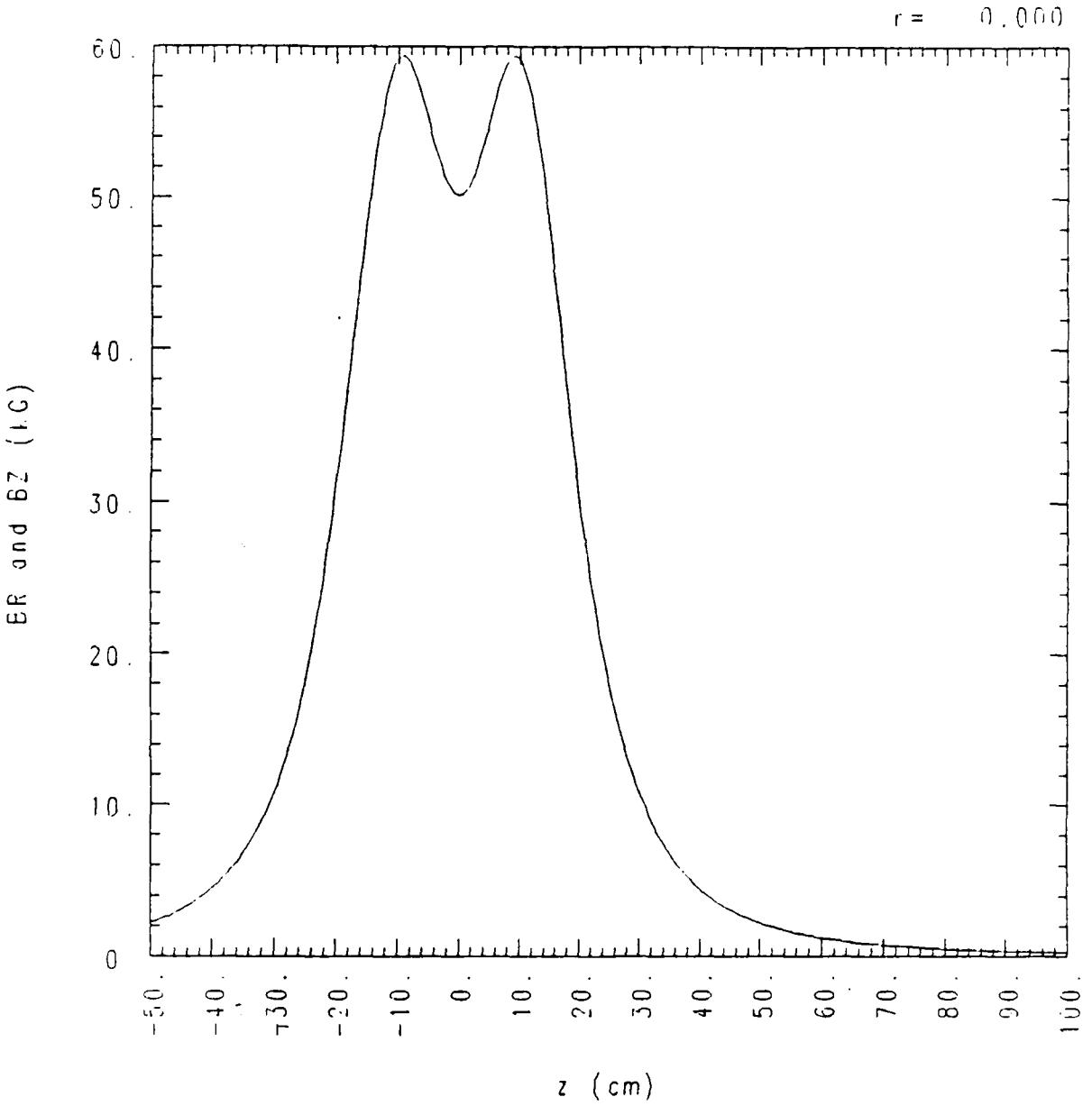
r = 0.000
60.
50.
40.
30.
20.
10.
0
ER and BZ (kG)
-50.
-40.
-30.
-20.
-10.
0.
10.
20.
30.
40.
50.
60.
70.
80.
90.
100.
z (cm)

Figure 29.

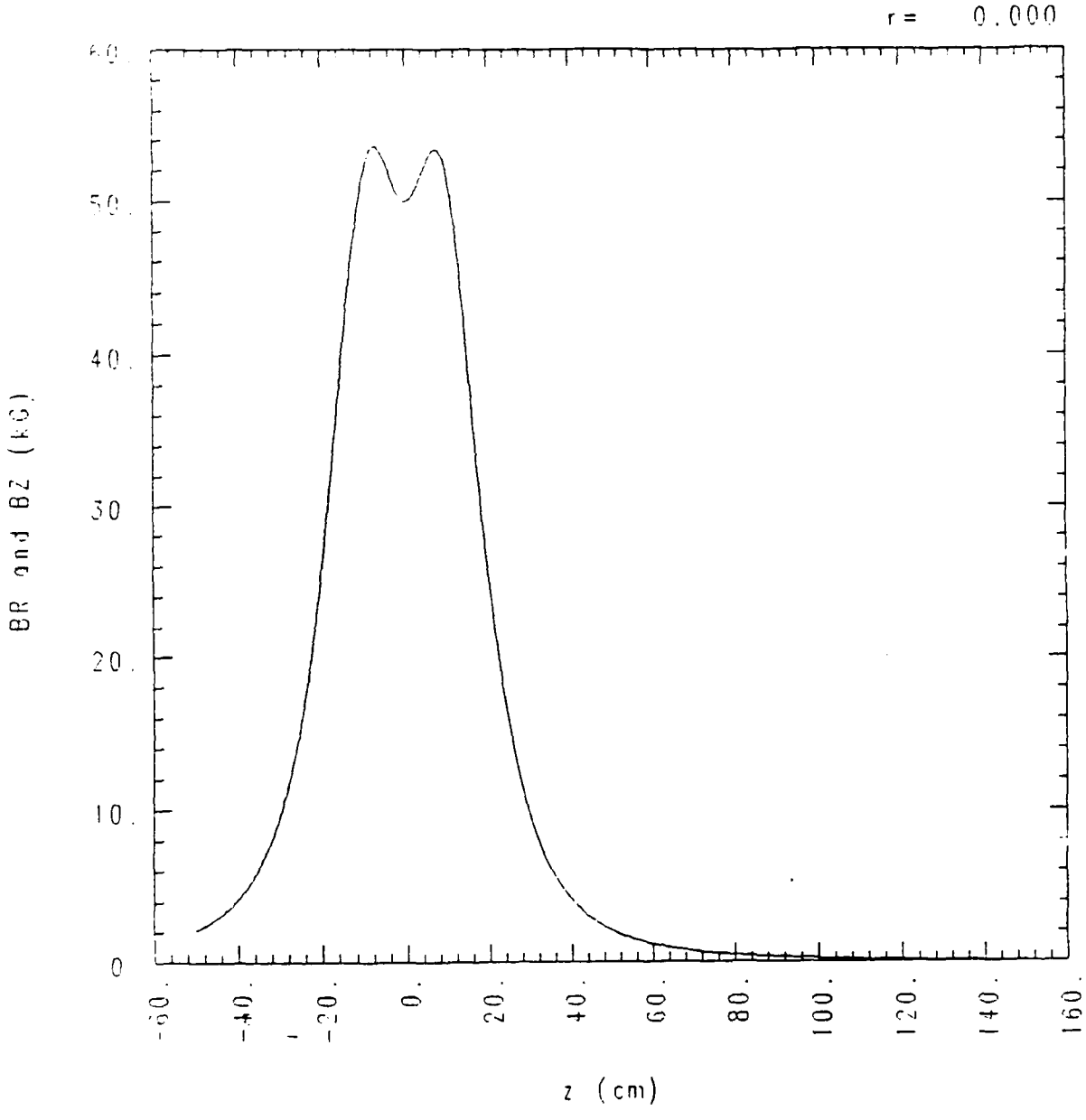
r = 0.000
BR and BZ (kG)
60.
50.
40.
30.
20.
10.
0
-60.
-40.
-20.
0.
20.
40.
60.
80.
100.
120.
140.
160.
z (cm)

Measurements were taken at the first and second maxima as well as the local minima between the two. The values and positions of these measurements were recorded for two different currents and compared to the theoretical field profile based on the claimed coil sizes and positions as calculated by a computer.[15] The values of these measurements are provided in Table 6. The results of this analysis are important for two reasons. They verify that the magnet coils are the size, strength and in the position that was specified by the manufacturer. Secondly they allow an accurate comparison of theoretical models with experimental results in the gyrotron.

At the time of these measurements, a new mirror holding system was designed.[16] Figure 30 shows the assembled mirror holders in place for operation. While the preceding experiment did allow external adjustment of the QO cavity mirrors it was limited to the 81 cm cavity length used, with a total variation of less than 2.5 cm. The new mirror holding system could continuously vary the length of the cavity a total of 10 cm at any one time. The cavity could also be expanded step wise by means of conflat spacers added to the cross-bore of the magnet. This feature would allow operation from less than 2 cm total length to well beyond the 28 cm that was used. In theory one could add any size spacers to the cross-bore of the magnet to get a cavity of arbitrary length though, in fact, other practical aspects would place an upper limit on the cavity length attainable.

---

15. ibid.

16. T.A. Hargreaves, M.L. Barsanti, R.P. Fischer, J.M. Burke, A.W. Fliflet, W.M. Manheimer, "The NRL Quasi-Optical Gyrotron Experiment", Conference Digest of the 12th Int. Conf. on IR and MMW, 1987, paper W8.1.

Table 6.

Axial Magnetic Field Measurements
American Magnetics 50kG Cross-bore Magnet

Magnet Current (Amps)	Position	B_z Measured (kG)	B_z Theory (kG)	Percent Diff. (%)
36.15	1st peak	24.82	25.00	-0.72
36.15	Cavity	26.69	26.80	-0.41
36.15	2nd Peak	26.58	26.71	-0.49
7.23	1st peak	5.01	5.00	0.20
7.23	Cavity	5.37	5.36	0.19
7.23	2nd Peak	5.37	5.34	0.56

QUASI-OPTICAL GYROTRON
(Cross-Bore Assembly)

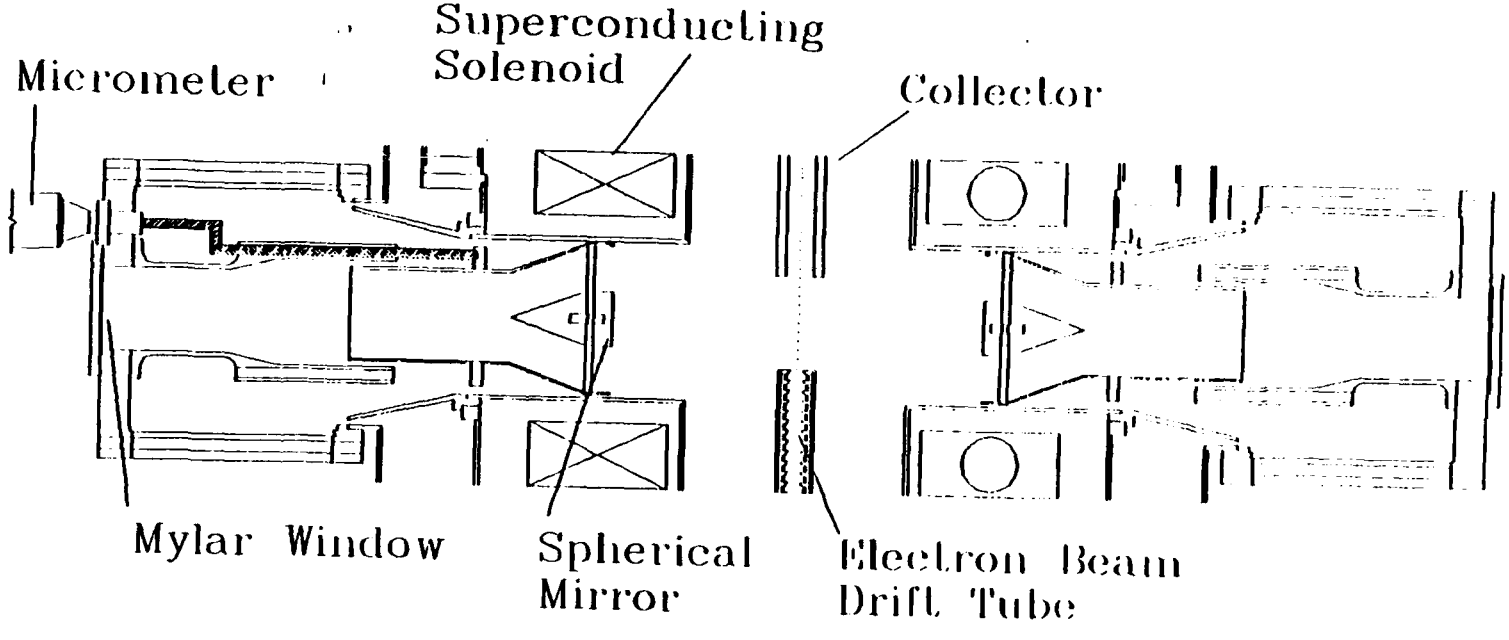

Figure 30.

Another important feature of this assembly is that it incorporates 0.013 cm thick mylar for the output windows. This material may not prove suitable for high average powers. It has the advantage, however, that the thickness is less than 10 percent of the wavelength of any operational frequencies. This makes the windows extremely broad band because they are not resonant at any of these frequencies.

A scale schematic of the entire assembly is shown on Figure 31. The new experiment was originally operated with a small mirror separations. This was done to compare the behavior of the QO qyrotron with a new magnet and mirror holders with the first QO gyrotron.[17] Both the power and efficiencies of the new experiment compared quite closely with the original one. The peak power versus current at various magnetic fields is given for 4 and 8 cm mirror separations in Figures 32 and 33 respectively. This was important for two reasons. One was that it provided a good means of verification of the old data. Second, and more importantly, this was a good way of proving that the new mirror design did not have any negative effects on the microwave properties of the tube.

There was however one major difference between the two experiments. The new experiment was easily multimoded. In fact the tendency was more toward multimoding than to single moded operation. One explanation for this difference was the fact that the original experiment was performed with a two microsecond voltage pulse. The new experiment was performed with a 13 microsecond pulse length. This pulse also had a much longer rise and fall time and a greater variation in voltage along the pulse. This voltage variation along with the increased rise and fall times of the

---

17. T.A. Hargreaves, K.J. Kim, J.H. McAdoo, S.Y. Park, R.D. Seeley, M.E. Read, "Experimental Study of a Single-Mode Quasi-Optical Gyrotron", Int. J. Electron., 1984, 57, 977.

Figure 31.

NRL QUASI-OPTICAL GYROTRON

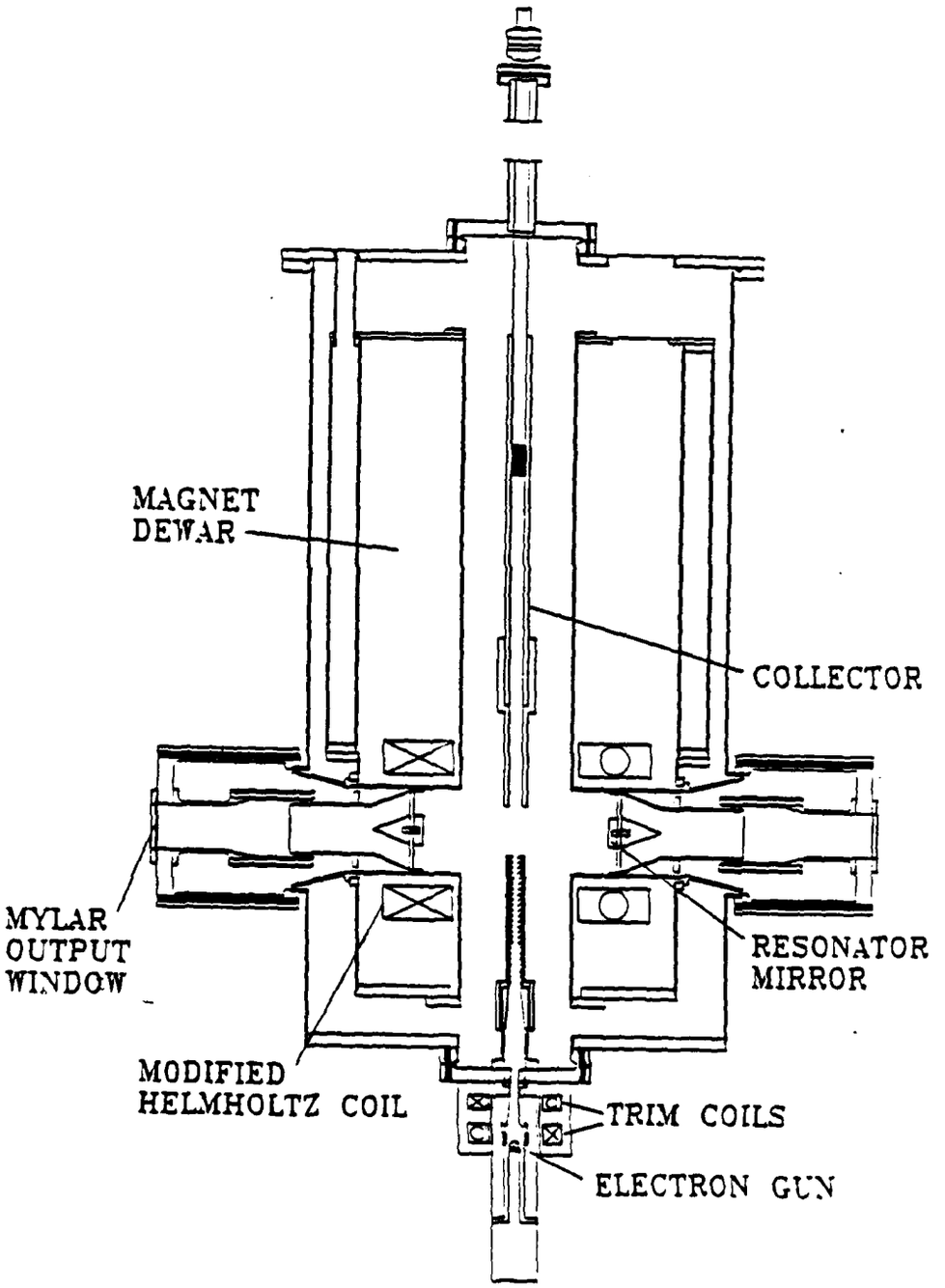

Figure 32.

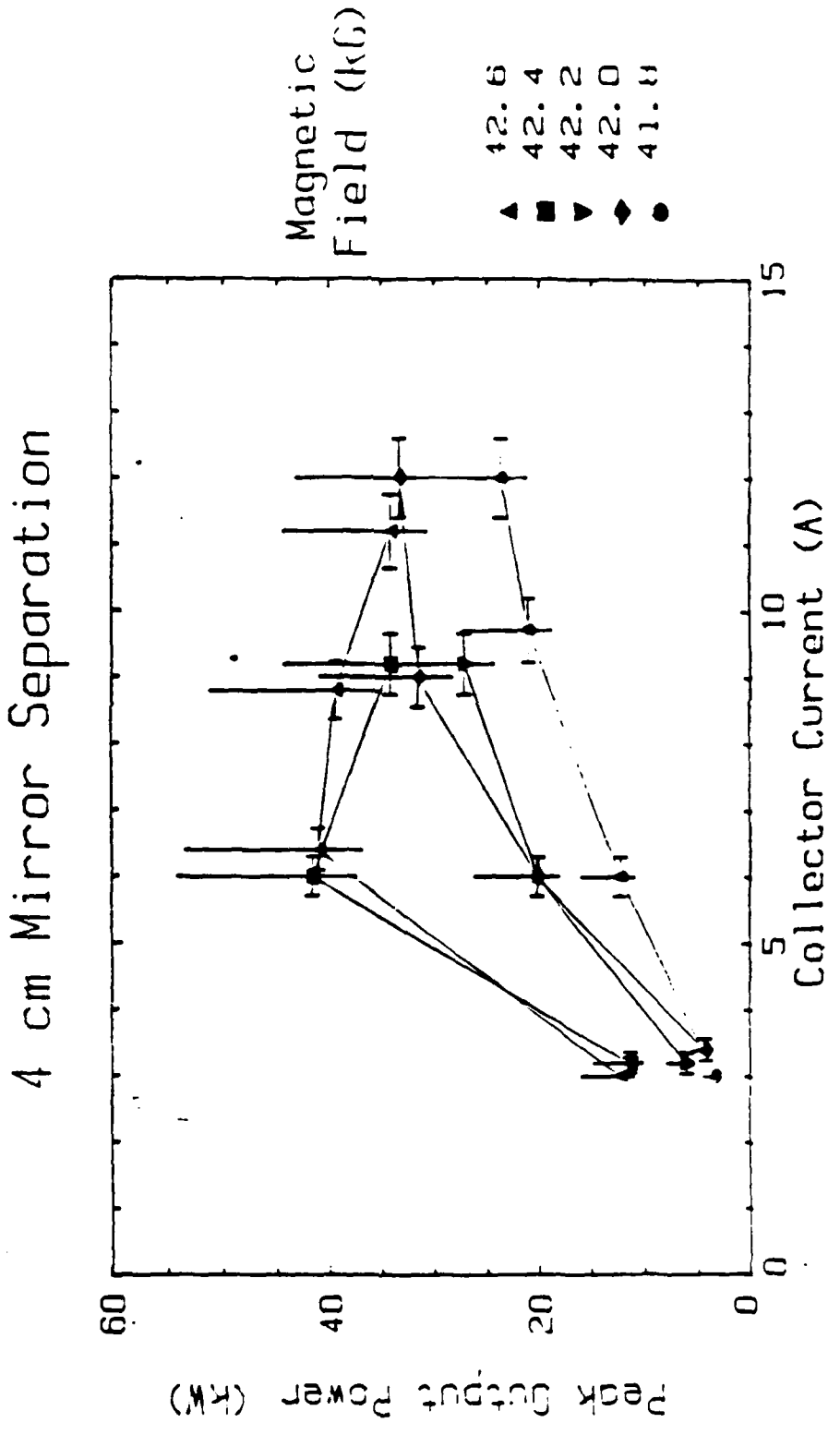
Magnetic Field (kG)
42.6
42.4
42.2
42.0
41.8
4 cm Mirror Separation
Collector Current (A)
0
5
10
15
Peak Output Power (kW)
0
20
40
60

Figure 33.

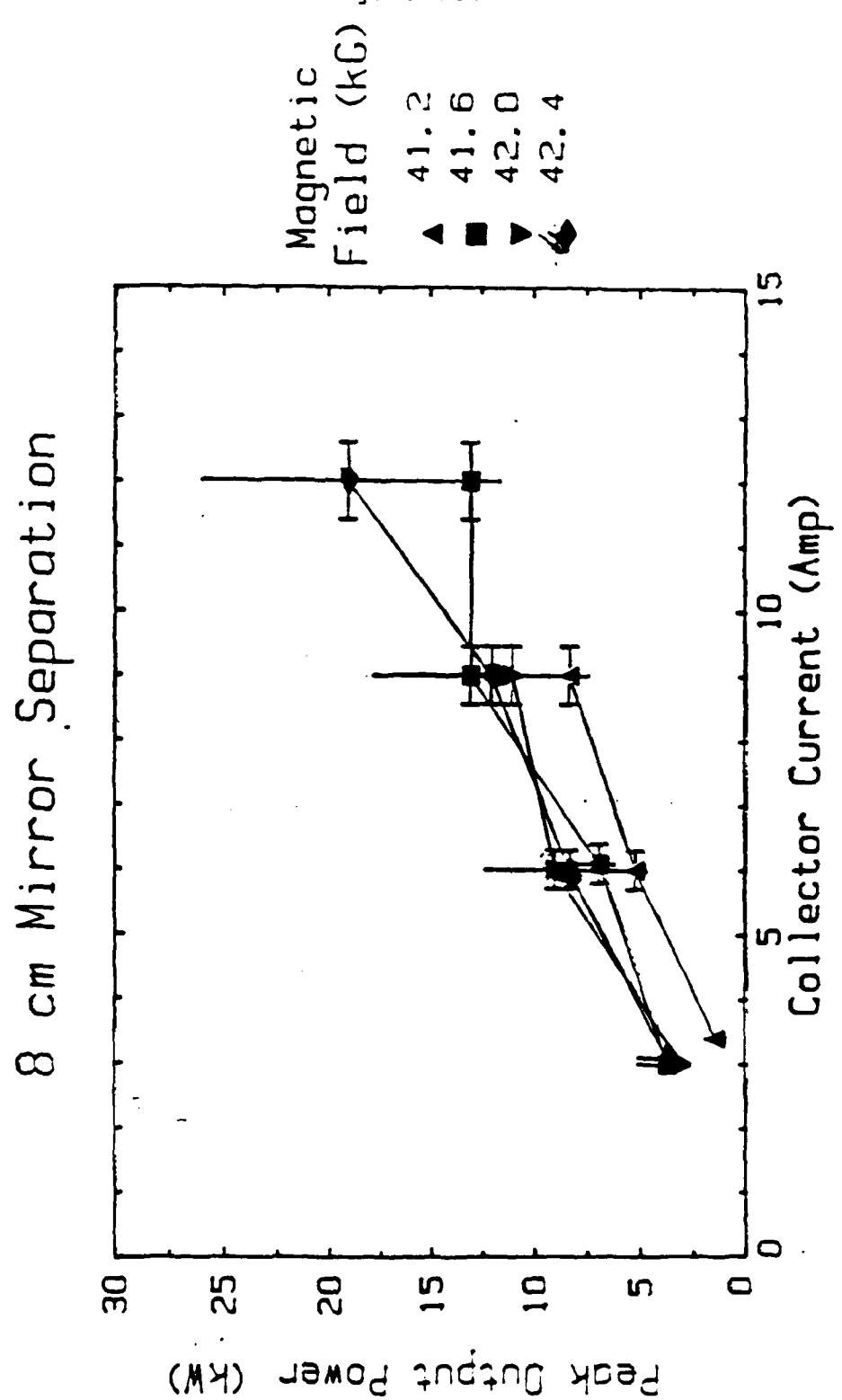
8 cm Mirror Separation
Magnetic Field (kG)
41.2
41.6
42.0
42.4
Peak Output Power (kW)
Collector Current (Amp)
0
5
10
15
20
25
30

pulse allowed more modes to evolve than was originally expected.

Cold Testing and Diagnostics

The quality factor of a microwave cavity is an important parameter. For the QO, the quality factor (Q) is on the order of hundreds of thousands. This makes it a difficult quantity to measure. Original attempts used millimeter-wave sources whose frequency jitter was too high for an accurate measurement. The current set up to measure high Q cavities such as this uses a 94 GHz impatt oscillator. This is a stable enough oscillator for Qs up to 200,000 to have been measured. This system uses six inch diameter mirrors to study the effects of coupling, alignment, separation and other properties of a quasi-optical resonator.

An existing Fabry-Perot interferometer has been thoroughly characterized. This interferometer is used in the bench measurement of Q. The interferometer has also been used as a frequency diagnostic on the operating experiments. It provides a good alternative to the heterodyne in that this is a more linear device than the heterodyne. The use of two alternate frequency diagnostics is important in that they can be compared with each other, discrepancies investigated and corrected. This greatly reduces the possibility of erroneous frequency measurements.

It is difficult to measure the quality factor of the QO in-situ because there is no access to the cavity. The bench measurements are done by injecting the microwaves directly into the cavity by means of small coupling holes in the center of the cold test mirrors that do not exist in the actual resonator mirrors. High order radial and azimuthal modes have been examined in both the six inch cavity and the interferometer. Because this set up has measured Qs of up to 200,000, it is suitable for measuring Qs for all the quasi-optical cavities of immediate interest.

A great deal of effort has gone into making accurate frequency and mode amplitude measurements. The schematic of the basic components of the heterodyne is provided in Figure 34. To this end a heterodyne frequency measuring system was put to use for the QO. Its first application, as mentioned earlier in this report, was with the large cavity QO. While frequency information was easily gathered from the heterodyne, it was later determined that to get information about relative mode strengths would require much more development.

It was determined that the variations in the output power of the YIG (a GaAs solid state microwave source known for its frequency stability) tuned oscillator as the frequency was swept, made it impossible to keep the local oscillator (LO) input power within the operating range of the harmonic mixer. Original attempts at leveling the LO power included varying the input voltages to the YIG oscillator. This method was immediately abandoned because it had a greater effect on the operating frequency than on the output power. A variable attenuator was then placed between the YIG and the harmonic mixer. The settings of the attenuator were checked periodically throughout a frequency sweep in an attempt to limit input power variations. Finally a feedback loop which monitored the power into the mixer, compared it to a preselected power level, and automatically adjusted a PIN diode variable attenuator, until the two levels matched, was incorporated. The time constant of this circuit was faster than the variance in power anywhere in the frequency range of the YIG, thus ensuring a constant level of LO power during a measurement.

A pair of harmonic mixers have been tested under various conditions to model the experiment. Several problems have been discovered with the mixers that required factory modifications. These modifications have been completed and the mixers appear to have a small enough frequency dependance to be useful for amplitude measurements.

Heterodyne Diagnostic

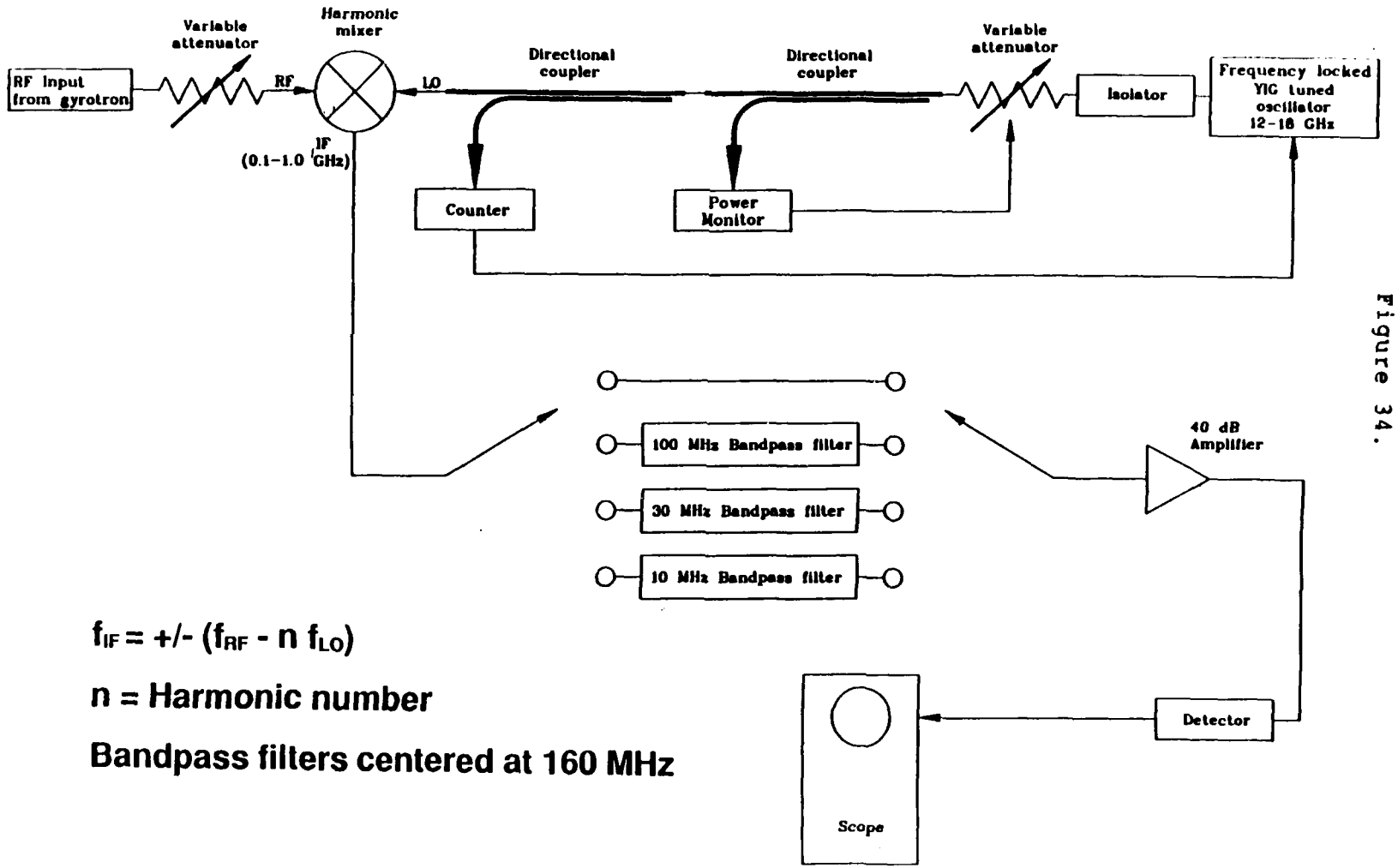

$f_{IF} = +/- (f_{RF} - n f_{LO})$

n = Harmonic number

Bandpass filters centered at 160 MHz

Figure 34.

A test was also performed on the waveguide used to transmit signals back to the control room. The waveguide had large frequency-dependant losses due to mode conversion. The heterodyne system was then moved next to the experiment in order to eliminate this section of waveguide. Frequency measurements of the various QO modes are now much more believable.

New Large Mirror Separation Experiments

The next step was the installation of a different cavity. This cavity consisted of mirrors with a radius of curvature about 1/4 of that of the previous mirrors, and about 1/4 greater in diameter. The cavity would be operated over a variable length of 20-28 cm. This would create a cavity with a Q about 10-20 times greater than the previous one. Data on the two cavities is provided in Tables 7 and 8. This cavity length was considered cw relevant since it would reduce ohmic heating of the mirrors to an acceptable level.

At this time a cold test was done to determine at what distance from the center of the cavity a metal tube coaxial with the electron beam could be placed without measurably affecting the microwave properties of the cavity. The result of this measurement was that for cavities of interest the tube could be placed approximately two waist lengths from the center of the cavity. The beam waist is the minima of the Gaussian beam formed between the two mirrors; this is where the wave front between the two mirrors is planar. The beam waist location and length can be easily calculated for a given cavity. For a symmetrical cavity such as this, the waist is centered between the two mirrors. Coinciding with the introduction of the new cavity, the drift tube and the collector were both extended so that they were each about one inch from the center of the cavity, or a total of two inches apart. This distance places both pieces

Table 7.

Cavity 1

Radius of curvature (R_c)	160 cm
Mirror diameter (2a)	3.8 cm
Mirror separation (d)	2, 4, 8 cm
Frequency (f)	110 GHz
Wavelength (λ)	0.27 cm
Longitudinal mode spacing ($\delta f/f$)	6.8, 3.4, 1.7 %
Radiation waist radius (ω_0)	1.05, 1.24, 1.47 cm
ω_0/λ	3.8, 4.6, 5.4
μ (E=60 keV, α=1)	7.6, 9.0, 10.7
Q (2 cm)	3800 (measured)
Q (4.5 cm)	7200 (measured)
Q (8 cm)	3865 (calculated)
Transmission (round trip, 8 cm)	9.5 % (calculated)
Ohmic Losses	0.25 %
Fresnel number ($a^2/\lambda d$)	6.6, 3.3, 1.7
G ($(1-d/R_c)a_1/a_2$)	0.99, 0.98, 0.95

Table 8.

Cavity 4

Radius of curvature (R_c)	38.7 cm
Mirror diameter (2a)	5.0 cm
Mirror separation (d)	21, 25, 29 cm
Frequency (f)	110 GHz
Wavelength (λ)	0.27 cm
Longitudinal mode spacing ($\delta f/f$)	0.65, 0.55, 0.47 %
Radiation waist radius (ω_0)	1.2, 1.3, 1.3 cm
ω_0/λ	4.5, 4.6, 4.7
μ (E=60 keV, α=1)	8.9, 9.1, 9.3
Q (calculated)	79400, 40600, 41200
Transmission (round trip)	1.2, 2.8, 3.2 %
Ohmic Losses	0.25 %
Fresnel number ($a^2/\lambda d$)	1.1, 0.92, 0.79
G ($(1-d/R_c)a_1/a_2$)	0.46, 0.35, 0.25

about 1 inch each from the cavity center. Looking again at Table 8 one can see that 1 inch, which is 2.54 cm, is very close to twice the waist length of the cavity over its entire range of mirror separations. The drift tube and collector were formally over four inches apart. They were extended in order to limit the space charge build up in the cavity region. This would allow a higher quality beam in the interaction region of the gyrotron without adversely affecting the cavity.

Also at this time the problem of trim coil overheating was addressed. The trim coils originally used on the large cavity IGC experiment and on the small cavity AMI experiment were commercially made items. Both failed after a limited amount of use. It was originally thought that the magnets had overheated and had melted their insulation, partially shorting the coils. A new magnet with thermal cutout switches was ordered as a replacement. In conjunction with this new protection a new heat exchanging system based around an automotive radiator was installed. This system which was an air cooled heat exchanger was placed in series with the water cooled exchanger already in service. At this time a cooling leg from this circuit was installed on the collector to allow for a greater duty cycle. The new trim coil failed again shortly after its installation. It was later determined that this failure, at least, was not the result of overheating but an unexplained chemical deposition on the coils. The improved heat exchanging capabilities, however, allowed the use of the original trim coil from the first QO to be used over much higher current levels than was previously possible.

With the new larger cavity several groups of studies were undertaken.[18] The first group was a series of

---

18. High Power Electromagnetics Branch,"Review of the NRL Quasi- Optical Gyrotron Program", presented to DOE, June 22, 1988.

threshold current studies. Measuring the effects of magnetic field, mirror separation and beam position on start currents. The results of these studies are summarized in Figures 35 through 37. The second set of studies were efficiency and power studies. Comparisons were made of the effects of voltage, current, magnetic field, magnetic field taper across the cavity and mirror separation. See Figures 38 through 46. Another set of studies were made of the frequency tuning capabilities of the QO. The findings of these studies are shown in Figures 47 and 48.

These studies resulted in several accomplishments.[19] A maximum peak power of 150 kW was demonstrated. This was nearly double the previous power levels of any NRL QO experiment. Power enhancement was demonstrated by the use of tapered magnetic fields. The QO was operated across a large parameter space where efficiency was over 10 percent. Magnetic field frequency tuning was demonstrated from 98-130 GHz. This was limited on the high side by the maximum field of the magnet and on the low side by the cutoff frequency of the diagnostics. Voltage tuning of 4 percent was also demonstrated. These accomplishments show the QO to be an extremely wide band high power source.

Higher Power Experiments

Conceptual designs for the next set of experiments on the QO had begun. A collection of these concepts is shown on Figure 49. These include the use of a double mylar window to better protect the new Varian VUW-8144 electron gun. A probe is to be placed on the collector end, between the two peaks of the magnetic field, to measure space charge build up during the pulse. Provisions are to be made for an accelerating voltage at the tip of the collector assembly, to reduce the effects of spacecharge. The beam collection will be outside the magnet dewar for enhanced cooling and

---

19. Ibid.

Figure 35.

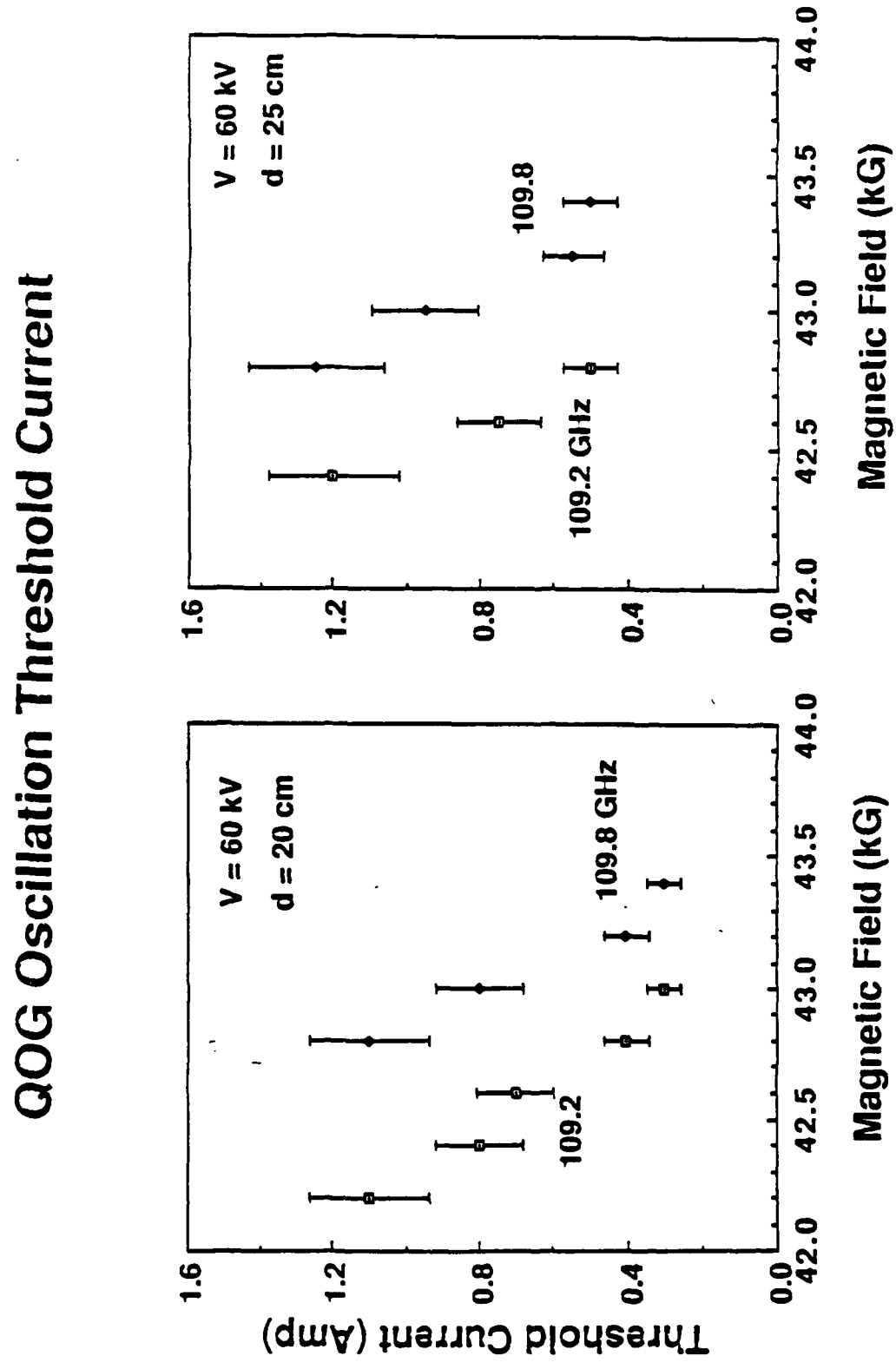
QOG Oscillation Threshold Current
Threshold Current (Amp)
V = 60 kV
d = 20 cm
109.2
109.8 GHz
V = 60 kV
d = 25 cm
109.8
109.2 GHz
Magnetic Field (kG)
Magnetic Field (kG)
1.6
1.2
0.8
0.4
0.0
42.0
42.5
43.0
43.5
44.0

Figure 36.

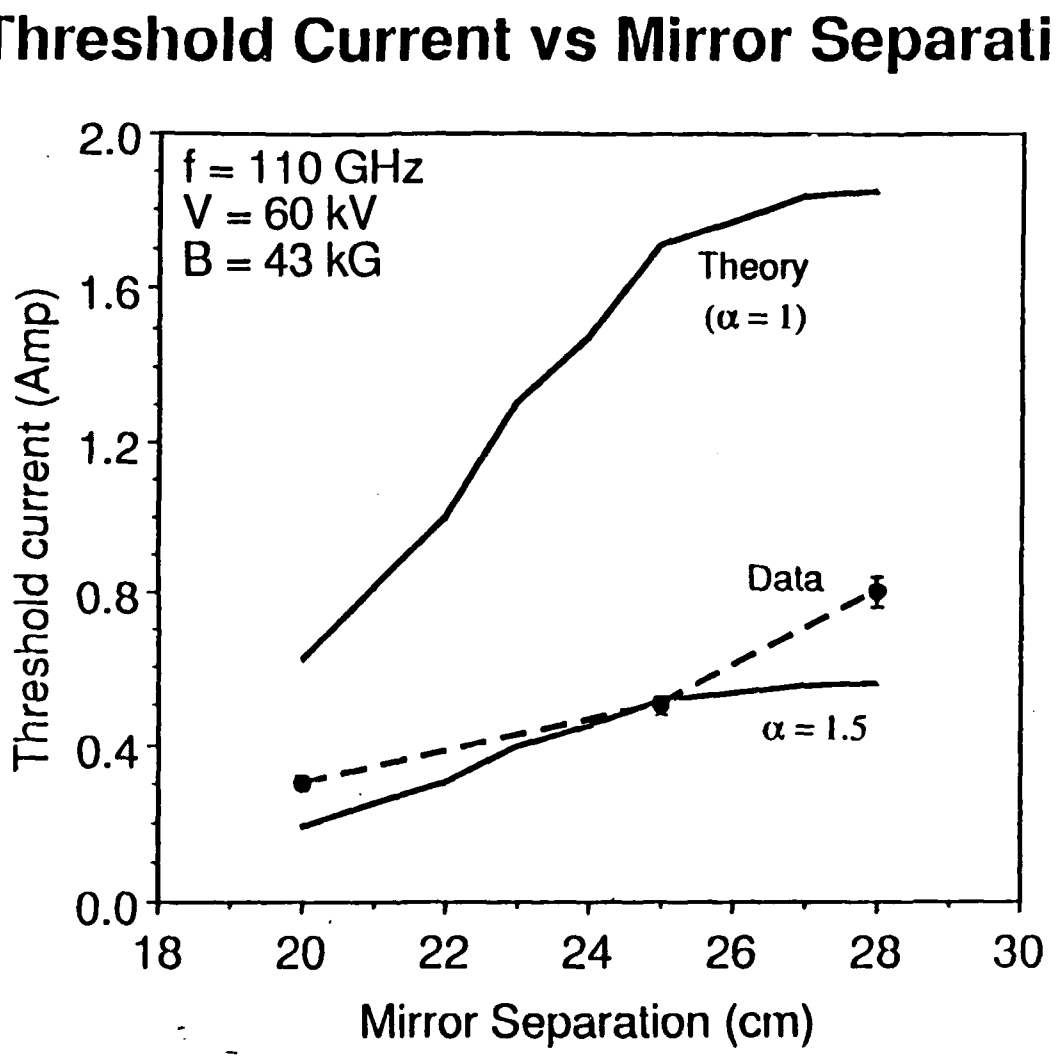
Threshold Current vs Mirror Separation
f = 110 GHz
V = 60 kV
B = 43 kG
Theory
(α = 1)
Data
α = 1.5
Threshold current (Amp)
2.0
1.6
1.2
0.8
0.4
0.0
18
20
22
24
26
28
30
Mirror Separation (cm)

Figure 37.

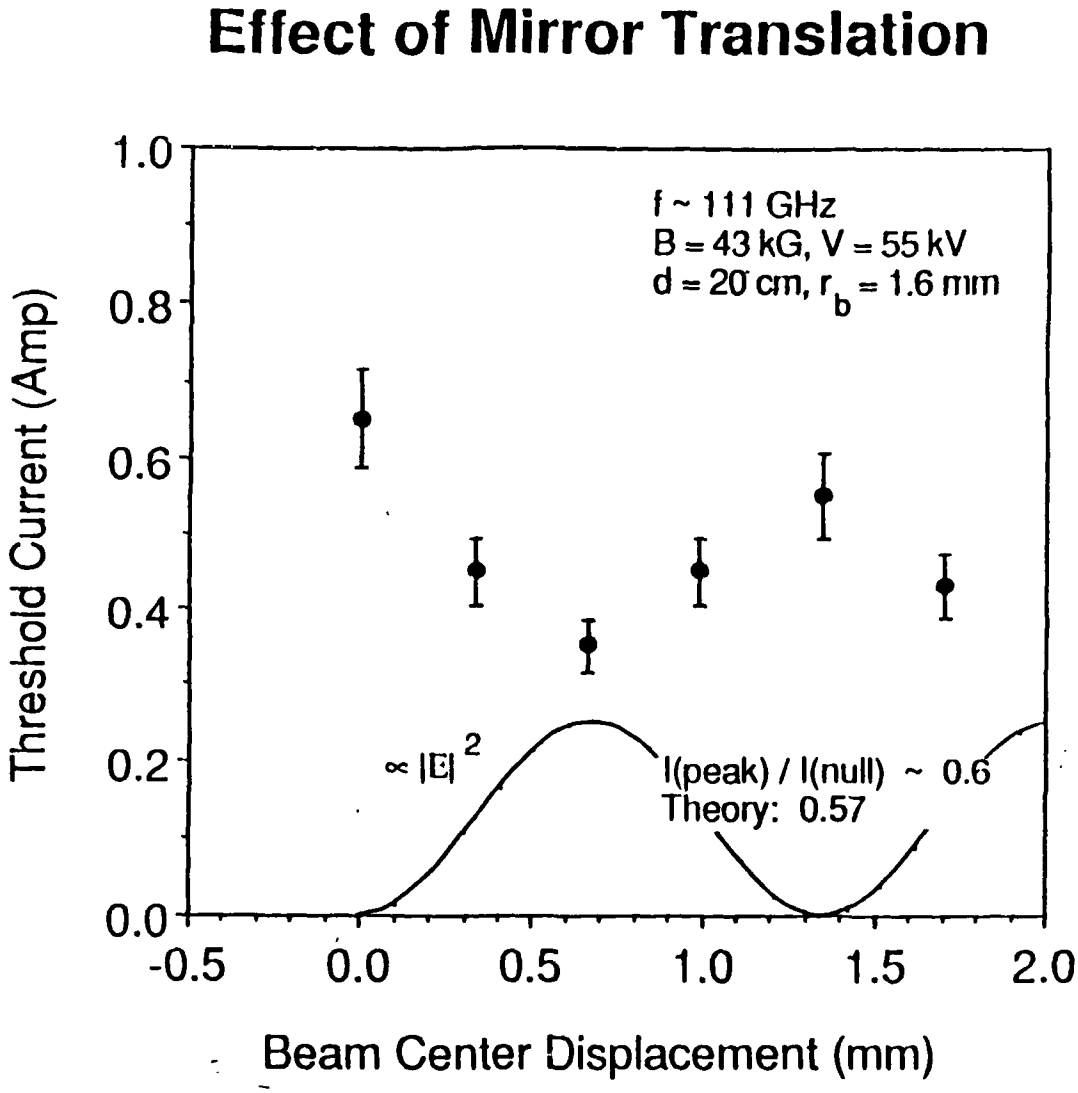
Effect of Mirror Translation
f ~ 111 GHz
B = 43 kG, V = 55 kV
d = 20 cm, r_b = 1.6 mm
∝ |E|^2
I(peak) / I(null) ~ 0.6
Theory: 0.57
Threshold Current (Amp)
Beam Center Displacement (mm)
1.0
0.8
0.6
0.4
0.2
0.0
-0.5
0.0
0.5
1.0
1.5
2.0

Figure 38.

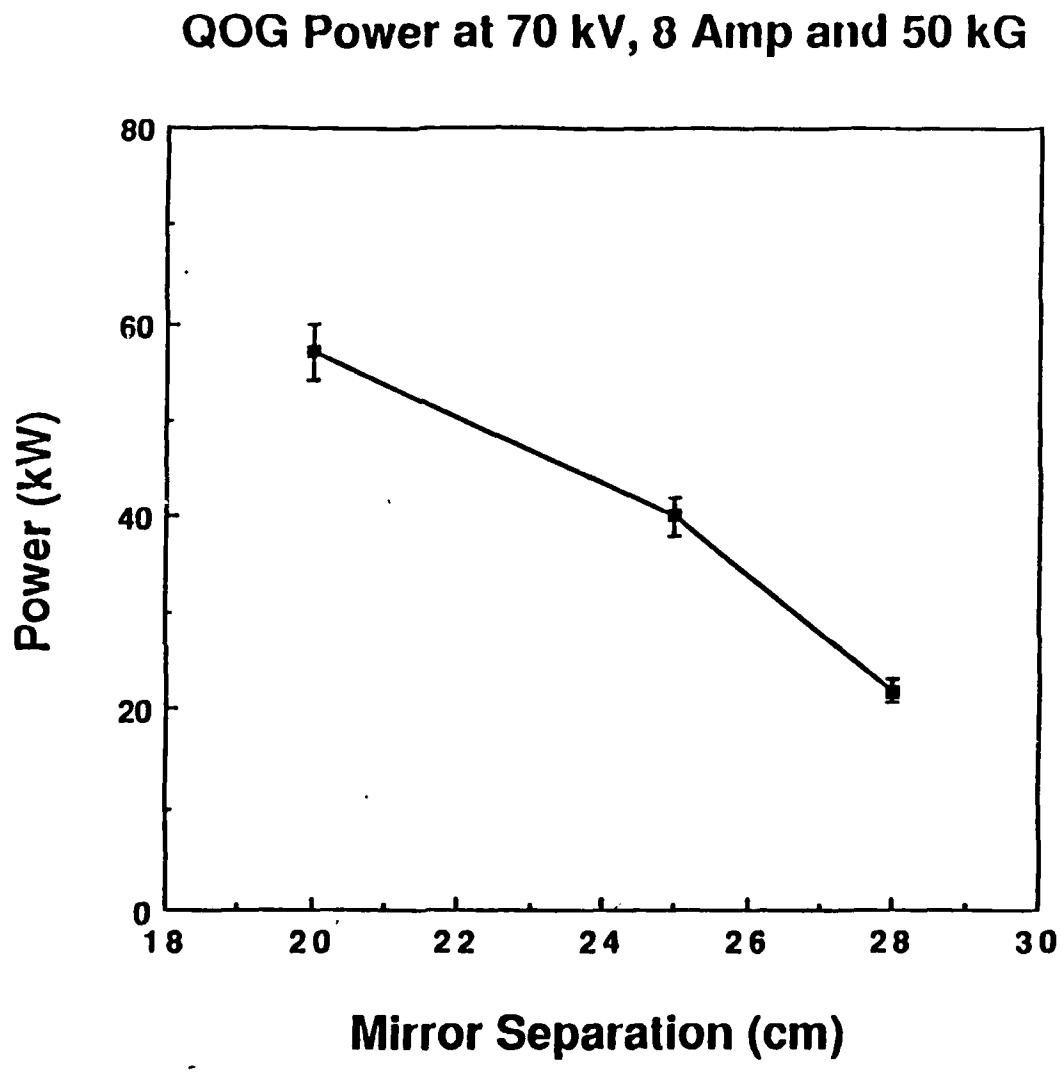
QOG Power at 70 kV, 8 Amp and 50 kG
Power (kW)
80
60
40
20
0
18
20
22
24
26
28
30
Mirror Separation (cm)

Figure 39.

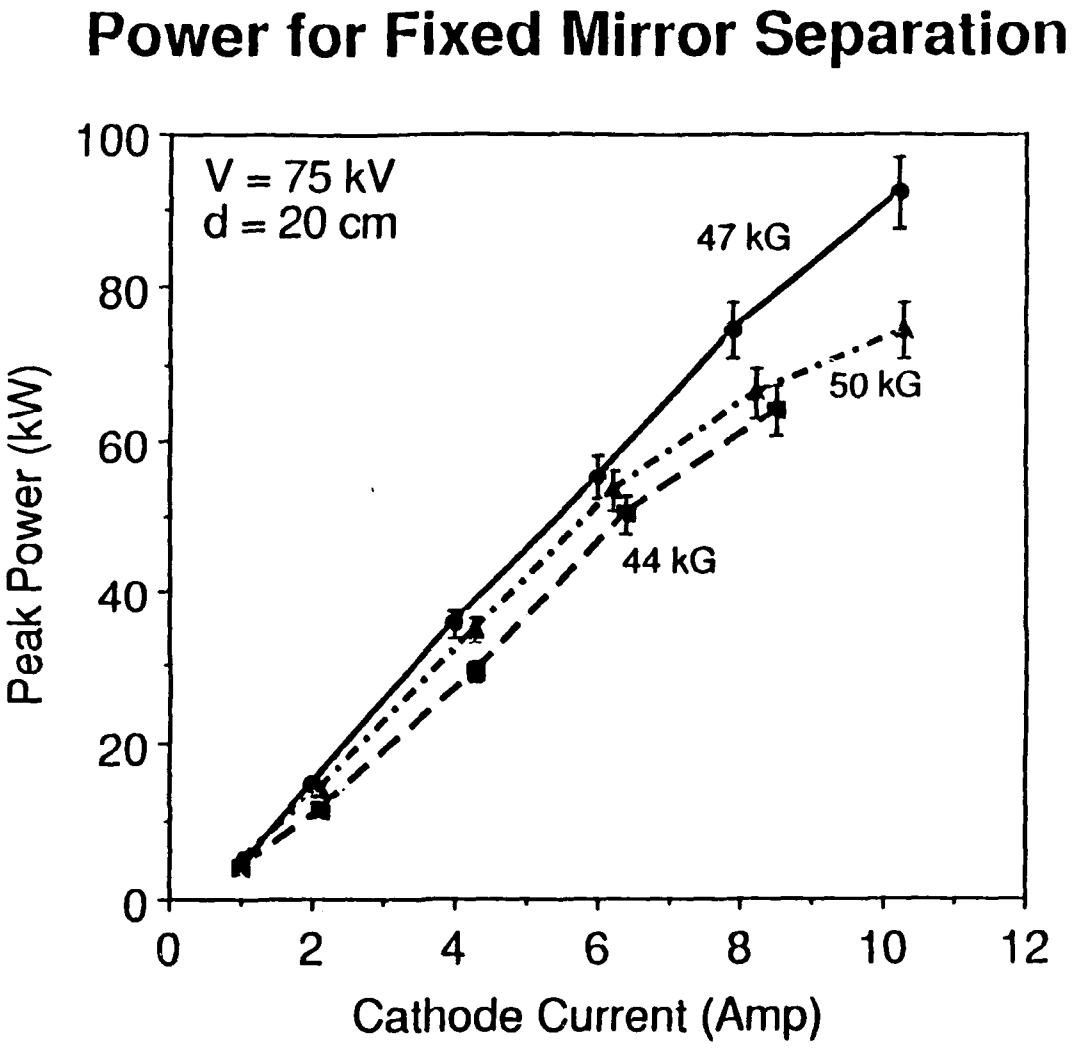
Power for Fixed Mirror Separation
V = 75 kV
d = 20 cm
47 kG
50 kG
44 kG
Peak Power (kW)
Cathode Current (Amp)
0
20
40
60
80
100
0
2
4
6
8
10
12

Figure 40.

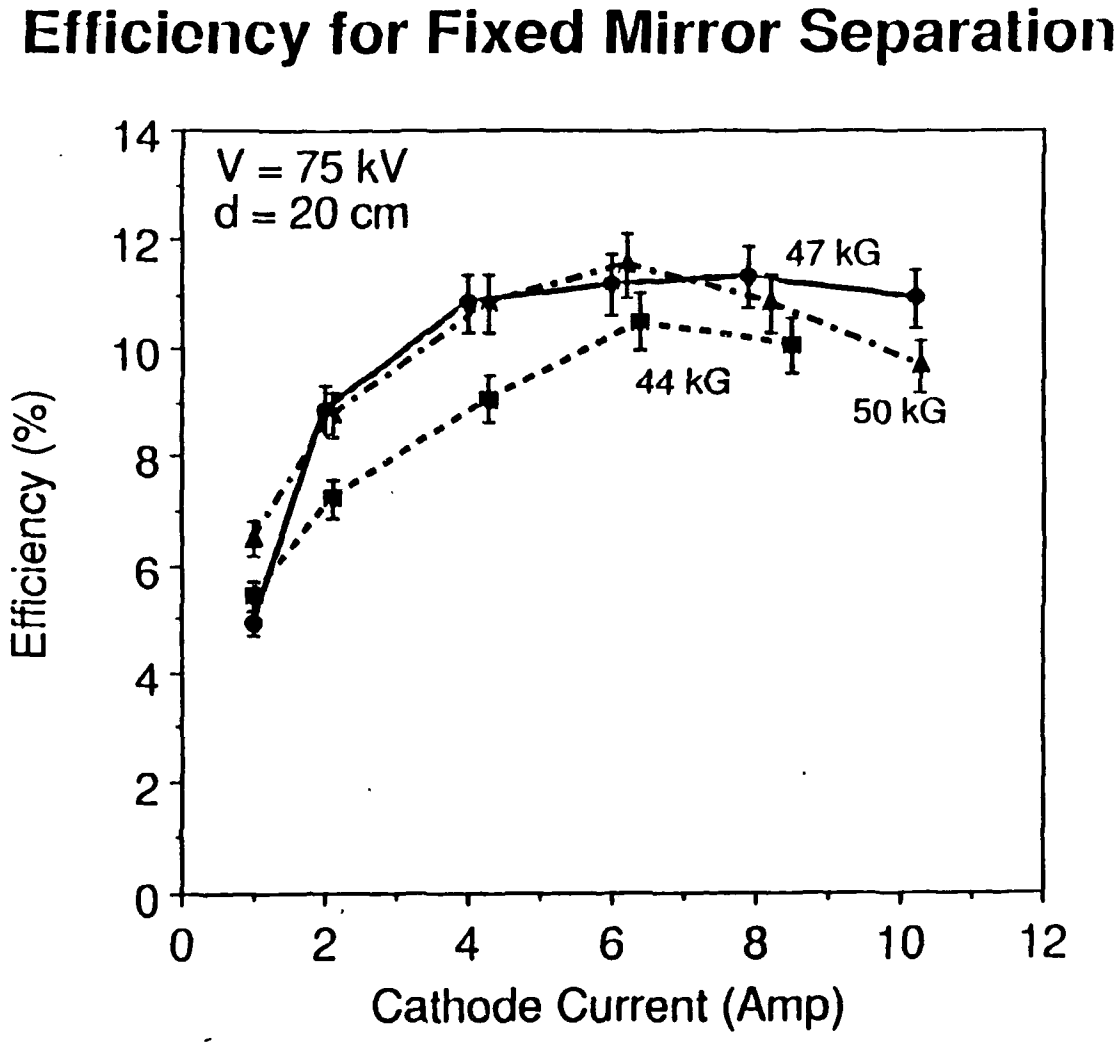
Efficiency for Fixed Mirror Separation
V = 75 kV
d = 20 cm
47 kG
44 kG
50 kG
Efficiency (%)
Cathode Current (Amp)
0
2
4
6
8
10
12
14

Figure 41.

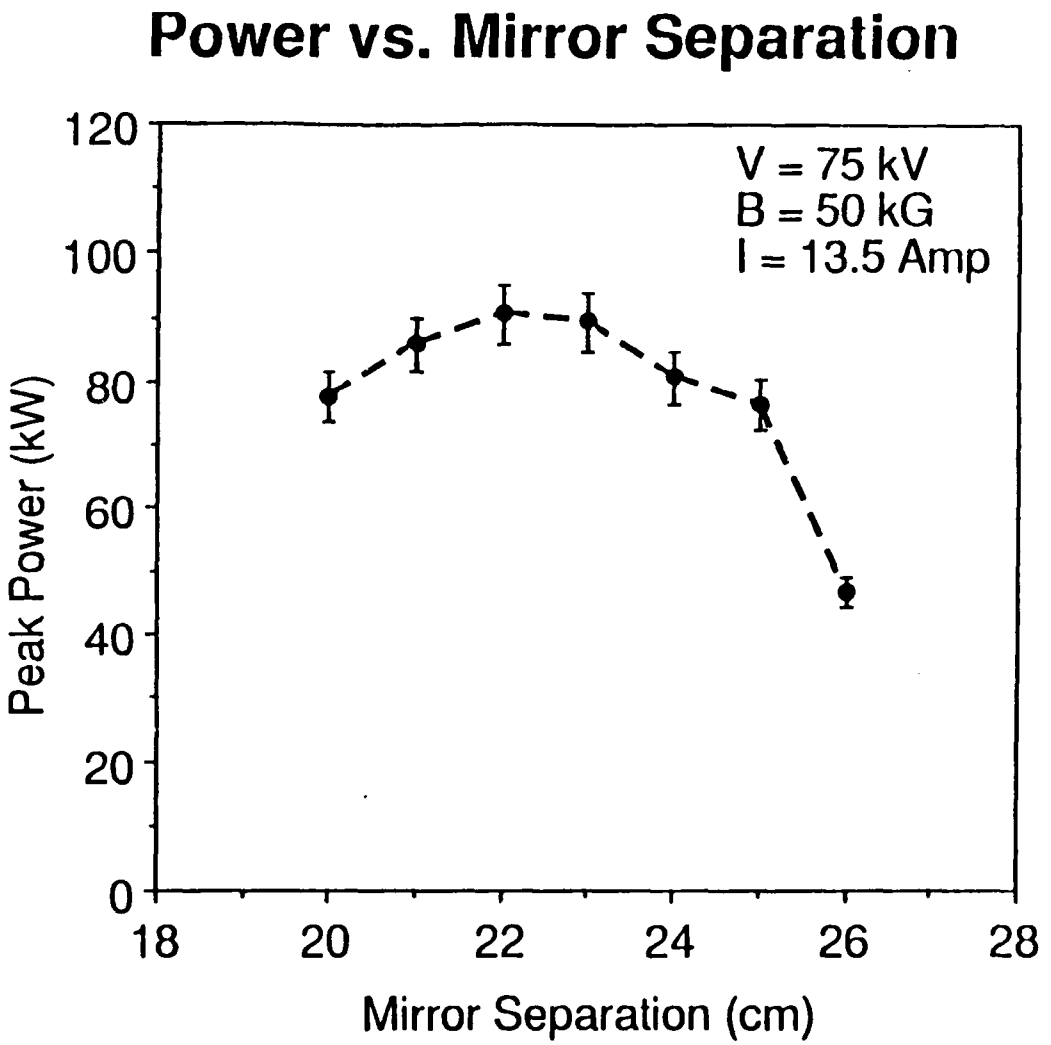
Power vs. Mirror Separation
V = 75 kV
B = 50 kG
I = 13.5 Amp
Peak Power (kW)
120
100
80
60
40
20
0
18
20
22
24
26
28
Mirror Separation (cm)

Figure 42.

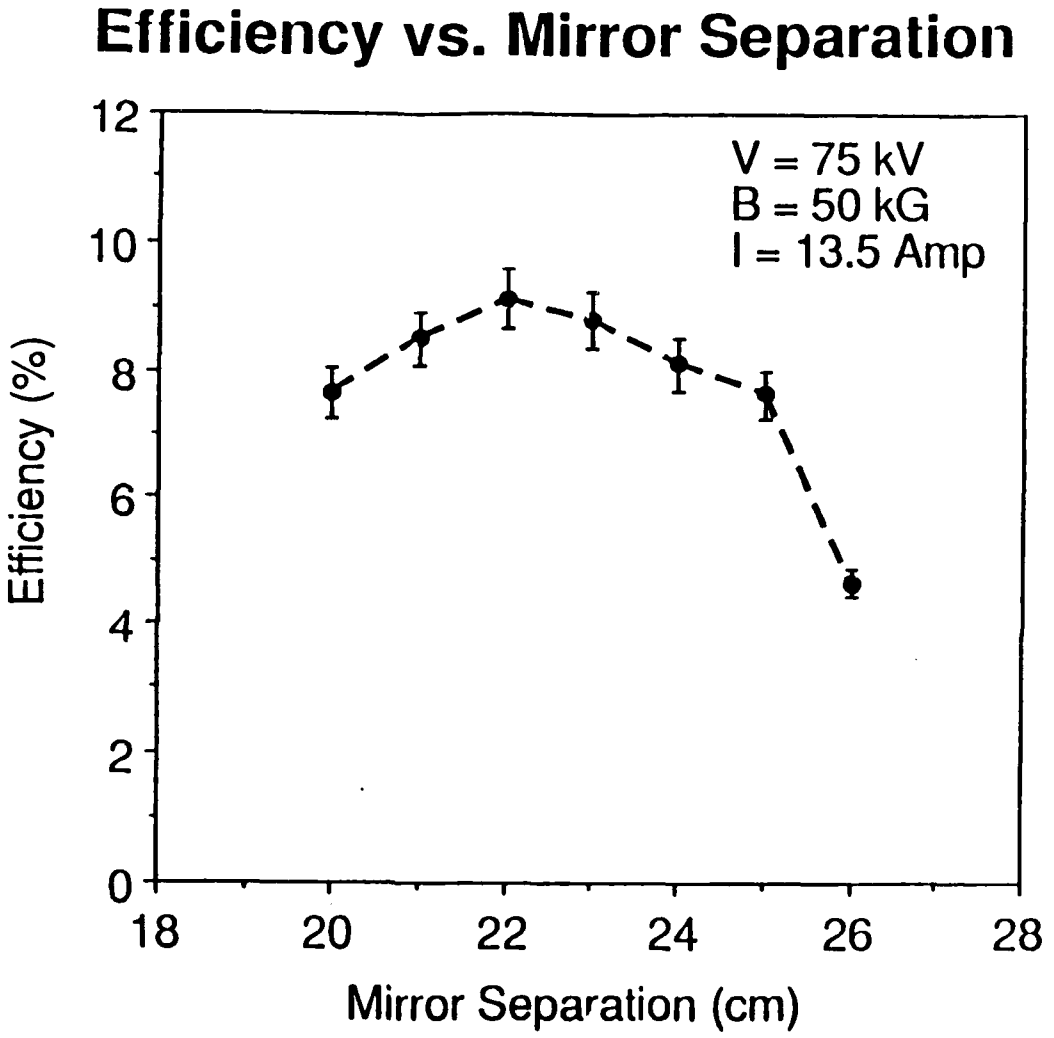
Efficiency vs. Mirror Separation
V = 75 kV
B = 50 kG
I = 13.5 Amp
Efficiency (%)
0
2
4
6
8
10
12
18
20
22
24
26
28
Mirror Separation (cm)

Figure 43.

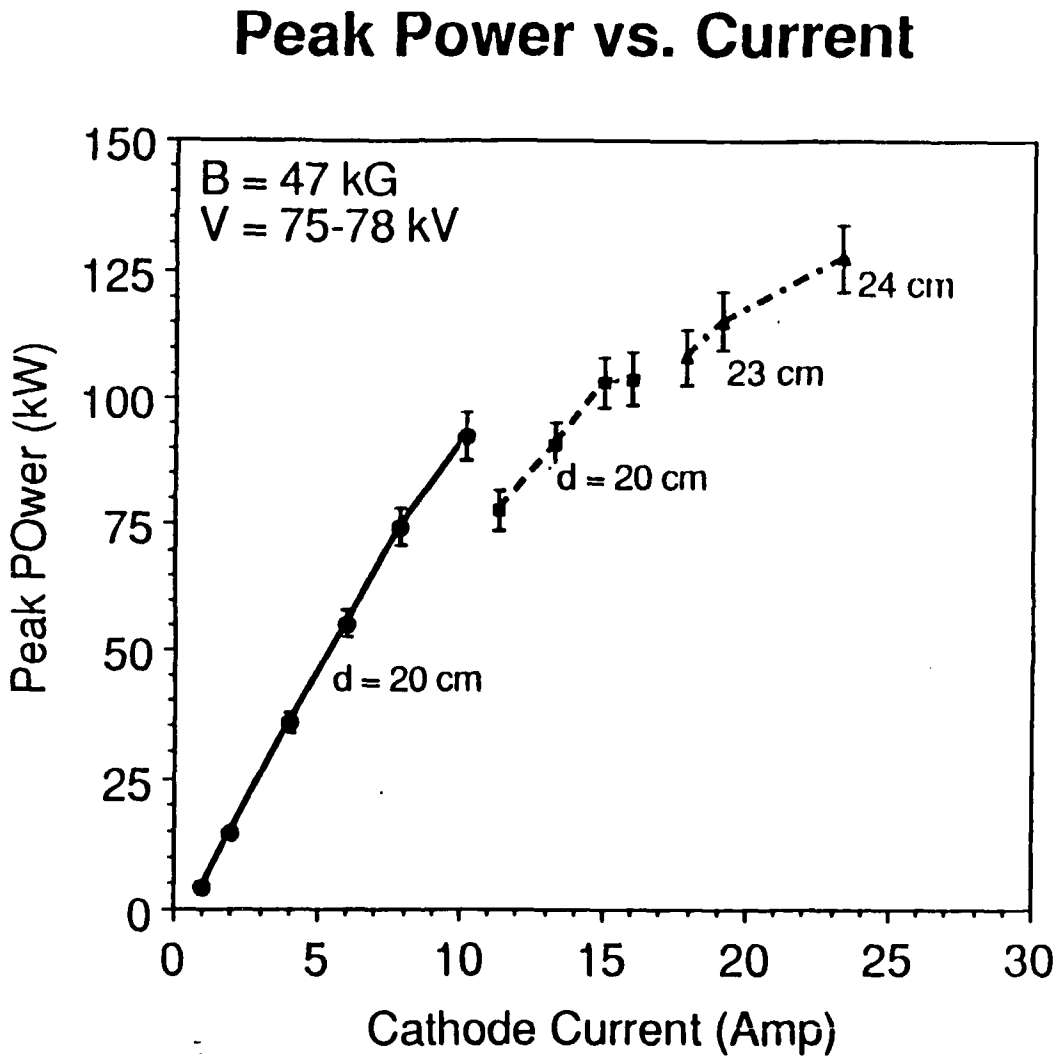
Peak Power vs. Current
B = 47 kG
V = 75-78 kV
d = 20 cm
d = 20 cm
23 cm
24 cm
Peak POwer (kW)
Cathode Current (Amp)
0
25
50
75
100
125
150
0
5
10
15
20
25
30

Figure 44.

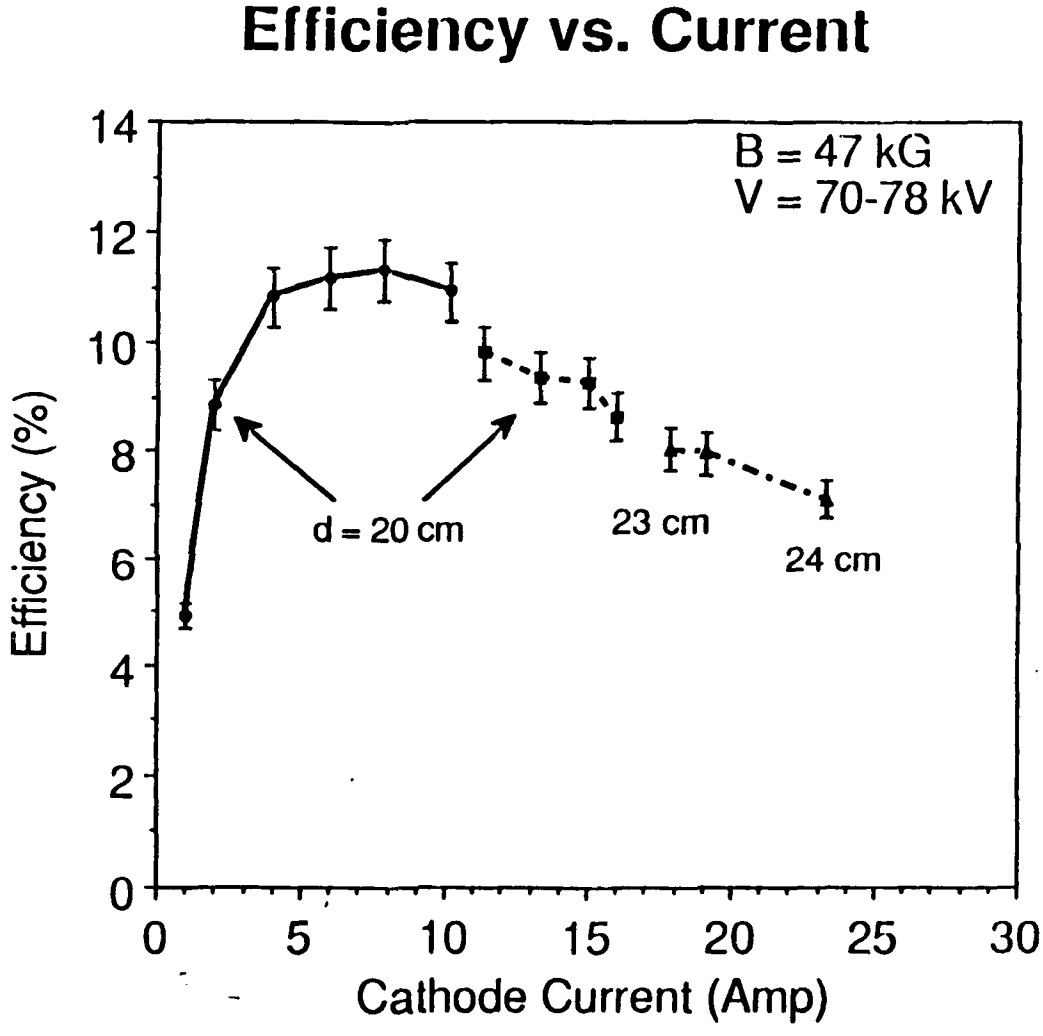
Efficiency vs. Current
B = 47 kG
V = 70-78 kV
d = 20 cm
23 cm
24 cm
Efficiency (%)
Cathode Current (Amp)
0
2
4
6
8
10
12
14
0
5
10
15
20
25
30

Figure 45.

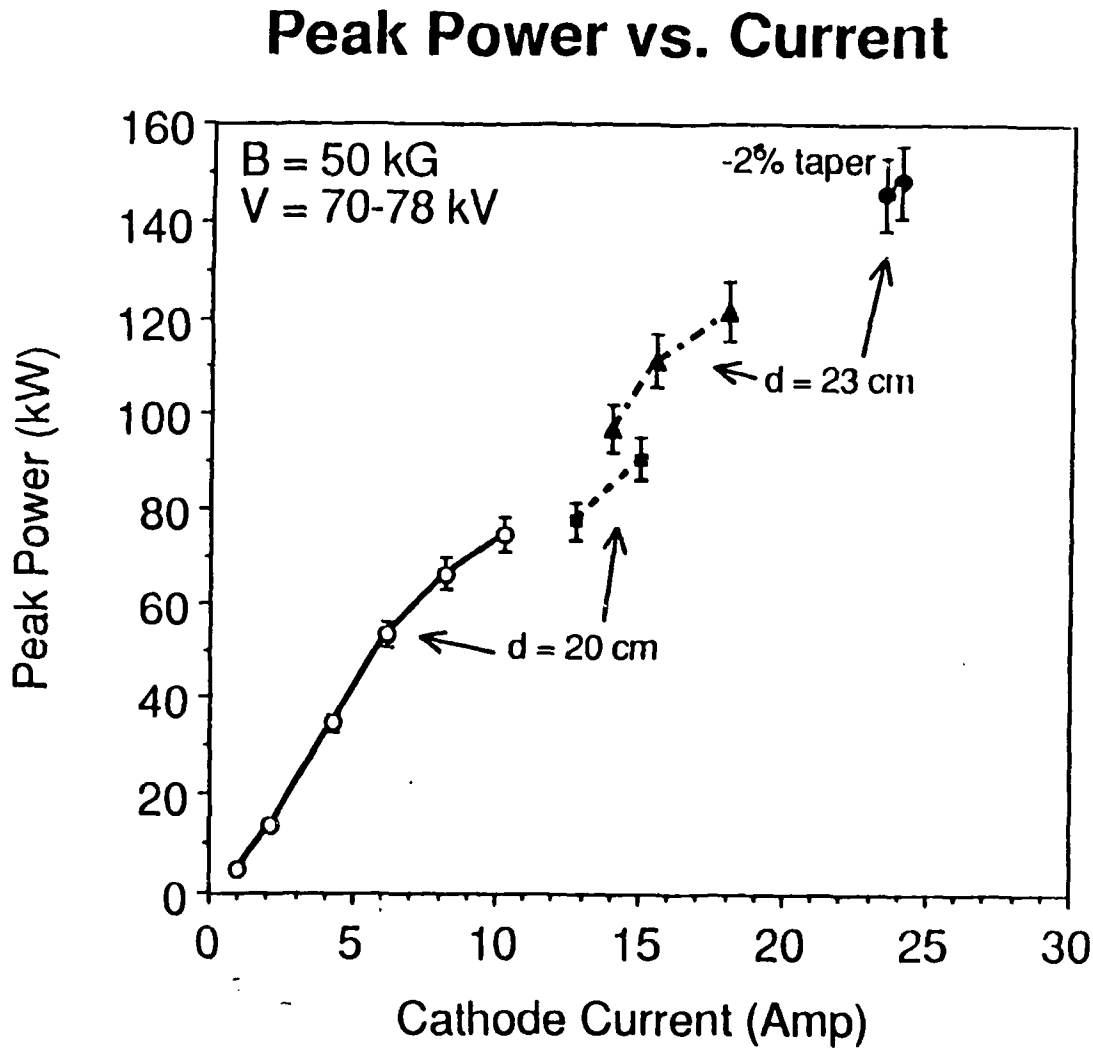
Peak Power vs. Current
B = 50 kG
V = 70-78 kV
-2% taper
d = 23 cm
d = 20 cm
Peak Power (kW)
Cathode Current (Amp)
0
20
40
60
80
100
120
140
160
0
5
10
15
20
25
30

Figure 46.

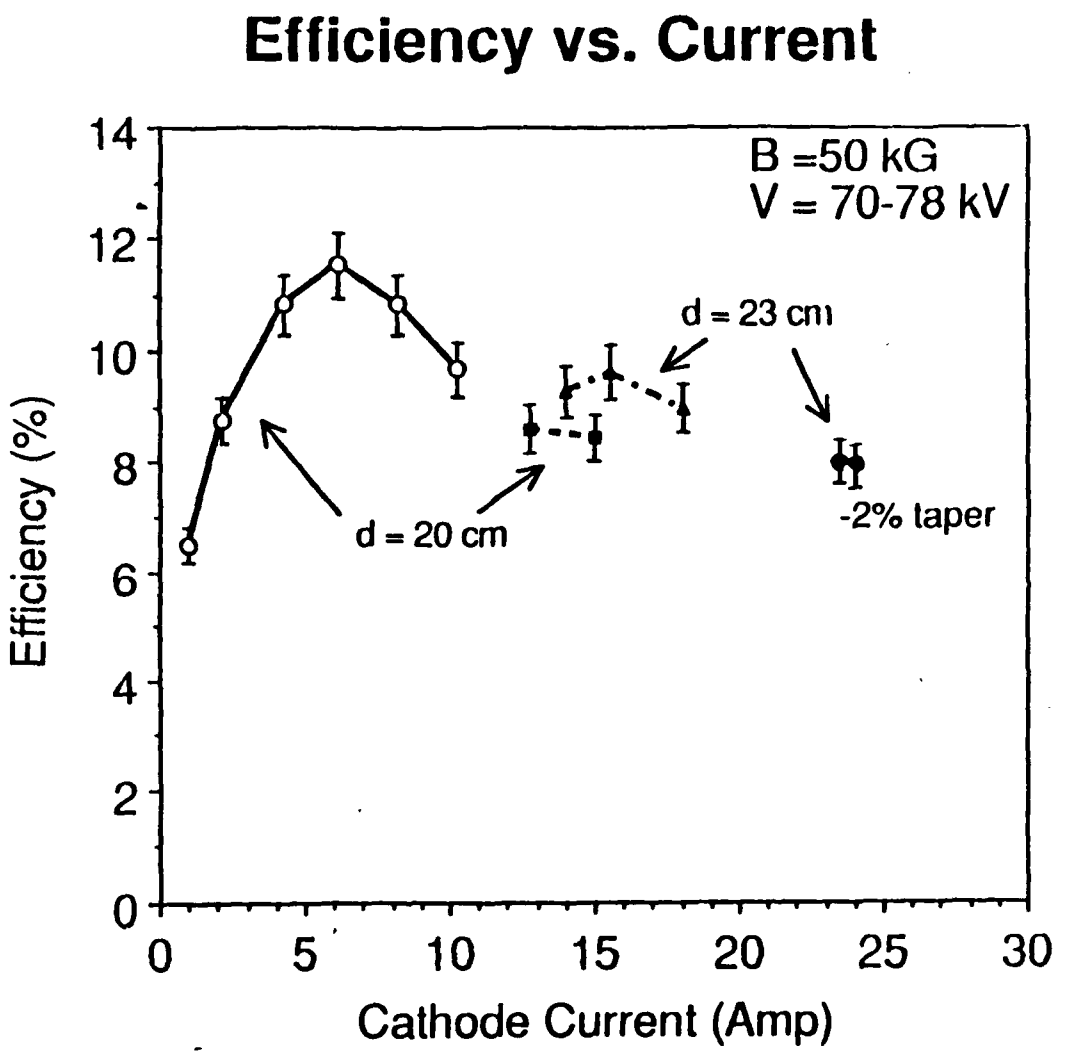
Efficiency vs. Current
B =50 kG
V = 70-78 kV
d = 23 cm
d = 20 cm
-2% taper
Efficiency (%)
Cathode Current (Amp)
0
2
4
6
8
10
12
14
0
5
10
15
20
25
30

Figure 47.

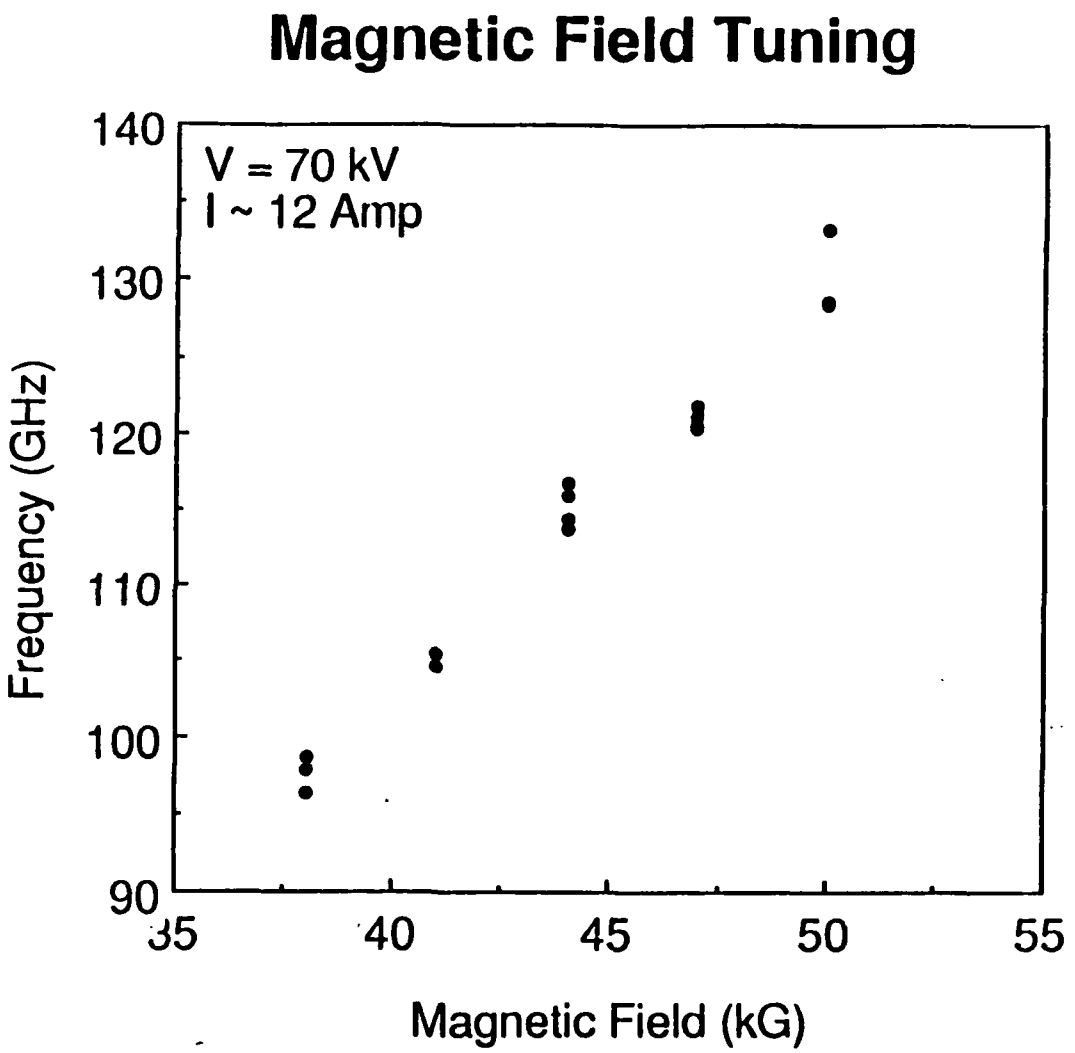
Magnetic Field Tuning
V = 70 kV
I ~ 12 Amp
Frequency (GHz)
140
130
120
110
100
90
35
40
45
50
55
Magnetic Field (kG)

Figure 48.

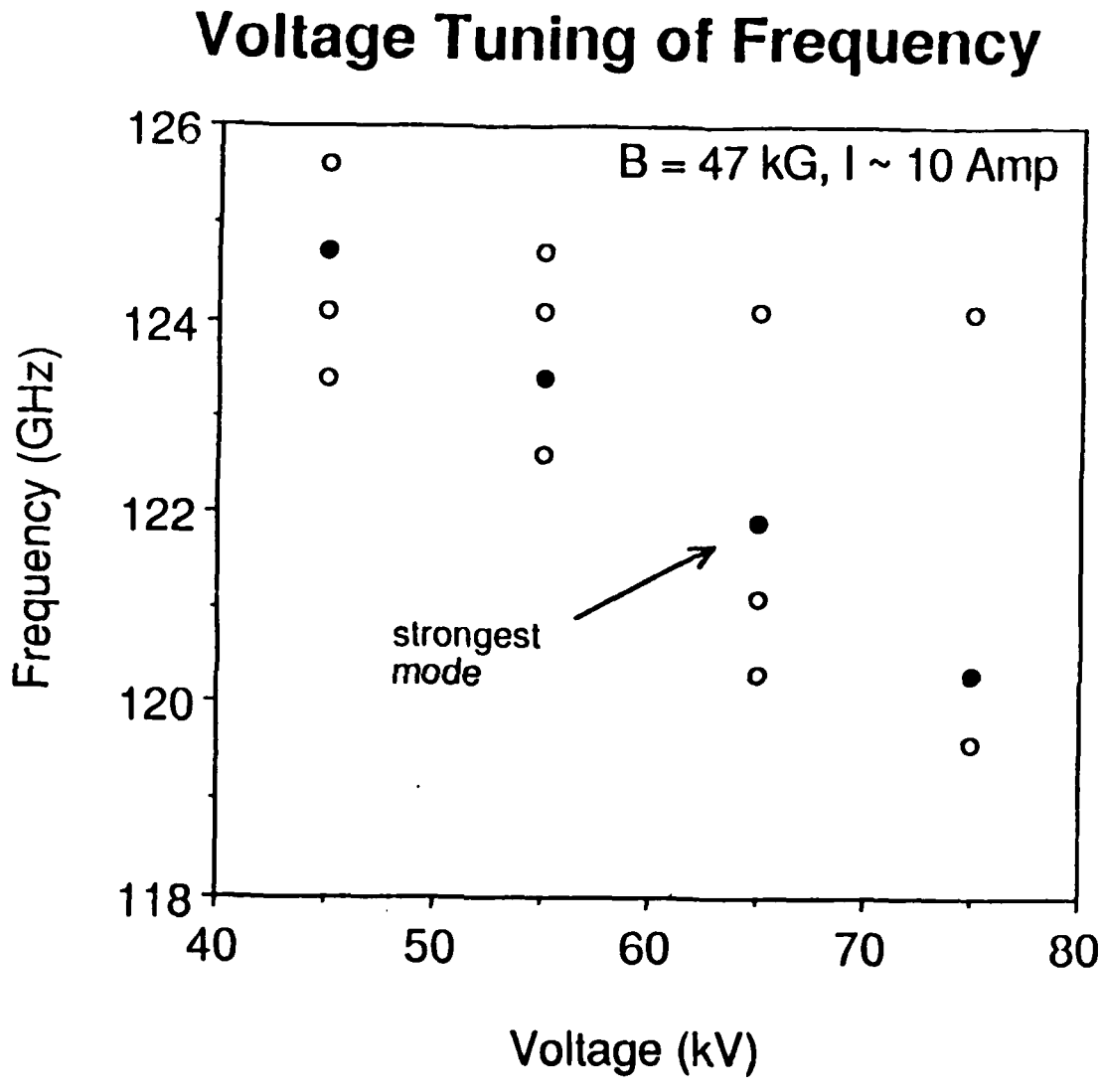
Voltage Tuning of Frequency
B = 47 kG, I ~ 10 Amp
strongest
mode
Frequency (GHz)
126
124
122
120
118
40
50
60
70
80
Voltage (kV)

Figure 49.

NRL HIGH POWER QUASI-OPTICAL GYROTRON

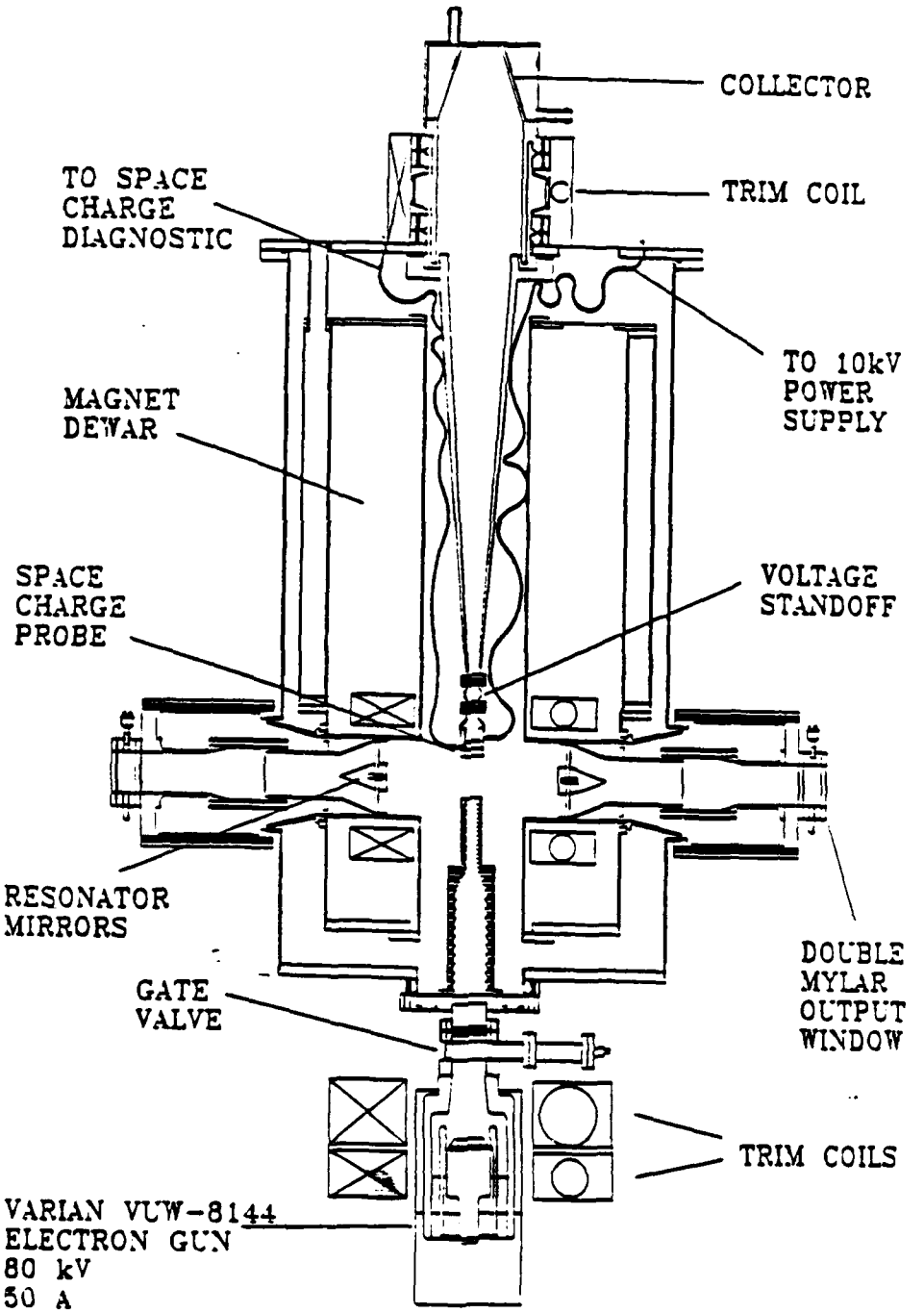

possible adaptation to a depressed collector scheme. Also included is an enhanced drift tube to handle the larger beam of the new gun.

APPENDIX A

```
c
c                              F5FIT.FOR
c
c     This program calculates  the  least squares fit between
      far field
c     data points and theory for  two modes. The data is read
      in from
c     field.dat. A logarithmic fit is used.

      parameter (npts=37,n5=5*51,k=3125,jmax=5)
      real theta(npts), pdata(npts), y(5), lsmin(jmax)
      real  x(10),   p(npts),   a(10),   b(10),  s(10),  s2,
ls(k),pmax2

      integer mi(5), ier, m(10), iw(9), ip, n,imin(jmax)
      external field5, minimum

      data mi/1,1,1,1,1/
      data y/8.53632,5.33144,14.86359,11.70600,1.84118/

c     m corresponds to the TEm,n mode
c     y is the Bessel root
c     ak  is  the  waveguide  radius  times  the  free  space
      wavenumber
c     x(i) refers to the amplitude/phase of mode i
c
c     The calculations match  those  from field5.for and were
      derrived
c     from the paper by Zhang.

      ak = 19.802
      pi = 3.14159

      open(unit=1,file='DATA',status='OLD')
      open(unit=2,file='OUTPUT',status='UNKNOWN')
999   format(1x,f5.1,1x,f5.1)

c     INPUT DATA

      do 10 i=1,npts
      read(1,999) theta(i), pdata(i)
 10   continue

      pmax2 = 0.0
      do 20 i=1,npts
      pdata(i) = pdata(i) + 40.
c      pdata(i) = 10.**((pdata(i)-pmax2)/10.)
 20   continue

c     GENERATE STARTING POINTS.
```

```
c       do 30 i=1,5
c       a(i) = 0.0
c       b(i) = 1.0
 30    continue

       a(1) = 0.2
       b(1) = 0.6
       a(2) = 0.2
       b(2) = 0.6
       a(3) = 0.
       b(3) = 0.3

       a(4) = 0.
       b(4) = 0.3

       a(5) = 2.5
       b(5) = 4.


 40    continue


c       do 120 nphi=1,10
c       do 100 nphi2=1,10

       nphi =  1
       nphi2 = 1
       x(6)=  (nphi-1) *10.*pi/180.
       x(7) = (nphi2-1)*10.*pi/180.

C     CALL IMSL ROUTINE WHICH GENERATES POINTS.

       ip = 0
       n=5

       do 80 j=1,k
       call zsrch(a,b,n,k,ip,s,m,iw,ier)

       sum = 0.0
       do 49 i=1,4
       sum = sum +s(i)
 49    continue

       do 51 i=1,4
       x(i) = s(i)/sum
c       x(i+6) = s(i+2)
 51    continue

       x(5) = s(5)
```

```
C     CALL SUBROUTINE WHICH CALCULATES THE FAR FIELD PATTERN.
C     INPUTS ARE THE MODE AMPLITUDES AND PHASES (X(10)).
C     OUTPUT IS THE PATTERN (P(NPTS)).

      call field5(x,npts,theta,y,mi,ak,p,n5)

c     Convert linear data (normalized to one) to logarithmic.

      do 58 i=1,npts
      p(i) = 10.*alog10(p(i)) + 40.
 58   continue

C     CALCULATE THE LEAST SQUARES FIT (S2).

      s2 = 0.0
      do 60 i=1,npts
      s2 = s2 +(pdata(i) - p(i))**2
 60   continue

C     PLACE EACH LEAST SQUARES FIT INTO ARRAY (LS(K)).

      ls(j) = s2

 80   continue

      do 85 i=1,jmax
      lsmin(i) = 10000.

 85   continue

      call minimum(jmax,ls,lsmin,k,imin)

C     THE FOLLOWING SECTION  FINDS  THE STARTING POINTS WHICH
      GIVE
C     THE BEST LEAST SQUARES FIT.

c       do 31 i=1,5
c       a(i) = 0.0
c       b(i) = 1.0
 31   continue


411   continue

      ip = 0


C     CALL IMSL ROUTINE WHICH GENERATES POINTS.

      do 81 j=1,k
      call zsrch(a,b,n,k,ip,s,m,iw,ier)
```

```
      sum = 0.0
      do 511 i=1,4
      sum = sum +s(i)
 511   continue

      do 512 i=1,4
      x(i) = s(i)/sum
c      x(i+6) = s(i+2)
512   continue

      x(5) = s(5)


      do 52 i=1,jmax
      if(j.eq.imin(i)) then
      write(2,997)x(1),x(2),x(3),x(4),x(5),imin(i)
      write(2,996)x(6),x(7),x(8),x(9),x(10)
      write(2,*)
      endif
 52   continue

 81   continue

      do 90 i=1,jmax
      write(2,998) nphi,nphi2, imin(i),lsmin(i)
 90   continue
998   format(1x,i5,1x,i5,1x,i5,2x,f9.1)
997   format(1x,5f7.3,i5)
996   format(1x,5f7.3)

100   continue
120   continue

      stop
      end



      subroutine minimum(jmax,ls,lsmin,k,imin)

      real ls(k),lsmin(jmax)
      integer imin(jmax)

c     This subroutine determines the minimum least squares
      fit.

      do 95 i=1,k
      ipla = 0
      do 85 j=jmax,1,-1
      if(ls(i).lt.lsmin(j)) ipla = j
 85   continue
```

```
      if(ipla.eq.1) then
      do 86 j=jmax,2,-1
      lsmin(j) = lsmin(j-1)
 86   continue
      lsmin(1) = ls(i)
      imin(1) = i

          else
          if(ipla.ne.0) then
          do 87 j=jmax,ipla,-1
          lsmin(j) = lsmin(j-1)
 87       continue
          lsmin(ipla) = ls(i)
          imin(ipla) = i
      endif
      endif
 95   continue

      return
      end

      subroutine field5(x,npts,theta,y,mi,ak,p,n5)

      real x(10),  theta(npts),y(5),  ak, p(npts), par(255),
f(5,51)
      real f2(2,51),term1,term2,term3,term4, tan1,tan2
      integer mi(5), n52
c
c     This  subroutine  calculates  power  as  a  function of
      angle.

      pi = 3.1416
c     The following DO LOOPS calculate f(theta).

      do 200 i=1,2
      do 100 j=1,npts

      yx=y(i)
      if(yx.eq.0.0) then
      f(i,j) = 0.0

      else
      sinthet=sin(theta(j)*pi/180.)
      costhet=cos(theta(j)*pi/180.)
      arg=ak*sinthet
      bonk=sqrt(1.-(yx/ak)**2)
      gamma=((1.-bonk)/(1.+bonk))**2
      x1=bonk +costhet-gamma*(bonk - costhet)
      x2=1.-(sinthet*ak/yx)**2
      f(i,j)=x1*bj(mi(i),yx)*bjprime(mi(i),arg)/x2

      x3 = 1.+bonk*costhet + gamma*(1.-bonk*costhet)
```

```
      abssin = abs(sinthet)
          if(abssin.lt.1.0e-04) then
          f2(i,j)=x3*bj(mi(i),yx)*0.5*mi(i)
          else
          f2(i,j)=x3*mi(i)*bj(mi(i),yx)*bj(mi(i),arg)/arg
          endif


      endif


100   continue
200   continue


c     The next DO LOOP initializes the parameters par(1) thru
c     par(102).

      mm=1
      do 500 j=1,npts
      do 400 i=1,2

      par(mm) = f(i,j)
      mm=mm+1

400   continue
500   continue

      mm = 103
      do 501 j=1,npts
      do 401 i=1,2
      par(mm) = f2(i,j)
      mm = mm +1
401   continue
501   continue


c     The values of  x(1)  thru  x(4)  are the electric field
      values.
c     x(5) is the  phase  difference,  x(6)  and x(7) are the
      polarization
c     angles.

      c6 = cos(x(6))
      s6 = sin(x(6))
      c7 = cos(x(7))
      s7 = sin(x(7))

c     The following equation calculates the power.

      pmax = 0.0
      do 600 i=1,npts
      ii = (i-1)*2
      np2 = npts*2 +1
```

```
      p(i)=(par(ii+1)*x(2)*c6)**2+(par(ii+1)*x(1)*s6)**2
     & +(par(ii+2)*x(4)*c7)**2 + (par(ii+2)*x(3)*s7)**2 +
     & 2*cos(x(5))*par(ii+1)*par(ii+2)*
     & (x(2)*c6*x(4)*c7+x(1)*s6*x(3)*s7)
     & + (par(ii+np2)*x(2)*s6)**2 +(par(ii+np2)*x(1)*c6)**2
     &                +              (par(ii+1+np2)*x(4)*s7)**2
+(par(ii+1+np2)*x(3)*c7)**2
     &
+2*cos(x(5))*par(ii+np2)*par(ii+1+np2)*(x(2)*x(4)*s6*s7
     & + x(1)*c6*x(3)*c7)
     & + 2*par(ii+1)*par(ii+2)*sin(x(5))*
     & (x(1)*s6*x(4)*c7 - x(2)*c6*x(3)*s7)
     & + 2*par(ii+np2)*par(ii+np2+1)*
     & sin(x(5))*(x(1)*c6*x(4)*s7-x(2)*s6*x(3)*c7)


      if(p(i).gt.pmax) pmax = p(i)
600   continue

      do 700 i=1,npts
      pnorm = p(i)/pmax
      p(i) = abs(pnorm)
700   continue

      return
      end
```

APPENDIX B

```
c
c                              FIELD5.OK
c
c     This program calculates the far field pattern for up to
c     five modes out of  a  circular waveguide. Present modes
      are TE13,
c     TE33, TE11, TE12, TE14.  The  output  is the power as a
      function of
c     theta. This data can be used for disspla.

      integer n, itmax,ier,m(5)
      real
wk(418),x(10),fnorm,par(1000),theta(200),y(5),f(5,200)
      real p(200)
      data m/1,3,1,1,1/
      data y/8.53632,11.34592,1.84118,5.33144,11.70600/

c     m corresponds to a TEm,n mode
c     ak  is  the  waveguide  radius  times  the  free  space
      wavenumber
c     y is the Bessel root
c     theta is the azimuthal angle
c     x(i) is the amplitude/phase of the i-th mode

c     The  equations used in this program were adapted from a
      paper
c     by Zhang et. al.,IPF-83-5, Institut Fur Plasmaforschung
      memo,
c     Stuttgart, June 1983.  Bessel functions were calculated
      by the
c     subroutine bes.

      do 5 i=1,200
      theta(i)= -55.+ (i-1)*110./200.
 5    continue

      pi=3.1416
      ak= 11.56
c      ak = 19.80
      open(unit=1,file="R15TEST",status="UNKNOWN")


c     The following DO LOOPS calculate f(theta).

      do 200 i=1,5
      do 100 j=1,200

      yx=y(i)
      if(yx.eq.0.0) then
      f(i,j) = 0.0
```

```
      else
      sinthet=sin(theta(j)*pi/180.)
      costhet=cos(theta(j)*pi/180.)
      arg=ak*sinthet
      bonk=sqrt(1.-(yx/ak)**2)
      gamma=((1.-bonk)/(1.+bonk))**2
      x1=bonk +costhet-gamma*(bonk - costhet)
      x2=1.-(sinthet*ak/yx)**2
      f(i,j)=x1*bj(m(i),yx)*bjprime(m(i),arg)/x2
      endif


100   continue
200   continue


c     The next DO LOOP initializes the parameters par(1) thru
c     par(1000).

      mm=1
      do 500 j=1,200
      do 400 i=1,5

      par(mm) = f(i,j)
      mm=mm+1

400   continue
500   continue

c     The values of x(1) thru  x(5) are the amplitudes of the
      modes.
c     x(6) thru x(10) are the phases.

      x(1)= 0.
      x(2)=1.
      x(3)=0.
      x(4)=0.
      x(5)=0.0
      x(6)=0.
      x(7)=0.
      x(8)= 0.0
      x(9)= 0.0
      x(10)=0.0
c     The following equation calculates the power.

      pmax = 0.0
      do 600 i=1,200
      ii = (i-1)*5

      p(i)=.5*(
(x(1)*par(ii+1))**2+(x(2)*par(ii+2))**2+(x(3)*par(ii+3))**2
     !+(x(4)*par(ii+4))**2+(x(5)*par(ii+5))**2 )
```

```
!  +x(1)*x(2)*par(ii+1)*par(ii+2)*cos(x(7)) +
!x(1)*x(3)*par(ii+1)*par(ii+3)*cos(x(8))
!+x(1)*x(4)*par(ii+1)*par(ii+4)*cos(x(9))
!  +x(1)*x(5)*par(ii+1)*par(ii+5)*cos(x(10))
!+x(2)*x(3)*par(ii+2)*par(ii+3)*cos(x(8)-x(7))
!  +x(2)*x(4)*par(ii+2)*par(ii+4)*cos(x(9)-x(7))
!+x(2)*x(5)*par(ii+2)*par(ii+5)*cos(x(10)-x(7))
!+x(3)*x(4)*par(ii+3)*par(ii+4)*cos(x(9)-x(8))
!  +x(3)*x(5)*par(ii+3)*par(ii+5)*cos(x(10)-x(8))
!+x(4)*x(5)*par(ii+4)*par(ii+5)*cos(x(10)-x(9))

      if(p(i).gt.pmax) pmax = p(i)
600   continue

      do 700 i=1,200
      pnorm = p(i)/pmax
      pnorm = abs(pnorm)
      p(i) = 10.*alog10(pnorm)
      if(p(i).lt.-40.) p(i)=-40.0
      write(1,999) theta(i),p(i)
999   format(1x,2f7.2)
700   continue
      write(1,*) pmax


      stop
      end
```

APPENDIX C

```
c
c                    CALPERP.TH
c
c     This program calculates the absorption of microwaves by
      the
c     calorimeter. This version is for the electric field
      polarized
c     perpendicular to the plane of incidence. Theta is
      varied as the
c     coat thickness is held constant.

c     d is the coat thickness
c     gamma is the lossy propagation constant
c     losstan is the loss tangent
c     refl is the reflection coefficient
c     theta is the angle of incidence
c     f is the frequency

      real e,pi,f,c,lambda,k,d,losstan,e2,refl,di
      complex ix,x1,x2,r,r2,epsln,gamma,sint,cost,x3

      f= 85.e+09
      ix = cmplx(0,1)
      e = 2.718281828
      pi = 3.141593
      c = 3.0e+08
      lambda = c/f
      k = 2. * pi/lambda

      losstan = 0.8
      e2 = 10.0
      epsln = e2*(1.0 - ix*losstan)
      gamma = k* csqrt(epsln)

      open(unit=1,file='CALPERP',status='UNKNOWN')
      do 10 i=1,201
      theta = (i-1)*pi/400.
      d = lambda*0.21
      sint = sin(theta)/csqrt(epsln)
      cost = csqrt(1.0 - sint**2)

      x2 = -2.*ix *gamma *d*cost
      x3 = csqrt(epsln)*cost/cos(theta)
      x1 = ((1. + cexp(x2))/(1.0 - cexp(x2)))* x3

      r = (1.-x1)/(1.+x1)
      r2 = conjg(r)
      refl = r*r2

      theta = theta *180/pi
      write(1,999) theta,refl
999   format(1x,2f7.3)

 10   continue
      stop
      end
```